

Dissertation zur Erlangung des Doktorgrades
der Fakultät für Chemie und Pharmazie
der Ludwig-Maximilians-Universität München

Influence of the Antibody Variable Domain on FcRn-Dependent Pharmacokinetics

Angela Susanne Schoch

aus

Heidelberg, Deutschland

2014

Erklärung

Diese Dissertation wurde im Sinne von §7 der Promotionsordnung vom 28. November 2011 von Herrn Prof. Dr. Gerhard Winter betreut.

Eidesstattliche Versicherung

Diese Dissertation wurde eigenständig und ohne unerlaubte Hilfe erarbeitet.

München, 11.09.2014

.....

Angela Schoch

Dissertation eingereicht am: 11.09.2014

1. Gutachter: Prof. Dr. Gerhard Winter

2. Gutachter: Prof. Dr. Wolfgang Frieß

Mündliche Prüfung am: 16.10.2014

Für meine Eltern

ACKNOWLEDGMENTS

The presented work has been acquired within a research cooperation between the Department of Pharmaceutical Technology and Biopharmaceutics at the Ludwig-Maximilians-University Munich and Roche Diagnostics Penzberg.

First of all, I would like to express my gratitude to my doctoral supervisor Prof. Dr. Gerhard Winter for the possibility to join his research group and for his professional guidance. I highly appreciate his scientific input and ongoing interest in the progress of my work as well as the opportunity to participate scientific and social events at his chair.

My thankfulness also goes to Dr. Thomas Emrich from Roche Diagnostics for his supervision, the scientific input and advice over the last years.

Also, I like to thank Dr. Hubert Kettenberger for his co-supervision regarding analytical aspects and his outstanding contribution to this work.

Many thanks go to Dr. Julia Heinrich and Dr. Apollon Papadimitriou for provision of the thesis topic and for giving me the opportunity to do my PhD thesis in an excellent working atmosphere. My tremendous gratitude is expressed to all my colleagues from LMBA. I very much appreciate the scientific and personal support from each of you: Claudia Goss, Ying Guo, Janine Müller, Kari Damhjell, Andreas Wolfert, Kerstin Birkner, Thomas Stuchly, Christian Künzel, Achim Lutz, Dr. Gregor Lotz, Gregor Jordan, Uwe Dahl, Miriam Moheysen-Zadeh, Alexander Pöhler, Dr. Roland Staack, Andreas Kalbe, Meike Zaspel, Dr. Sabine Lohmann, Dr. Cordula Jany, Steven Challand, Julian Meir, Sylvia Rottach, Maria Viert, Dr. Martin Schäfer, Anita Müller and Martina Savaete. A special thanks to Klaus Mackeben, Markus Zadak, Uwe Wessels and Dr. Kay Stubenrauch for sharing their lab with me and enduring me over the last years.

I like to thank my analytical lab for introducing me into all analytical methods and answering endless questions. I know your kind support was not self-evident and

therefore I am very thankful to Barbara Saur, Elke Liebig, Eva Greiter, Melanie Elsner, Andrea Haggenmüller, Alexander Knaupp and Andreas Adlberger. Furthermore I want to thank Michaela Schuster, Holger Kley, Xaver Reiser, Achim Gärtner and Daniela Matscheko for their help and contribution to this work.

I want to thank Dr. Julia Engert for her scientific and personal support, for proof reading of the publications and this thesis. Furthermore I thank Dr. Tilman Schlothauer for his support and helpful discussions. Also, I am thankful to Prof. Dr. Wolfgang Frieß for his interest in my work and for kindly being the co-referee of this work.

Many thanks go to Dr. Martin Bader, Dr. Sabine Imhof-Jung, Susanne Gegner and Ursula Schwarz as well as Dr. Petra Rüger and Nina Meissler for production and purification of all antibodies.

I want to thank Dr. Irmgard Thorey, Monika Lechner and especially Marco Friedrich for conducting all animal experiments.

I like to thank Dr. Olaf Mundigl, Doris Ziegler-Landsberger and Heike Seul for conducting the in vitro cell assay experiments.

Florian Lipsmeier and Stefan Klostermann, I want to thank for their support in statistical and bioinformatical issues.

I want to thank Frieda Schwegler, Sibylle Christ and Anja Schmalz for their encouragement and friendship in the last years. Also, I am thankful to my aunt and uncle, Helmtraud and Klaus Strein, for their support.

My deepest gratitude goes to my parents, Bärbel and Bruno Schoch, for their support in all aspects who made my studies and my PhD thesis possible in the first place. Furthermore I like to thank my siblings Marisa, Julian and Dominic as well as Corinna and Goentje for their encouragement and backup in the last years.

TABLE OF CONTENT

1.	INTRODUCTION.....	1
1.1.	Antibodies	1
1.1.1.	Antibody structure	1
1.1.2.	Antibody function	3
1.1.3.	Therapeutic antibodies	4
1.2.	FcRn	7
1.2.1.	FcRn structure	7
1.2.2.	FcRn expression.....	7
1.2.3.	FcRn function.....	8
1.2.3.1.	FcRn-IgG binding mechanism	8
1.2.3.2.	Regulating IgG homeostasis	9
1.2.3.3.	Passive humoral immunity	10
1.2.3.4.	Regulating antigen presentation.....	11
1.2.3.5.	Regulating IgG concentration in specialized cell types	11
1.2.4.	Human FcRn transgenic mouse model	12
1.2.5.	IgG-engineering	13
1.3.	Antibody model system.....	16
1.3.1.	Briakinumab and Ustekinumab.....	16
1.3.2.	Bevacizumab and Bevacizumab-variant.....	18
1.4.	Aim of the thesis	19
2.	MATERIAL	21
2.1.	Reagents and chemicals	21
2.2.	Kits	22
2.3.	Instruments and chromatography columns	23
2.4.	Antibodies and proteins.....	25

2.5.	Mice	27
2.6.	Buffer compounds.....	27
2.7.	Software	29
2.8.	Consumable supplies	30
3.	METHODS	31
3.1.	Production	31
3.2.	Biochemical characterization	33
3.2.1.	Determination of mAb concentration	33
3.2.2.	Determination of mAb molecular weight	33
3.2.3.	Determination of mAb size.....	34
3.2.4.	Determination of mAb hydrophobicity	35
3.2.5.	Analysis of stressed mAbs.....	36
3.2.6.	Determination of mAb isoelectric point	36
3.2.7.	Charge distribution analysis	37
3.2.8.	IdeS cleavage	38
3.2.9.	Complex of mAb and IL-12	39
3.3.	Functional characterization.....	40
3.3.1.	Interaction with human IL-12	40
3.3.1.1.	ELISA	40
3.3.1.2.	SPR	42
3.3.2.	Interaction with IL-12 and IL-23 of different species	43
3.3.3.	Interaction with mouse FcγRI	43
3.4.	FcRn-mAb interaction.....	44
3.4.1.	FcRn-mAb affinity at pH 6.0.....	44
3.4.2.	FcRn-mAb dissociation	44
3.4.2.1.	FcRn-mAb dissociation using SPR	44
3.4.2.2.	FcRn-mAb dissociation using FcRn affinity chromatography	45
3.4.2.3.	FcRn affinity chromatography using a pH gradient	45

3.4.2.4.	FcRn affinity chromatography under high ionic strength conditions	46
3.4.2.5.	FcRn affinity chromatography using a salt gradient.....	46
3.5.	<i>In vivo</i> PK study	48
3.5.1.	Mice	48
3.5.2.	Study design.....	48
3.5.3.	Determination of human antibody serum concentrations	50
3.5.4.	Pharmacokinetic analysis	52
3.5.5.	Statistical analysis	53
3.5.6.	Detection of drug/ADA immune complexes	53
3.6.	Second model antibody system	57
4.	RESULTS.....	60
4.1.	Production	60
4.2.	Biochemical characterization.....	64
4.2.1.	Determination of mAb concentration	64
4.2.2.	Determination of mAb molecular weight by CE-SDS	64
4.2.3.	Determination of mAb size by SEC.....	66
4.2.4.	Determination of mAb hydrophobicity.....	66
4.2.5.	Analysis of stressed mAbs	68
4.2.6.	Determination of mAb isoelectric point	71
4.2.7.	Charge distribution analysis.....	72
4.2.8.	IdeS cleavage	75
4.3.	Functional characterization	77
4.3.1.	Interaction with human IL-12	77
4.3.1.1.	ELISA	77
4.3.1.2.	SPR	79
4.3.2.	Interaction with IL-12 and IL-23 of different species	81
4.3.3.	Interaction with mouse FcγRI.....	82
4.4.	FcRn-mAb interaction.....	83

4.4.1.	FcRn-mAb affinity at pH 6.0.....	83
4.4.2.	FcRn-mAb dissociation	84
4.4.2.1.	FcRn-mAb dissociation using SPR	84
4.4.2.2.	FcRn affinity chromatography using a pH gradient	85
4.4.2.3.	FcRn affinity chromatography using a salt gradient.....	96
4.5.	<i>In vivo</i> studies	98
4.5.1.	<i>In vivo</i> study in human FcRn transgenic mice.....	98
4.5.2.	<i>In vivo</i> study in FcRn knockout mice	102
4.6.	Second model antibody	105
4.6.1.	Biochemical characterization.....	106
4.6.1.1.	Charge distribution analysis	107
4.6.2.	Functional characterization.....	108
4.6.3.	FcRn-mAb dissociation	109
5.	DISCUSSION	110
5.1.	Biochemical characterization	111
5.2.	Functional characterization.....	114
5.3.	FcRn-mAb interaction.....	116
5.4.	<i>In vivo</i> studies	121
5.5.	Transferability to other mAbs.....	128
5.6.	FcRn affinity column as analytical tool	129
6.	FINAL SUMMARY AND CONCLUSIONS	130
7.	ADDENDUM.....	134
7.1.	Tables.....	134
7.2.	List of abbreviations	138
7.3.	List of figures.....	142

7.4.	List of tables.....	145
7.5.	References	147
7.6.	Presentations and publications	161
7.7.	Curriculum Vitae	162

1. Introduction

This thesis deals with the interaction between the neonatal Fc receptor and immunoglobulin G antibodies. The introduction gives a brief summary on antibodies, the neonatal Fc receptor and the model antibodies used in this work.

1.1. Antibodies

In 1890, Emil von Behring and Shibasaburo Kitasato first described the use of antitoxins in serum therapy. They suggested that antibodies could specifically eliminate diphtheria and tetanus toxins (Behring and Kitasato 1890). This finding was the key to establish an effective vaccination against diphtheria. Today, diphtheria vaccination is available to almost every child.

Since that time, antibodies have been studied and characterized in detail. The first therapeutic antibody was a murine monoclonal antibody (mAb) named Muromonab-CD3 in 1986 which had severe side effects (Perens et al. 2007). The development from murine to chimeric and later to humanized and human antibodies reduced the occurrence of side effects (Reff and Heard 2001). Furthermore the indication areas grew steadily in the last years, including cancer, autoimmune, viral, inflammatory and ophthalmic diseases. However, the development of new applications and approaches for antibodies will continue in the next years.

1.1.1. Antibody structure

Antibodies are members of the immunoglobulin (Ig) family (Campbell and Reece 2006). They are classified by their function and pharmacokinetic properties into five isotypes: immunoglobulin alpha (IgA), delta (IgD), epsilon (IgE), gamma (IgG) and my (IgM) (Lobo et al. 2004). In mammals, antibodies of the IgG type constitute

one of the immune system's major components for the defense against pathogens such as bacteria, viruses and fungi. They are secreted by plasma B cells and represent approximately 75% of serum immunoglobulins in healthy humans (Janeway et al. 2001).

Human IgG (~150 kDa) is a protein consisting of four polypeptide chains, including two identical heavy chains (HC) and two identical light chains (LC) assembled by disulfide bonds (Figure 1-1) (Campbell and Reece 2006).

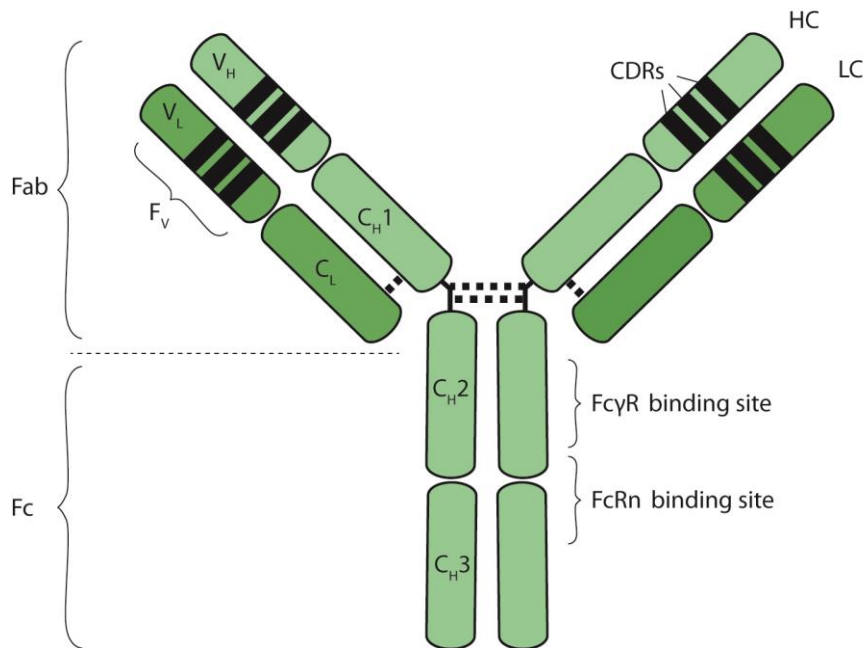


Figure 1-1: Schematical IgG structure

IgG consists of two identical heavy (HCs) and light chains (LCs) which are covalently linked by disulfide bonds. The HC consists of three constant domains (C_{H1} , C_{H2} , C_{H3}) and a variable domain (V_H). The LC consists of one constant domain (C_L) and a single variable domain (V_L). The antigen binding fragment (Fab) consists of the LC and of the C_{H1} and V_H domains of the HC. The variable region of the Fab (F_v) consists of the V_H and V_L domains and includes the complementarity determining regions (CDRs). The crystallizable fragment (Fc) comprises the C_{H2} and C_{H3} domains.

IgGs are divided into four subclasses according to their HC sequence (Janeway et al. 2001; Lobo et al. 2004): IgG1, IgG2, IgG3 and IgG4. Most therapeutic antibodies belong to the IgG-isotype and the IgG1 subclass, therefore this work focusses on IgG1 as antibody-isotype. Each HC has a molecular weight (MW) of about 50 kDa and consists of four domains: Three domains in the constant region C_{H1} , C_{H2} , C_{H3}

and a single domain in the variable domain V_H . C_{H1} and C_{H2} are connected to each other via the hinge region that is responsible for the high structural flexibility of IgGs (Janeway et al. 2001; Khawli et al. 2010; Reff and Heard 2001).

Table 1-1: Properties of human IgG subclasses

The IgG subclasses are named in order of their serum abundance, starting with IgG1 as most abundant. Data reported by Janeway et al. (2001).

	IgG1	IgG2	IgG3	IgG4
Mean serum level [mg/mL]	9	3	1	0.5
Serum half-life [d]	21	20	7	21

IgGs can be further classified by their LC sequence into kappa (κ) and lambda (λ) (Janeway et al. 2001). Each LC has a MW of about 25 kDa and consists of two domains: the constant domain C_L and the variable domain V_L .

Antibodies have two functional domains, namely the antigen binding fragment (Fab) and the crystallizable fragment (Fc). The constant domains C_{H2} and C_{H3} form the Fc region. The Fc region interacts with effector molecules such as complement proteins and Fc receptors (FcRs) (Jefferis 2009; Raghavan and Bjorkman 1996; Reff and Heard 2001).

The Fab fragment consists of the two LC and the two HC domains C_{H1} and V_H and is responsible for recognizing and binding the antigen. The variable region of the Fab (Fv) contains the V_H and V_L domains and includes the complementarity determining regions (CDRs) that are responsible for highly specific antigen binding (Mould and Green 2010). Each antibody has two Fab regions and can therefore bind two antigens simultaneously (Reff and Heard 2001).

1.1.2. Antibody function

IgGs are major components of the immune system. The Fab region comprises the antigen binding site and is responsible for the ability of the IgG to specifically recognize diverse antigens. The high specificity is due to the CDRs in the Fab region which recognize defined antigen structures, the so-called epitopes (Campbell and Reece 2006).

The Fc part of an IgG does not bind to antigens but couples the antibody to immune effector pathways to target and eliminate pathogens and foreign molecules:

- Interaction with the C1q-component of the complement system leads to phagocytosis and complement dependent cytotoxicity (CDC) (Jefferis 2009; Montano and Morrison 2002).
- Binding to Fcγ receptors (FcγRs) leads to phagocytosis and antibody dependent cellular cytotoxicity (ADCC) (Keizer et al. 2010; Montano and Morrison 2002; Mould and Green 2010; Reff and Heard 2001).
- Interaction with neonatal Fc receptor (FcRn) influences IgG homeostasis resulting in prolonged serum half-life (Lobo et al. 2004; Mould and Green 2010; Roopenian and Akilesh 2007).

1.1.3. Therapeutic antibodies

The generation of the first monoclonal antibody by hybridoma technology in 1975 was one of the starting points for the development of therapeutic antibodies (Köhler and Milstein 1975).

Therapeutic antibodies in modern medicine play a major role in the treatment of various diseases, e.g. cancer and autoimmune diseases. The importance of therapeutic antibodies to the drug market increases continuously. To date, more than 30 monoclonal antibodies have been approved by the US Food and Drug Administration (FDA) and it is estimated that over 300 other antibodies are currently in development (Benson et al. 2011; Yamada 2011). Thus, the number of therapeutic antibodies is going to increase in the following years. It is therefore important to understand pharmacokinetic (PK) aspects of these potentially life-saving protein drugs.

Therapeutic antibodies are mainly administered parenterally via intravenous (i.v.) or subcutaneous (s.c.) application due to their large molecular size, high polarity and gastric instability (Tabrizi et al. 2006). The PK profile of therapeutic antibodies is described by absorption (except for i.v. administration), distribution and elimination

processes and is on a molecular level mainly dependent on the target antigen and on the antibody structure itself (Ternant and Paintaud 2005; Wang et al. 2008).

Antibodies directed against soluble targets (e.g. cytokines) are internalized via fluid-phase endocytosis into cells, where the target is degraded. These antibodies in general show a dose-proportional behavior with linear clearance because the clearance is limited to catabolic processes (Mould and Green 2010).

In contrast, antibodies directed against targets on cell surfaces can also be internalized via receptor-mediated endocytosis and may therefore show target-mediated clearance (Wang et al. 2008). Target-mediated clearance is usually a saturable process; uptake and elimination of the therapeutics are dependent on the expression of the target and the antibody dose. Antibodies that undergo target-mediated clearance show therefore typically a nonlinear clearance (Keizer et al. 2010).

Besides the influence of the target antigen, the antibody structure itself can also influence PK. The charge of an antibody for example can influence PK by affecting the electrostatic interaction between the antibody and negatively charged groups on the surface of cells (Khawli et al. 2002).

Furthermore antibodies having the tendency to form aggregates can show an altered PK profile. The formation of aggregates is often caused by hydrophobic regions of an antibody and can impact immunogenicity, which is defined as the ability to provoke an immune response (Putnam et al. 2010). In the course of an immune response anti-drug antibodies (ADAs) can be formed against the therapeutic antibody which in turn influence PK by formation of drug/ADA immune complexes that induce a quick elimination (Brinks et al. 2011; Pendley et al. 2003).

Finally, structural heterogeneities in the Fc region of an antibody can alter the interaction with Fc receptors and consequently influence PK. For example, differences in the glycosylation pattern in the Fc region can affect binding to Fcγ receptors and complement proteins and subsequently influence PK by altered CDC or ADCC. However, of particular importance is the Fc region of an IgG

antibody, because of its interaction with the neonatal Fc receptor. Human IgGs of subclasses 1, 2, and 4 have a prolonged half-life of up to 21 days which is mediated by the interaction with FcRn (Chaudhury et al. 2003; Ghetie and Ward 2000). The long serum persistence and the high specificity of IgGs are the main reasons why IgGs are widely used as therapeutic proteins.

1.2. FcRn

The neonatal Fc receptor was first described by Brambell et al. in 1964 and is therefore also known as the Brambell-receptor (Brambell et al. 1964; Junghans 1997). The Fc receptor was named neonatal due to its initially identified function of transporting maternal IgG to the fetus and thereby building the humoral immunity of the fetus (Brambell 1966). Today, it is known that FcRn is also expressed in adults and has several important functions (1.2.3) but for historical reasons it is still called the neonatal Fc receptor.

1.2.1. FcRn structure

Human FcRn is a heterodimeric glycoprotein consisting of a 42-44 kDa class I major histocompatibility complex (MHC I)-like heavy chain (α -FcRn) and a non-covalently associated 12 kDa β_2 microglobulin (β_2m) light chain (Kuo et al. 2010; Low and Mezo 2009; Rodewald 1976; Simister and Rees 1985). The heavy chain is membrane-bound and is composed of three extracellular domains (α_1 , α_2 , α_3), a single transmembrane domain and a short cytoplasmic sequence domain (Bjorkman and Parham 1990; Simister and Mostov 1989). The α domains, especially the α_2 domain, represent the binding site to IgG (Giragossian et al. 2013).

Mouse, rat and monkey FcRn amino acid sequences share 66 %, 65 % and 95 % sequence identity with human FcRn, respectively (Giragossian et al. 2013).

1.2.2. FcRn expression

In adults, FcRn is primarily expressed in vascular endothelial cells or the reticuloendothelial system (RES) (Mould and Green 2010). More precisely, FcRn is mainly expressed by endothelial cells of muscle, skin, liver, spleen, kidney, blood-brain barrier, blood-ocular barrier and circulating monocytes (Akilesh et al. 2007; Blumberg et al. 1995; Borvak et al. 1998; Cianga et al. 2011; Kim et al. 2008; Schlachetzki et al. 2002). In most cell types the steady state cell-surface expression levels of FcRn are low (Ward and Ober 2009).

1.2.3. FcRn function

FcRn plays a major role in several processes:

- in IgG and albumin homeostasis
- in passive humoral immunity
- in regulating antigen presentation
- in regulating IgG concentration in brain and kidney

The key feature of the FcRn-IgG interaction and also of the FcRn-albumin interaction is pH-dependent binding (Chaudhury et al. 2003; Datta-Mannan et al. 2007), although IgG and albumin have independent binding sites on the FcRn (Kim et al. 2006).

1.2.3.1. FcRn-IgG binding mechanism

The cognate FcRn binding site is located at the C_H2-C_H3 interface of an IgG. The FcRn-IgG interaction occurs in a 1:2 stoichiometry, with one IgG binding to two FcRn molecules via its two heavy chains (Figure 1-2) (Huber et al. 1993; Sanchez et al. 1999).

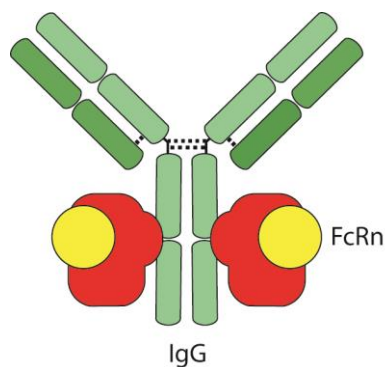


Figure 1-2: FcRn-IgG interaction

The heterodimeric FcRn molecule is illustrated as MHC I-like HC in red and β_2m in yellow. The cognate FcRn binding site is at the C_H2-C_H3 domain of the IgG (green).

The interaction between IgG and FcRn is strictly pH-dependent, showing nanomolar affinity at endosomal pH of 5-6 and negligible binding at physiological pH of 7.4 (Goebel et al. 2008; Ober et al. 2004a; Ober et al. 2004b). Responsible for this pH-

dependent binding are histidine residues located at the C_H2-C_H3 interface of the IgG which interact with acidic residues on the FcRn surface at acidic pH (Raghavan et al. 1994). Increasing pH values result in deprotonation of the histidine residues of the IgG and in dissociation of the FcRn-IgG complex. In addition to this ionic interaction, there are hydrophobic interactions between isoleucine residues of the IgG and tryptophan residues of the FcRn (Raghavan et al. 1995; Roopenian and Akilesh 2007).

1.2.3.2. Regulating IgG homeostasis

Human IgGs of subclasses 1, 2 and 4 have an average serum half-life of 21 days, which is longer than that of any other known serum protein (Waldmann and Strober 1969). This long half-life is predominantly mediated by the interaction of IgGs with FcRn (Chaudhury et al. 2003; Ghetie and Ward 2000). The underlying mechanism is illustrated in Figure 1-3: IgGs are subject to unspecific pinocytosis by various cell types (Akilesh et al. 2007; Montoyo et al. 2009). Afterwards IgGs encounter and bind FcRn in the acidic endosome at a pH of 5-6 (Rodewald 1976; Roopenian and Akilesh 2007). The endosome is divided into two parts, either containing molecules bound to FcRn or molecules not bound to FcRn. IgGs bound to FcRn are transported to the cell surface and are released in the extracellular space at physiological pH of 7.4, thereby protecting IgGs from lysosomal degradation (Ghetie and Ward 2000; Raghavan and Bjorkman 1996). Afterwards FcRn is transported back in the cell following exocytotic fusion with the cell membrane, which in turn results in low steady-state levels of FcRn on the plasma membrane (Ghetie et al. 1996; Ober et al. 2004b). Molecules that are not bound to FcRn in the endosome, like weakly interacting antibodies, antigens or serum proteins, are degraded in the lysosomes. The strict pH-dependent bind-and-release mechanism is critical for IgG-recycling and any deviation of the binding characteristics at different pHs may strongly influence circulation half-lives of IgGs (Schlothauer et al. 2013; Vaccaro et al. 2005).

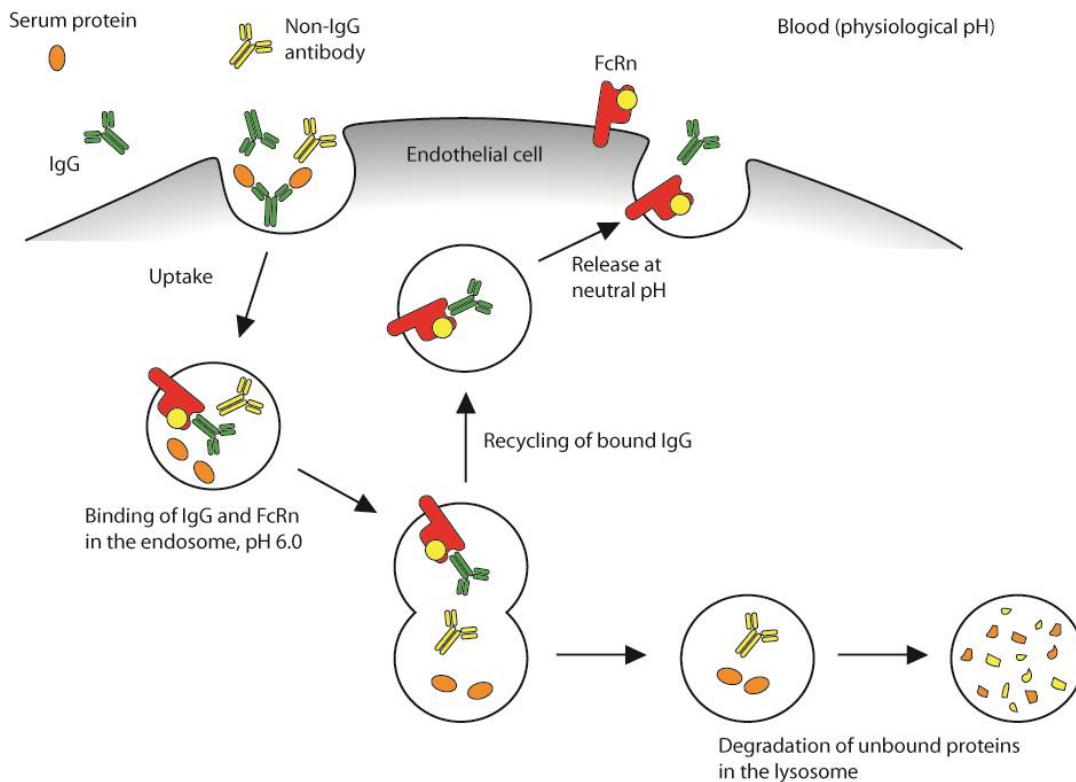


Figure 1-3: IgG-recycling mechanism

IgGs are subject to unspecific pinocytosis. Afterwards IgGs encounter and bind FcRn in the acidic endosome at a pH of 5-6 and are subsequently transported back to the cell surface. Finally, IgGs are released in the extracellular space at physiological pH of 7.4. In contrast, antigens, serum proteins and unbound antibodies are degraded in the lysosome. The figure was modified from Roopenian and Akilesh (2007).

Although IgG3 also binds to FcRn, IgG3 has a serum half-life of only 7 days. This can be explained by the intracellular competition between IgG1 and IgG3 that inhibits FcRn-mediated IgG3-recycling (Stapleton et al. 2011).

1.2.3.3. Passive humoral immunity

FcRn transfers IgG from mother to fetus via transcytosis across a polarized cell layer. The underlying mechanism differs between rodents and humans. In rodents, FcRn transports maternally derived IgG in ingested milk across the epithelial-cell layer of the proximal small intestine (Jones and Waldmann 1972). In humans on the other hand, FcRn transports maternal IgG across the placenta to the fetus. Here, FcRn is expressed by syncytiotrophoblasts, where it transports maternal IgG to the fetal capillaries of the placental villi (Leach et al. 1996; Simister et al. 1996).

1.2.3.4. Regulating antigen presentation

FcRn is also expressed in antigen presenting cells (APCs) like monocytes, macrophages and dendritic cells (Zhu et al. 2001). In these cells, FcRn regulates IgG homeostasis (Akilesh et al. 2007) but it can also enhance antigen presentation by directing antigen-IgG immune complexes into lysosomes in dendritic cells (Qiao et al. 2008). This results in the higher phagocytic activity of monocytes relative to natural killer (NK) cells that do not express FcRn (Ward and Ober 2009).

1.2.3.5. Regulating IgG concentration in specialized cell types

FcRn is also expressed in several specialized cell types like in the blood brain barrier, the kidney and multiple ocular tissues. The exact functions of FcRn at the blood-ocular barrier, cornea or retina remain currently unknown (Kim et al. 2008).

FcRn is expressed in brain microvasculature and in the choroid plexus epithelium at the blood–brain barrier (BBB) (Schlachetzki et al. 2002). The blood–brain barrier prevents the passive diffusion of macromolecules, like IgG, into the central nervous system (CNS) (Roopenian and Akilesh 2007). In response to inflammatory mediators, like tumor-necrosis factor alpha (TNF α), the blood–brain barrier can open transiently (Ballabh et al. 2004). In these situations, IgG would flood into the CNS down its steep concentration gradient and FcRn probably mediates reverse transcytosis of IgG from the CNS back into the circulation to maintain low levels of potentially inflammatory antibodies in the CNS (Roopenian and Akilesh 2007; Ward and Ober 2009).

The kidney functions as plasma filter using a size-selective barrier at the level of the glomeruli. Macromolecules of 70 kDa and larger cannot enter the barrier, whereas smaller molecules are excreted in the primary urine. IgG and albumin are both serum proteins with high molecular weight and are therefore excluded from the primary urine (Akilesh et al. 2007). These serum proteins could clog the kidney filter if they were not efficiently removed (Ward and Ober 2009). FcRn is expressed by epithelial cells of the glomerulus (podocytes) and transports deposited IgG from the basolateral surface of the podocyte into the primary urine of the glomerulus via transcytosis

(Haymann et al. 2000). FcRn is also expressed by epithelial cells of the proximal convoluted tubule to transcytoses IgG back into the systemic circulation (Kobayashi et al. 2002).

1.2.4. Human FcRn transgenic mouse model

Pharmacokinetics of therapeutic antibodies is often analyzed in mice during preclinical tests, before usage in humans (Ober et al. 2001). Human PK cannot be fully reflected by conventional mouse models, because binding of FcRn and IgG is a species-specific interaction (Roopenian et al. 2010). Murine FcRn binds IgG of several species, e.g. human, mouse, rabbit, guinea pig, bovine, sheep and rat IgG (Ober et al. 2001). On the contrary, human FcRn only binds human, rabbit and guinea pig IgG but not mouse IgG (Vaccaro et al. 2006; Zhou et al. 2005). Furthermore conventional mouse model systems do not reliably describe the pharmacokinetics of humanized antibodies and Fc-fusion proteins, because these antibodies have an abnormally high affinity for mouse FcRn, resulting in an artificially prolonged serum persistence (Ober et al. 2001; Petkova et al. 2006; Ternant and Paintaud 2005). These species-specific differences in affinity occur probably due to different glycosylation patterns in humans and rodents (Kuo et al. 2009).

To overcome the limitation in the conventional rodent model, the human FcRn transgenic mouse model is often used. This model mimics the interaction between human FcRn and human IgGs and is therefore an appropriate model to gain information about the prospective PK profile of human IgGs in humans (Roopenian et al. 2010). IgG elimination is dependent on the FcRn expression level, therefore the FcRn expression level is higher in homozygous mice than in heterozygous mice. Furthermore Roopenian et al. (2010) described three transgenic mouse lines that express different levels of FcRn: FcRn knockout mice (mFcRn $-/-$) expressing no FcRn, the human FcRn transgenic mice Tg276 and Tg32 expressing moderate and high levels of FcRn, respectively. To investigate PK differences of antibodies the use of heterozygous human FcRn transgenic mice Tg276 (B6.Cg- $\text{tm}1\text{Dcr}$ >Tg(FCGRT)276Dcr) is best suited (Roopenian et al. 2010).

Human FcRn transgenic mice lack endogenous mouse FcRn and instead express human FcRn (Petkova et al. 2006). As mouse IgG has only little affinity to human FcRn resulting in a fast clearance of mouse IgG, these mice show immunodeficiency. An accurate animal husbandry minimizes the risk of bacterial infections (Qiao et al. 2008).

An even more significant alternative to the FcRn transgenic mouse model would be the cynomolgus monkey model, but access to this model is limited due to ethical and cost reasons (Ward and Ober 2009).

1.2.5. IgG-engineering

FcRn plays a key role in regulating IgG homeostasis, therefore modulating the interaction between IgG and FcRn through protein engineering is an attractive method to modulate target-independent PK properties (Ghetie et al. 1997; Shields et al. 2001). In some cases antibodies with prolonged half-life are desired to lower the application dose or to reduce the application frequency of therapeutic antibodies in order to improve patient convenience and patient compliance (Hinton et al. 2004; Hinton et al. 2006). In other cases, antibodies with reduced half-life in the blood circulation are desired. For example, drugs for intravitreal application should preferentially have a long half-life in the eye and a short half-life in the circulation of the patient. Such antibodies could then have the advantage of increased exposure to a disease site, e.g. in the eye.

Different mutations that influence FcRn binding and therewith the half-life in the blood circulation are known.

FcRn binds to the Fc region at the C_H2-C_H3 domains of IgG, therefore modifications in that binding area can directly influence FcRn-IgG interaction (Raghavan et al. 1995; Roopenian et al. 2010; Roopenian and Akilesh 2007). Specific manipulations of the Fc region are known to affect PK characteristics by altering the interaction between Fc region and FcRn especially at pH 6.0 and such modifications have been used to design therapeutic antibodies with specific PK properties (Dall'Acqua et al. 2006; Petkova et al. 2006).

A triple mutation M252Y/S254T/T256E (YTE) in the Fc region of an antibody against respiratory syncytial virus (MEDI-524) resulted in a 10-fold increase in its FcRn affinity at pH 6.0 and subsequently in a nearly 4-fold increase in serum half-life in cynomolgus monkeys (Petkova et al. 2006; Yeung et al. 2009).

A single mutation (N434A) in the Fc region resulted in a 4-fold improvement in pH 6.0 binding and a 2-fold decrease in clearance in cynomolgus monkeys compared to the wild type antibody (Yeung et al. 2009).

Importantly, in another case, a single mutation (N434W) increased pH 6.0 binding 80-fold but did not result in prolonged half-life compared to the wild type antibody. This PK behavior was explained by the simultaneously improved binding to FcRn at pH 7.4, highlighting the importance of preserving the efficient pH-dependent release of IgGs at pH 7.4 when engineering antibodies with increased terminal half-lives (Suzuki et al. 2010; Wang et al. 2011).

In addition to the specific interaction of the Fc region with FcRn, the Fab regions have also been suggested to contribute to the FcRn-IgG interaction (Igawa et al. 2010; Schlothauer et al. 2013; Wang et al. 2011).

Wang et al. (2011) reported that IgGs with different target specificities and Fab regions but identical Fc sequences can have different FcRn affinities. Fab-mediated residual binding at near physiological pH was correlated with the pharmacokinetic properties of a set of therapeutic antibodies indicating that IgGs with excessive binding to FcRn at pH 7.3 suffer from reduced terminal half-lives.

Recently, Schlothauer et al. (2013) have described a novel pH-gradient FcRn affinity chromatography method that closely mimics physiological conditions for the dissociation between FcRn and IgG. Furthermore, they showed that IgGs with identical Fc regions differ in their dissociation from FcRn *in vitro*, thereby indicating the influence of the Fab region on FcRn-IgG interaction.

However, the underlying mechanism of the distal Fab region's influence on FcRn binding is hitherto only poorly understood. A deep understanding of the FcRn-IgG interaction is of high interest, especially in drug development and FcRn-dependent

antibody-engineering. Therefore the Fab influence on FcRn-IgG interaction needs to be further investigated.

1.3. Antibody model system

For systematic analysis of the Fab influence on FcRn-IgG interaction, an appropriate antibody model system is needed. The model antibodies should have similar Fc regions, but differences in their terminal half-lives. Furthermore, model antibodies should have identical target specificities to exclude target-dependent effects on PK. Therefore, Briakinumab (OzespasTM) and Ustekinumab (StelaraTM) were used as a model system to systematically investigate the influencing factors of the Fab region on FcRn-mediated IgG homeostasis.

1.3.1. Briakinumab and Ustekinumab

Briakinumab and Ustekinumab are two therapeutic antibodies both directed against soluble interleukin 12 (IL-12) and interleukin 23 (IL-23). IL-12 and IL-23 are heterodimeric, pro-inflammatory cytokines consisting of p40/p35 subunits and of p40/p19 subunits, respectively (Elliott et al. 2009; Gandhi et al. 2010). Briakinumab and Ustekinumab specifically bind to the shared p40-subunit of IL-12 and IL-23 and prevent them from binding to their cell surface receptor complexes, thereby blocking inflammatory pathways (Ding et al. 2008; Kurzeja et al. 2011). Briakinumab and Ustekinumab are not cross-reactive to mouse IL-12 and IL-23 (Luo et al. 2010; Traczewski and Rudnicka 2012), thus target-mediated clearance can be excluded when performing a PK study in mice.

Briakinumab, developed by Abbott, was intended to be used for the treatment of moderate to severe chronic plaque psoriasis in adults who failed to respond to, or who have a contraindication to, or are intolerant to other systemic therapies including ciclosporin, methotrexate and psoralen ultraviolet A (PUVA). In January 2011, Abbott withdrew its application for marketing authorization due to occurrence of major adverse cardiovascular events (MACEs) after Briakinumab treatment (European Medicines Agency 2011). The initial dose for Briakinumab was 200 mg as s.c. application. Followed by injection of 200 mg after 4 weeks and afterwards of 100 mg every 4 weeks (Inzinger et al. 2012).

Ustekinumab, developed by Centocor Ortho Biotech Inc., is indicated in the EU for

use in adults with moderate to severe plaque psoriasis who have not responded to or cannot use other systemic treatments for psoriasis, such as ciclosporin, methotrexate or PUVA. Furthermore it is used to treat adults with active psoriatic arthritis, when the condition has not responded well enough to other treatments called disease-modifying antirheumatic drugs (European Medicines Agency 2009b). Ustekinumab is administered as s.c. injection at a concentration of 45 mg. The second dose is given 4 weeks after the initial dose and afterwards every 12 weeks. The dose is adjusted to 90 mg for patients weighing more than 100 kg (Weber and Keam 2009).

Briakinumab and Ustekinumab are two fully human monoclonal IgG1 antibodies (Lima et al. 2009; Weger and Weger 2010). Both antibodies have nearly identical Fc domains with minor differences in several allotype-specific amino acids in this region.

Briakinumab is an IgG1 λ antibody with variable heavy and light chain domains of the V_H3 and V λ 1 germline families. Ustekinumab is an IgG1 κ antibody with variable heavy and light chain domains of the V_H5 and V κ 1D germline families, respectively. Briakinumab has an estimated bioavailability of approximately 42% after single dose s.c. application (Lima et al. 2009). Maximum serum concentrations (c_{\max}) were achieved after 3-4 days (T_{\max}) (Gottlieb et al. 2007; Weber and Keam 2009). Ustekinumab had an estimated bioavailability of 57.2% after single s.c. dose and a slow absorption with T_{\max} of approximately 12 days (Zhu et al. 2009). Interestingly, Ustekinumab has a median terminal half-life of 22-24 days (Kauffman et al. 2004), whereas Briakinumab has a terminal half-life of only 8-9 days after i.v. administration (Lima et al. 2009).

In summary, Briakinumab and Ustekinumab have the same target specificity and nearly identical Fc sequences but show different terminal half-lives in humans. Therefore these antibodies were chosen to elucidate the role of the Fab region on FcRn-dependent PK.

1.3.2. Bevacizumab and Bevacizumab-variant

To confirm the results of the Briakinumab-Ustekinumab model system, a second model system with Bevacizumab (Avastin®) and a specifically engineered variant of Bevacizumab was used.

Bevacizumab is a humanized monoclonal IgG1 antibody with variable kappa light chains directed against the vascular endothelial growth factor (VEGF) (Braghiroli et al. 2012; European Medicines Agency 2009a). VEGF is a signal protein that stimulates vasculogenesis and angiogenesis. Bevacizumab binds to VEGF and slows the growth of new blood vessels, thereby inhibiting the blood supply to cancer cells and subsequently inhibiting tumor growth and proliferation (European Medicines Agency 2009a).

Bevacizumab, developed by Hoffmann-La Roche, is used for the treatment of several cancer types including for example cancer of the colon or rectum, metastatic breast cancer and/or advanced or metastatic kidney cancer (Braghiroli et al. 2012; Rosen 2005). The recommended dose is between 5 and 15 mg/kg of body weight every two or three weeks, depending on the type of cancer being treated. Bevacizumab is administered as an i.v. infusion (European Medicines Agency 2009a).

Bevacizumab has a reported terminal half-life of up to 21 days in humans and of about 6.8 days in mice (Lin et al. 1999; Vieira and Rajewsky 1988).

1.4. Aim of the thesis

In recent years the importance of therapeutic antibodies has been rapidly increasing. Therefore it is necessary to understand pharmacokinetic and pharmacodynamic aspects of these protein drugs. Due to their large molecular size, antibodies are expected to show poor bioavailability following oral administration. In addition, antibodies can undergo denaturation due to the acidic pH of the stomach, and proteolytic degradation within the stomach and intestine (Tabrizi et al. 2006). Thus, antibodies are administered parenterally via i.v. or s.c. application which is inconvenient for patients and can reduce the patient compliance. Therefore antibodies with prolonged half-life are desired to lower the application dose or reduce the application frequency of the therapeutic antibodies. In other cases, antibodies with reduced half-life in the blood circulation are desired, for example antibodies used for intravitreal application. These antibodies should have a high concentration at the desired site of action, which is inside the eye, but a low concentration in circulation to reduce systemic side effects. In conclusion, modulating antibody PK to reduce or prolong terminal half-lives in early development stages is of high interest.

The IgG interaction with FcRn is important in regulating IgG homeostasis, therefore modulating the interaction between IgG and FcRn through protein engineering is an attractive method for modulating target-independent PK properties. Specific manipulations of the Fc region are known to affect PK characteristics by altering the interaction between Fc region and FcRn, especially at pH 6.0, and have been used to design therapeutic antibodies with specific PK properties (Dall'Acqua et al. 2006). However, antibodies having the same Fc regions do not simply have to have a similar PK profile. An additional contribution of the Fab region to FcRn binding has been reported, but the underlying mechanism remained unknown (Schlothauer et al. 2013; Wang et al. 2011; Zalevsky et al. 2010).

The aim of this thesis was to elucidate the influencing structural element of the Fab region and the underlying mechanism that influences FcRn-IgG interactions and FcRn-dependent PK. Two IgG1 antibodies, Briakinumab and Ustekinumab, that

have similar Fc regions but very different terminal half-lives in human, were therefore chosen as model system. Systematically engineered variants of Briakinumab and Ustekinumab with cross-over exchanges and modified charge distribution in the Fab region were produced to localize the influencing structural element of the Fab region and to analyze if the interaction was charge-mediated. These antibodies were biochemically and functionally characterized to confirm that antibodies were produced correctly and to look for reasons explaining differences in PK. The interaction with FcRn was studied to elucidate the contribution of the FcRn-IgG interaction on PK. Afterwards, antibodies differing in their FcRn-IgG interaction were analyzed in *in vivo* PK studies. Finally, the transferability of the previous results to a second model antibody system was tested.

2. Material

In the following chapter all reagents, chemicals, kits, mice strains and instruments used in this work are listed.

2.1. Reagents and chemicals

The reagents and chemicals used in this work are listed in Table 2-1:

Table 2-1: Reagents and chemicals

Description	Provider
ABTS	Roche Diagnostics GmbH, Mannheim, Germany
10mM sodium acetate, pH 4.5	GE Healthcare, United Kingdom
DTT	Sigma-Aldrich Chemie GmbH, Germany
HBS P+, pH 7.4	GE Healthcare, United Kingdom
HCl (37%, Ph.Eur.)	Carl Roth GmbH, Germany
Histidine ($\geq 98.5\%$, Ph.Eur.)	Carl Roth GmbH, Germany
H ₃ PO ₄ (85%, Ph.Eur.)	Carl Roth GmbH, Germany
Isoflurane	CP-Pharma GmbH, Germany
KCl ($\geq 99\%$, Ph.Eur.)	Carl Roth GmbH, Germany
KH ₂ PO ₄ ($\geq 98\%$, Ph.Eur.)	Carl Roth GmbH, Germany
MES ($\geq 99\%$, Ph.Eur.)	Carl Roth GmbH, Germany

Methyl cellulose	Proteinsimple, USA
Mouse Pool Serum (C57BL/6J mice)	Roche Diagnostics GmbH, Mannheim, Germany
NaCl ($\geq 99\%$, Ph.Eur.)	Carl Roth GmbH, Germany
NaOH (0.1 mol/L)	Carl Roth GmbH, Germany
NaH ₂ PO ₄ ($\geq 99\%$, Ph.Eur.)	Carl Roth GmbH, Germany
Na ₂ HPO ₄ ($\geq 98\%$, Ph.Eur.)	Sigma-Aldrich Chemie GmbH, Germany
Na ₃ PO ₄ ($\geq 98\%$, ACS)	Sigma-Aldrich Chemie GmbH, Germany
(NH ₄) ₂ SO ₄ ($\geq 99.5\%$, ACS)	Carl Roth GmbH, Germany
10 x PBS	Roche Diagnostics GmbH, Mannheim, Germany
Pharmalyte 3-10	Proteinsimple, USA
pI markers 7.05 & 9.77 (iCE)	Proteinsimple, USA
Streptavidin-sepharose	GE Healthcare, United Kingdom
TRIS ($\geq 99\%$, Ph.Eur.)	Carl Roth GmbH, Germany
Tween 20	Roche Diagnostics GmbH, Mannheim, Germany
Urea ($\geq 99.5\%$, Ph.Eur.)	Sigma-Aldrich Chemie GmbH, Germany

2.2. Kits

The following kits were used in this work:

Table 2-2: Kits

Description	Provider
Amine Coupling Kit (BiaCore)	GE Healthcare, United Kingdom
Bulk BirA	Avidity Biotechnologies, USA
FabRICATOR®	Genovis, Sweden
His Capture Kit	GE Healthcare, United Kingdom
Protein Series II Kit (Bioanalyzer)	Agilent Technologies, USA

2.3. Instruments and chromatography columns

The following instruments and chromatography columns were used:

Table 2-3: Instruments and chromatography columns

Description	Provider
<u>Instruments</u>	
Analytical balance (XS105 dual range)	Mettler Toledo, Switzerland
Anesthesia station	Fortec Medic Supplies Ltd, Kenya
Autosampler (iCE)	Prince Technologies, Netherlands
Biacore T100	GE Healthcare, United Kingdom
Bioanalyzer (2100)	Agilent technologies, USA
Electrical pipettes (50-1,200 µL)	Eppendorf, Germany
Filter (0.22 & 0.45 µm)	Pall Corporation, USA
Freezer (Liebherr premium, -20°C)	Liebherr, Switzerland

Material

Freezer (6485, -50- -85 °C)	GFL, Germany
HydroFlex™ (Microplate washer)	Tecan Group, Switzerland
iCE 280 system	Proteinsimple, USA
NanoDrop™1000 (Spectrophotometer)	Thermo Fisher Scientific, Germany
Pipettes (2.5-1,000 µL)	Eppendorf, Germany
Refrigerator (Liebherr comfort)	Liebherr, Switzerland
SevenEasy™ (pH-Meter)	Mettler Toledo, Switzerland
Sunrise™ (Photometer)	Tecan Group, Switzerland
Super-Q water systems	Millipore, Germany
Thermomixer comfort®	Eppendorf, Germany
Termoshaker (Grant bio PHMP-4)	Keison Products, United Kingdom
Uvikon® XL (UV VIS Photometer)	GOEBEL Instrumentelle Analytik GmbH, Germany
Vortex-Genie 2	Scientific industries, USA

Chromatography columns

FcRn affinity chromatography column (production see 3.4.2.2)	Roche Diagnostics GmbH, Mannheim, Germany (internal use only)
TSKgel Ether-5PW (10 µm, 7,5 mmx7,5 cm, HIC column)	Tosoh Corporation, Japan

Waters Biosuite™ 250 (7.8 x 300 mm, Waters Corporation, USA
SEC column)

2.4. Antibodies and proteins

Antibodies, receptors and cytokines used are listed in Table 2-4. Antibodies used as model antibodies and for the ELISA-measurements were produced only for internal use and are not commercially available.

Table 2-4: Antibodies and proteins

Description	Provider
<u>Model system antibodies</u>	
Briakinumab (sequence origin: PN WO2001014162-A2)	Roche Diagnostics GmbH, Mannheim, Germany
Ustekinumab (sequence origin: CAS Registry Number 815610-63-0)	Roche Diagnostics GmbH, Mannheim, Germany
mAb 1	Roche Diagnostics GmbH, Mannheim, Germany
mAb 2	Roche Diagnostics GmbH, Mannheim, Germany
mAb 3	Roche Diagnostics GmbH, Mannheim, Germany
mAb 4	Roche Diagnostics GmbH, Mannheim, Germany
mAb 5	Roche Diagnostics GmbH, Mannheim, Germany
mAb 6	Roche Diagnostics GmbH, Mannheim, Germany
mAb 7	Roche Diagnostics GmbH, Mannheim, Germany

Material

mAb 8	Roche Diagnostics GmbH, Mannheim, Germany
mAb 9	Roche Diagnostics GmbH, Mannheim, Germany
mAb 10	Roche Diagnostics GmbH, Mannheim, Germany
Bevacizumab (sequence origin: DB00112)	Roche Diagnostics GmbH, Mannheim, Germany
Bevacizumab-variant	Roche Diagnostics GmbH, Mannheim, Germany

Antibodies for ELISA measurements

<huFc>-Dig	Roche Diagnostics GmbH, Mannheim, Germany
<Dig>-POD	Roche Diagnostics GmbH, Mannheim, Germany
<muFc>-POD	Roche Diagnostics GmbH, Mannheim, Germany
<huFc>-Fab'-Bi	Roche Diagnostics GmbH, Mannheim, Germany
Calibration standard (conjugate of huIgG and muIgG)	Roche Diagnostics GmbH, Mannheim, Germany

Antibody for SPR measurements

<huFcPan>	Roche Diagnostics GmbH, Mannheim, Germany (internal use only)
-----------	---------------------------------------------------------------

Proteins

muFcγRI	R&D systems GmbH, USA
---------	-----------------------

huFcRn	Roche Diagnostics GmbH, Mannheim, Germany
huIL-12	Cell sciences, USA
huIL-23	R&D systems GmbH, USA
muIL-12	R&D systems GmbH, USA
muIL-23	R&D systems GmbH, USA

2.5. Mice

Animal studies were approved by the Government of Upper Bavaria, Germany (permit number 55.2-1-54-2532.2-28-10) and performed in an AAALAC accredited animal facility according to the European Union Normative for Care and Use of Experimental Animals. Mouse husbandry was carried out under specific pathogen free conditions and the animals were housed in standard cages having free access to food and water during the whole study period. The two following mice strains were used in this work:

Table 2-5: Mice

Description	Provider
B6.Cg- $\text{tg}(\text{FCGRT})276\text{Dcr}$ (human FcRn transgenic mice)	Jackson Laboratory, USA
B6.129X1-Fcgrt $\text{tm1Dcr}/\text{DcrJ}$ (FcRn knockout mice)	Jackson Laboratory, USA

2.6. Buffer compounds

The following buffer compounds were used in this work. All buffers were prepared using demineralized, sterile water and the pH was adjusted using hydrochloric acid and sodium hydroxide.

Table 2-6: Buffer compounds

FcRn column buffers, pH gradient

Eluent A, pH 5.5

MES	20 mM
NaCl	140 mM

Eluent B, pH 8.8

TRIS	20 mM
NaCl	140 mM

FcRn column buffers, salt gradient

Eluent A, pH 7.8

MES	10 mM
-----	-------

Eluent B, pH 7.8

MES	10 mM
NaCl	250 mM

FcRn column preparation buffers, pH 7.5

NaH ₂ PO ₄	20 mM
NaCl	150 mM

Formulation buffer, pH 6.0

Histidine	20 mM
NaCl	140 mM

HIC buffers, pH 7.0

Eluent A, pH 7.0

(NH ₄) ₂ SO ₄	1.5 M
Na ₃ PO ₄	25 mM

Eluent B, pH 7.0

Na ₃ PO ₄	25 mM
---------------------------------	-------

1 x PBS, pH 6.0/ pH 7.4

KH ₂ PO ₄	1 mM
---------------------------------	------

Na ₂ HPO ₄	10 mM
----------------------------------	-------

NaCl	137 mM
------	--------

KCl	2.7 mM
-----	--------

SEC buffer, pH 7.0

KH ₂ PO ₄	200 mM
---------------------------------	--------

KCl	250 mM
-----	--------

Wash buffer ELISA, pH 7.4

KH ₂ PO ₄	1 mM
---------------------------------	------

Na ₂ HPO ₄	10 mM
----------------------------------	-------

NaCl	137 mM
------	--------

KCl	2.7 mM
-----	--------

Tween 20	0.05 %
----------	--------

Universal buffer for ELISA

Produced by Roche Diagnostics, Mannheim, Germany (internal use only, compounds not published).

2.7. Software

The software systems used are listed in Table 2-7.

Table 2-7: Software

Description	Provider
Biacore T100 control/ evaluation	GE Healthcare, United Kingdom
Chromeleon	Dionex, Germany
DiscoveryStudio Pro, Version 3.5	Accelrys Inc., USA
European Molecular Biology Open Software Suite (EMBOSS)	European Bioinformatics Institute (EBI), United Kingdom
General Protein Mass Analysis for Windows (GPMW) 9.10	ChemSW, USA
Microsoft office 2010	Microsoft, USA
WinNonlin 5.3	Pharsight, USA
XLfit4	IDBS, United Kingdom

2.8. Consumable supplies

The following table gives information about the consumable supplies used.

Table 2-8: Consumable supplies

Description	Provider
BiaCore CM5 sensor chip	GE Healthcare, United Kingdom
26-gauge injection needle	B.Braun Melsungen AG, Germany
Hematocrit capillary	Hirschmann, Inc., USA
Microvette 500Z-Gel serum tubes	Nümbrecht, Germany
Streptavidin MTP (high capacity)	Roche Diagnostics GmbH, Mannheim, Germany
Preincubation MTP	Thermo Scientific, USA
1 mL syringe	Dispomed Witt oHG, Germany
1 ml XK column	GE Healthcare, United Kingdom

3. Methods

The method section is divided in 6 parts. In the first part, the production of the antibodies used in this work is described. Afterwards, in part 2 and 3, the antibodies were biochemically and functionally characterized to test the correct production and to check for reasons that could explain differences in PK. Part 4 deals with the analysis of the FcRn-mAb interaction to elucidate if PK differences are due to different FcRn interactions. The influence of different FcRn-mAb interactions on *in vivo* PK is investigated in part 5. Finally, the transferability of the previous results to another independent mAb model system is tested and is described in part 6.

3.1. Production

The antibodies used in this work were Briakinumab (ABT 874, J 695, Ozespa®, SEQ ID NO 36, PN WO2001014162-A2), Ustekinumab (CNTO 1275, Stelara®, CAS Registry Number 815610-63-0) as well as ten variants of Briakinumab and Ustekinumab, hereafter referred to as mAb 1 to mAb 10, respectively. In total, twelve IgGs were investigated.

All antibodies were kindly provided by the department of LMR Discovery (Roche Diagnostics GmbH, Mannheim, Germany, Site Penzberg). Briefly, synthetic genes were produced for Briakinumab, Ustekinumab, mAb 5 and mAb 6 at Geneart (Life technologies GmbH, USA). Site-directed mutagenesis was used to mutate specific amino acids to produce mAb 1, mAb 2, mAb 7, mAb 8, mAb 9 and mAb 10. MAb 3 was transfected with plasmids encoding Ustekinumab heavy chains and Briakinumab light chains and mAb 4 vice versa. All monoclonal antibodies used in the experiments were transiently expressed in HEK293 cells and purified using protein A chromatography and size exclusion chromatography (SEC) at the

department of Biochemical & Analyticals Research (Roche Diagnostics GmbH, Mannheim, Germany, Site Penzberg). Antibodies were formulated in buffer containing 20 mM histidine, 140 mM sodium chloride (NaCl), pH 6.0, and stored frozen at -80°C until analysis.

3.2. Biochemical characterization

The biochemical characterization of the mAbs included the analysis of protein concentration, size and molecular weight. Furthermore, hydrophobicity and charge distribution were analyzed and compared.

3.2.1. Determination of mAb concentration

Protein concentration was determined by photometric measurement of the absorbance at 280 nm and 320 nm after buffer blank subtraction. The absorbance at 320 nm was subtracted from the absorbance at 280 nm to correct light scattering and turbidity and this value was used to calculate the protein concentration according to the law of Lambert-Beer. The concentration was determined as average of three measurements. The absorbance spectrum is shown exemplarily for one antibody in Figure 3-1.

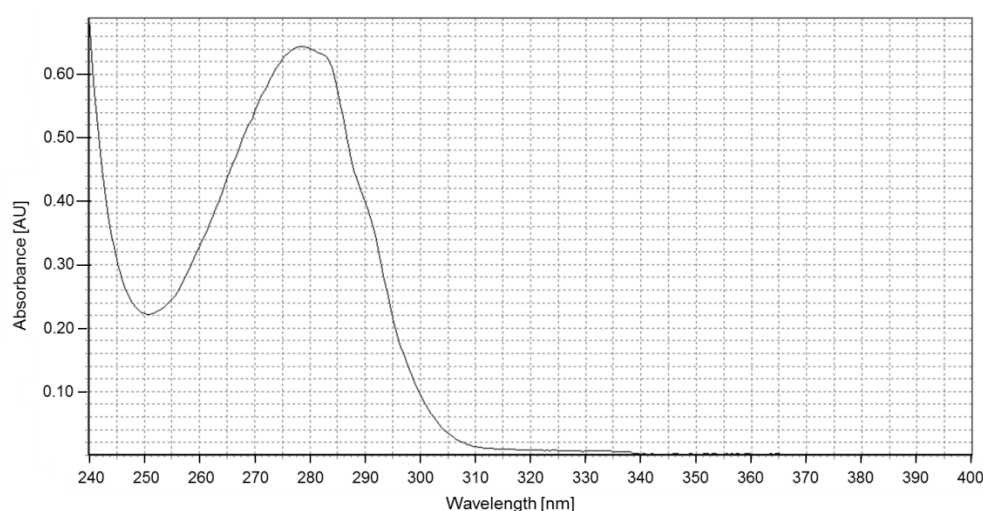


Figure 3-1: Photometric absorbance

Absorbance spectrum of an IgG1 antibody.

3.2.2. Determination of mAb molecular weight

The Agilent 2100 Bioanalyzer was used for analysis of the antibody molecular weight. In principle, the analysis is based on capillary electrophoresis on a chip system (CE-SDS), which provides sizing and quantitation information of the proteins. Samples were reduced into HCs and LCs using dithiothreitol (DTT).

Afterwards reduced and non-reduced samples were incubated with sodium dodecyl sulfate (SDS)-containing sample buffer at 90°C (Thermomixer comfort®, Eppendorf, Germany) for 5 min, centrifuged and loaded on the chip. Fluorescence dye molecules intercalated with protein-SDS micelles and the complexes were detected by laser-induced fluorescence. Data was translated into gel-like images (bands, Figure 3-2) and electropherograms (peaks). The size of each fragment in the sample was calculated with the use of a ladder containing proteins of known sizes. Integration of the electropherograms showed the percentage of fractions having the same molecular weight referred to total area of all fractions.

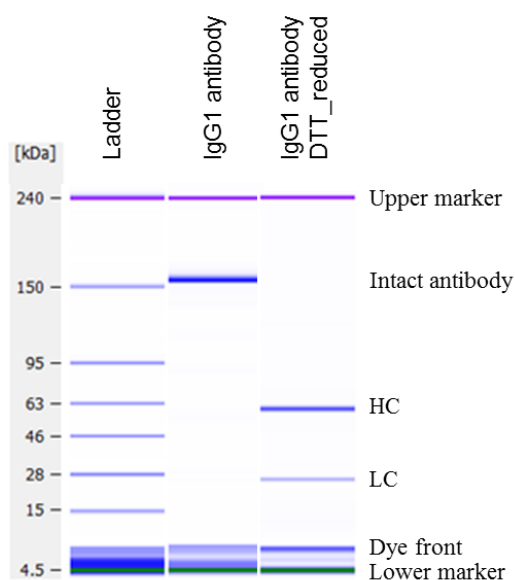


Figure 3-2: Purity and molecular weight

Gel-like images of an intact IgG1 antibody and of HCs and LCs after DTT-reduction.

3.2.3. Determination of mAb size

SEC analysis was used for determination of the antibody size or more accurately of the apparent hydrodynamic radius. SEC was conducted using a Waters Biosuite™ 250 column on a Summit HPLC-system. The elution peaks were monitored by UV absorption at 280 nm. Isocratic chromatography was conducted at room temperature (RT) using an aqueous buffer composed of 200 mM potassium dihydrogen phosphate and 250 mM potassium chloride at pH 7.0 and a flow-rate of 0.5 mL/min. Each sample contained 25 µg mAb per injection. The chromatograms were integrated

using the Chromeleon software. This is shown exemplarily in Figure 3-3. The fraction of higher molecular weight species (HMWs) includes dimers and larger soluble oligomers. It was determined as relative area of the respective peaks referred to the total area of all peaks including HMW peaks, the monomer peak and the peaks of the lower molecular weight species (LMWs).

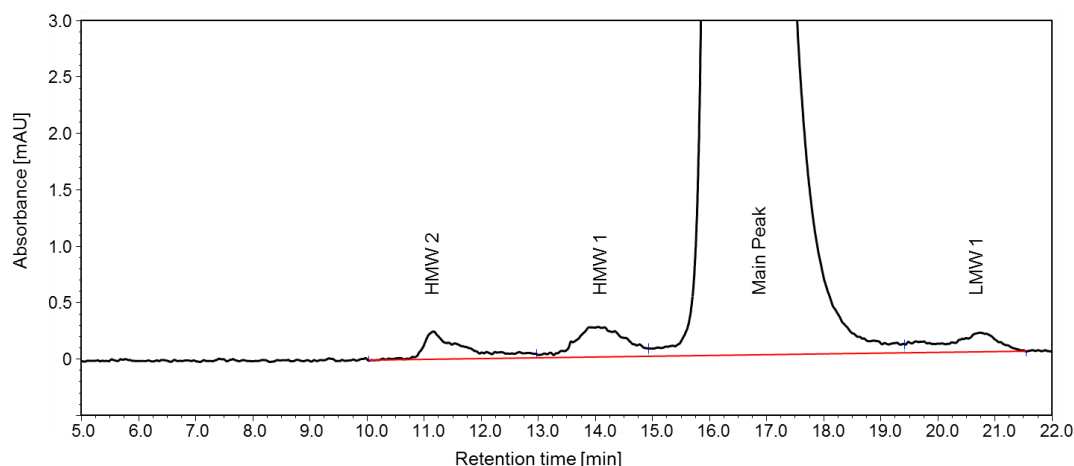


Figure 3-3: SEC chromatogram with included integration borders

HMWs including oligomers and dimers elute first, followed by monomer and LMWs.

3.2.4. Determination of mAb hydrophobicity

The apparent hydrophobicity of the antibodies was measured using hydrophobic interaction chromatography (HIC). HIC analysis was conducted using a TSKgel-5PW column on a Summit HPLC-system. The elution peaks were monitored by UV absorption at 280 nm. Decreasing salt-gradient chromatography was conducted at RT starting with aqueous buffer composed of 1.5 M ammonium sulfate, 25 mM sodium phosphate, pH 7.0, to 0 mM ammonium sulfate, 25 mM sodium phosphate, pH 7.0, and a flow-rate of 0.8 mL/min. Each sample contained 30 µg mAb per injection. The chromatograms were integrated using the Chromeleon software. Low and high hydrophobic reference samples (RS) were used to classify the antibodies according to their hydrophobic profile.

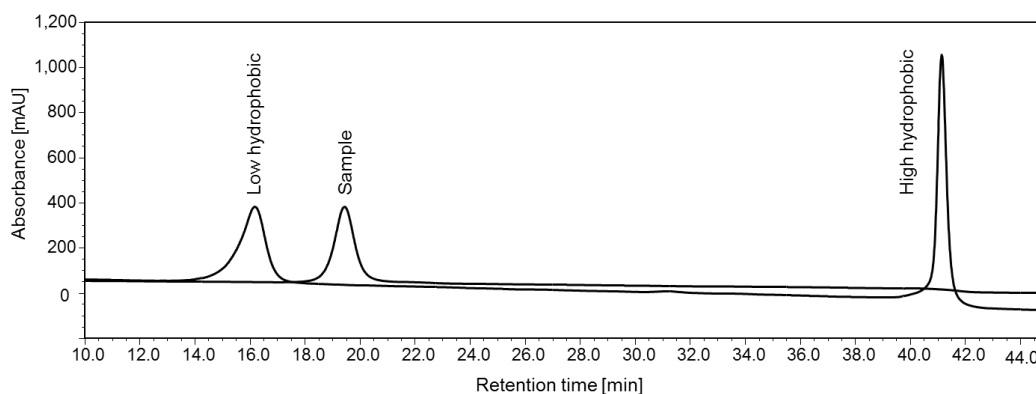


Figure 3-4: HIC chromatogram with reference samples

Low hydrophobic samples elute earlier than higher hydrophobic ones. The hydrophobicity of the sample is classified with the help of low and high hydrophobic reference samples.

3.2.5. Analysis of stressed mAbs

Stress-tests were used to analyze the protein stability and the tendency for aggregation of Briakinumab and Ustekinumab.

First, samples were tested for their response to freeze-thaw stress. Six freeze-thaw cycles were performed using 1 mL of the samples formulated in 20 mM histidine, 140 mM NaCl, pH 6.0. One cycle consisted of storage at -80°C and RT for 2 h until the samples were completely frozen and thawed, respectively. Afterwards the samples were analyzed for protein concentration and MW distribution according to the methods described above.

Second, the storage stability and the response to accelerated temperature stress was tested. Samples were diluted in 20 mM histidine, 140 mM NaCl, pH 6.0, and in PBS, pH 7.4, to a concentration of 1 mg/mL. Afterwards samples were stored at -80°C and 37°C , respectively, for 7 days. Then the samples were analyzed for protein concentration and MW distribution according to the methods described above.

3.2.6. Determination of mAb isoelectric point

The isoelectric point (pI) of the antibodies was determined using capillary isoelectric focusing (cIEF) with an iCE280 system connected to an autosampler. The separation cartridge in the iCE280 unit contained a fluorocarbon-coated fused-silica capillary with an internal diameter of 100 μm and a separation length of 5 cm. As anolyte and

catholyte, 80 mM phosphoric acid containing 0.1% w/w methyl cellulose and 100 mM sodium hydroxide containing 0.1% w/w methyl cellulose were used, respectively. Methyl cellulose was used to increase the viscosity of the matrix and thus the resolution. Samples were rebuffered in 10 mM histidine buffer and 40 μ L of the samples ($c = 1.2$ mg/mL) were added to 160 μ L of a mixture containing 3% v/v carrier Pharmalyte 3-10, 0.2% v/v pI markers 7.05 and 9.77, 0.35% w/w methyl cellulose and 30 % w/w urea. The pI markers were used to calibrate the pH gradient formed by the pharmalyte in the capillary. IEF was carried out for 30 sec at 500 volt followed by 6 min at 3000 volt. The chromatograms were integrated using the Chromeleon software. This is shown exemplarily in Figure 3-5.

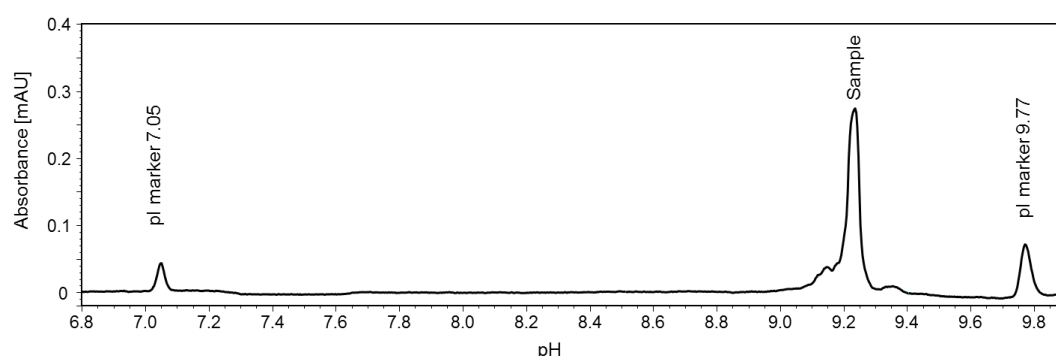


Figure 3-5: iCE chromatogram with pI markers

Upper and lower pI markers were used to calibrate the pH gradient.

The theoretical isoelectric points were also calculated by the protein sequence using GPMW (Version 9.10) and standard settings (Skoog and Wichman 1986). As plausibility check, calculated and measured pIs were compared.

In addition to the isoelectric points, the pH dependent net charge of the V_H , V_L and Fv domain of Briakinumab and Ustekinumab at pH 6.0 and pH 7.4 were calculated with the open-source program EMBOSS iep assuming all cysteines are involved in disulfide bridges.

3.2.7. Charge distribution analysis

The 3D-charge distribution in the Fv domain was calculated for all mAbs. Furthermore FcRn was studied for the presence of positively or negatively charged

regions. Generation of homology models and calculation of isopotential surfaces were kindly performed by Dr. Hubert Kettenberger (Biochemical & Analyticals Research, Roche Diagnostics GmbH, Mannheim, Germany, Site Penzberg).

Briefly, a homology model for the Briakinumab Fab fragment was generated using modeller 9v7 and PDB structure 1AQK (Faber et al. 1998) as a template. The isopotential surfaces for Briakinumab and Ustekinumab Fab fragments were calculated from this model (Briakinumab) or the crystal structure of Ustekinumab (PDB ID 3HMX), respectively. Structures were protonated using the “prepare protein” protocol with CHARMM force field in DiscoveryStudio Pro, Version 3.5 (Accelrys Inc., USA) at pH 7.4 and an ionic strength of 145 mM.

For the variants of Briakinumab and Ustekinumab, homology models of the Fab fragments were generated. For the Briakinumab variants, mAb 1, mAb 4, mAb 5 and mAb 7-10, the Fab fragment homology model was generated using the Briakinumab model described above. The Fab fragment homology model for the Ustekinumab variants, mAb 2, mAb 3 and mAb 6, was generated using the crystal structure of Ustekinumab (PDB ID 3HMX). The isopotential surfaces of the Fab fragments were calculated based on these models as described above.

The isopotential surface of FcRn was calculated using the published crystal structure of human FcRn (PDB 4N0U (Oganesyan et al. 2014)) as described above.

3.2.8. IdeS cleavage

Briakinumab and Ustekinumab were cleaved using the FabRICATOR® Kit (Genovis, Sweden). The enzyme FabRICATOR® consists of recombinant immunoglobulin-degrading enzyme from *Streptococcus pyogenes* (IdeS). IdeS is a proteolytic enzyme that cleaves IgG only at one specific site in the lower hinge region, resulting in F(ab')₂ fragment and Fc monomers (Figure 3-6) (Johansson et al. 2008). Antibodies were diluted in cleavage buffer consisting of 50 mM Na₃PO₄, 150 mM NaCl, pH 6.6, to a concentration of 1 mg/mL. To each µg antibody 1 unit FabRICATOR® was added and the solution was incubated for 30 min at 37°C. Afterwards the cleaved antibodies were tested using CE-SDS and analytical SEC.

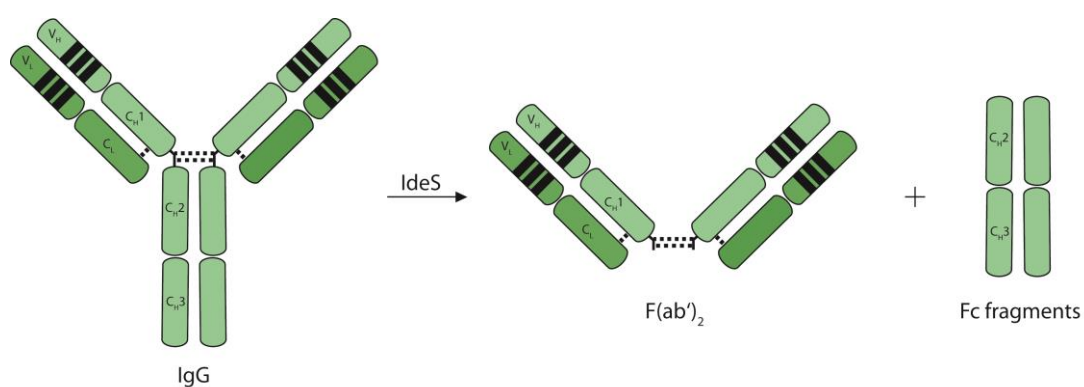


Figure 3-6: Antibody cleavage using IdeS

Antibody cleavage site is in the lower hinge region generating F(ab')₂ fragment and Fc monomers.

3.2.9. Complex of mAb and IL-12

Briakinumab and Ustekinumab were bound to their target IL-12 by mixing 0.3 nmol mAb with 0.2 nmol IL-12. In addition, a Briakinumab-IL-12 complex was assembled using an IL-12 excess by mixing 0.3 nmol mAb with 0.8 nmol IL-12. The mAb-IL12 complexes were incubated for 30 min at RT. Afterwards the mAb-IL-12 complex was analyzed for FcRn interaction (3.4.2.2).

3.3. Functional characterization

The functional characterization consisted of analysis of the interaction with human IL-12 and IL-12/-23 of different species. Furthermore the interaction with an mouse Fc γ receptor (muFc γ R) was analyzed by comparison of binding levels to the mouse Fc γ receptor I (muFc γ RI), which is the Fc γ R having the highest affinity to IgG1 (Nimmerjahn and Ravetch 2008).

3.3.1. Interaction with human IL-12

The interaction with human IL-12 was analyzed using a target-specific enzyme-linked immunosorbent assay (ELISA) and surface plasmon resonance (SPR).

3.3.1.1. ELISA

For the specific ELISA, biotinylated human IL-12 was used as capture reagent.

Recombinant human IL-12 (Cell sciences, USA) was reconstituted and biotinylated using the Bulk BirA biotinylation kit according to the manufacturer's instructions (Bulk BirA, Avidity Biotechnologies, USA). Biotin-protein ligase, birA enzyme, activates biotin to form biotinyl 5' adenylate and transfers the biotin to biotin-accepting proteins. To couple IL-12 with biotin, 1 mg IL-12 were mixed with 83 μ L of the following mixture: 2.5 mL PBS and 1 tablet complete protease inhibitor (cOmplete ULTRA tablets, Roche Diagnostics GmbH, Mannheim, Germany), 750 μ L Biomix A, 750 μ L Biomix B and 5 μ L BirA. The mixture was incubated overnight at RT. The biotinylated IL-12 was dialyzed against 50 mM potassium phosphate buffer, pH 7.4. After filtration using a 0.22 μ m filter, the concentration was measured by UV/Vis spectroscopy (NanoPhotometer, Implen Inc., USA). The biotinylated human IL-12 was stored frozen at -80°C until use.

For quantitative determination of the antibodies bound to human IL-12, a specific ELISA was used. The ELISA design is shown in Figure 3-7.

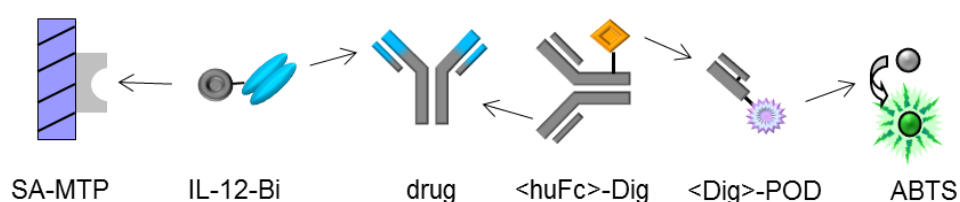


Figure 3-7: Principle of the specific ELISA

Streptavidin-coated MTPs were coated with biotinylated capture reagent (IL-12-Bi). Afterwards antibodies were added at various dilutions. Bound mAbs were detected by subsequent incubation with digoxigenin-labeled detection antibody (<huFc>-Dig), followed by incubation with anti-digoxigenin Fab fragments conjugated to horseradish peroxidase (<Dig>-POD). ABTS was used as HRP substrate to form a colored reaction product. Absorbance of the resulting reaction product was read at 405 nm with a reference wavelength at 490 nm.

Preparation: All reagents and buffers were raised to RT before usage. Dilutions were made in assay buffer (Universal buffer for ELISA). Incubation steps were performed under agitation at 500 rpm at RT and were followed by 3 washing steps using 300 μ L wash buffer (PBS, 0.05% Tween20) per well.

Capture reagent: A streptavidin-coated microtiter plate (MTP) was coated with 100 μ L/well biotinylated IL-12-solution (IL-12-Bi, concentration 100 ng/mL) and incubated for 60 min.

Samples: Antibody stock solutions were serially 1:2 diluted starting at 12 ng/mL. The resulting concentrations were 12, 6, 3, 1.5, 0.75, 0.38, 0.19 and 0 ng/mL. 100 μ L of each antibody dilution as well as positive and negative control samples were added to each well and incubated for 60 min. All samples were analyzed in duplicates.

First detection reagent: A volume of 100 μ L of digoxigenin-labeled antibody (50 ng/mL <huFc>-Dig) which binds to the Fc region of human IgGs was added to each well and incubated for 60 min.

Second detection reagent: 100 μ L of anti-digoxigenin Fab fragments conjugated to horseradish peroxidase (15 mU/mL <Dig>-POD) were added to each well and incubated for 60 min.

Substrate reaction: A volume of 100 μ L substrate solution 2,2'-azino-bis(3-

ethylbenzothiazoline-6-sulphonic acid) (ABTS) was added to the MTP per well and the extinction was measured at 405 nm with a reference wavelength of 490 nm. At an optical density (OD) of 2.0 the measurement was stopped.

Calculation: Using a 4-parameter fit (Wiener-Rodbard equation $= A + \frac{B}{(1+C \times x^D)}$) of the “XLfit4” software, the absorbance-concentration curves were calculated and compared to each other. Furthermore the concentration of each mAb was calculated using the fit of the Briakinumab calibration curve to obtain IL-12 binding relative to Briakinumab (Briakinumab = 100%).

Acceptance criteria: The standard calibration curve must consist of at least 5 values. The absorbance of the lowest calibration standard should be below 0.1 OD. For sample analysis at least two dilutions of the sample should be within the linear range of the standard calibration curve.

Accuracy: The accuracy of the ELISA was determined to be $\pm 20\%$ according to Roche internal guidelines.

3.3.1.2. SPR

Affinity of the mAbs to recombinant human IL-12 was analyzed by SPR with a BiaCore T100 instrument. The assay was performed using PBS including 0.05% Tween20, pH 7.4, as running and dilution buffer. An <huFcPan>-capture antibody recognizing the mAb's Fc region in 10 mM sodium acetate buffer, pH 4.5, was immobilized onto a CM5 chip to a level of 12,400 response units (RU). This capture antibody bound the mAbs at their Fc region to a level of about 50 RU using a flow rate of 10 μ L/min for 30 sec. Afterwards different dilutions of human IL-12 were prepared: 0.25, 0.75, 2.2, 6.7, 20, 60, 180 nM and each sample was injected at a flow rate of 30 μ L/min. Association and dissociation times of 120 and 600 sec were used, respectively. The chip was regenerated by injection of 100 mM phosphoric acid for 60 sec, followed by injection of 5 mM sodium hydroxide solution at a flow rate of 10 μ L/min. The equilibrium dissociation constant (K_D) was calculated using steady state affinity calculation at the BiaCore T100 evaluation software.

3.3.2. Interaction with IL-12 and IL-23 of different species

The interaction of the mAbs used in the *in vivo* study (Briakinumab, Ustekinumab, mAb 8 and mAb 9) with recombinant human IL-12, human IL-23, mouse IL-12 and mouse IL-23 was analyzed using a BiaCore T100 instrument. The assay was performed using PBS including 0.05% Tween20, pH 7.4 as running and dilution buffer. An <huFcPan>-capture antibody in 10 mM sodium acetate buffer, pH 4.5, was immobilized onto a CM5 chip to a level of 12,400 RU. This capture antibody bound the mAbs at their Fc region to a level of about 50 RU using a flow rate of 10 μ L/min for 30 sec. Afterwards 130 nM of human IL-12, human IL-23, mouse IL-12 and mouse IL-23 were injected at a flow rate of 30 μ L/min. Association and dissociation times of 120 and 600 sec were used, respectively. The chip was regenerated by injection of 100 mM phosphoric acid for 60 sec, followed by injection of 5 mM sodium hydroxide solution at a flow rate of 10 μ L/min. The binding levels of each antibody to each Interleukin were determined using BiaCore T100 evaluation software and compared to each other.

3.3.3. Interaction with mouse Fc γ RI

Binding levels of the mAbs used in the *in vivo* study (Briakinumab, Ustekinumab, mAb 8 and mAb 9) to the mouse Fc γ receptor I (muFc γ RI) were analyzed using a BiaCore T100 instrument. The assay was performed using HBS P+, pH 7.4 as running and dilution buffer. An <His>-capture antibody in 10 mM sodium acetate buffer, pH 4.5, was immobilized onto a CM5 chip to a level of 12,500 RU (His Capture Kit, GE Healthcare, United Kingdom). This capture antibody bound muFc γ RI to a level of about 410 RU using a flow rate of 30 μ L/min for 60 sec. Afterwards 25 nM of the mAbs were injected at a flow rate of 30 μ L/min. Association and dissociation times of 60 and 180 sec were used, respectively. The chip was regenerated by injection of 10 mM glycine-HCl, pH 1.5, at a flow rate of 30 μ L/min for 60 sec. The binding levels of each antibody to muFc γ RI were determined using BiaCore T100 evaluation software and compared to each other.

3.4. FcRn-mAb interaction

The FcRn-mAb interaction consists of two phases that are important to be analyzed: FcRn-mAb binding at pH 6.0 and FcRn-mAb dissociation at higher pHs. Therefore, the FcRn-mAb interaction was first studied by analyzing the FcRn-IgG affinity at pH 6.0 and afterwards by analyzing the FcRn-mAb dissociation at elevated pHs.

3.4.1. FcRn-mAb affinity at pH 6.0

The steady state binding levels and the K_{DS} for huFcRn and the mAbs were determined at pH 6.0 using a BiaCore T100 instrument. Human FcRn in 10 mM sodium acetate buffer, pH 4.5, was immobilized on a BiaCore CM5-biosensor chip via amine-coupling to a level of 50 RU. The assay was performed using PBS containing 0.05% Tween20 adjusted to pH 6.0 as running and dilution buffer. Different dilutions of the mAbs were prepared: 23, 47, 94, 188, 375, 750, 1500 nM and each sample was injected at a flow rate of 5 μ L/min. Association and dissociation times of 600 and 360 sec were used, respectively. The chip was regenerated by injection of PBS containing 0.05% Tween20 at pH 7.5. The K_D was calculated as steady state affinity using BiaCore T100 evaluation software and normalized to the K_D of Ustekinumab. The measurements were performed in triplicate and the mean and standard deviation was determined.

3.4.2. FcRn-mAb dissociation

The dissociation of FcRn and the mAbs was analyzed using SPR and FcRn affinity chromatography.

3.4.2.1. FcRn-mAb dissociation using SPR

The steady state binding levels and the K_{DS} for huFcRn and the mAbs were determined at different pH-values to evaluate the pH dependency of the FcRn affinity. The experimental setup is the same as in 3.4.1, except that the running buffers used were PBS containing 0.05% Tween20 adjusted to pH 6.4, pH 6.6, pH 6.8, pH 7.0 and pH 7.2, respectively.

3.4.2.2. FcRn-mAb dissociation using FcRn affinity chromatography

FcRn was biotinylated using the Bulk BirA biotinylation kit according to the manufacturer's instructions (Bulk BirA, Avidity Biotechnologies, USA). To couple FcRn with biotin, 3 mg FcRn were mixed with 250 μ L of the following mixture: 2.5 mL PBS and 1 tablet complete protease inhibitor (cOmplete ULTRA tablets, Roche Diagnostics GmbH, Mannheim, Germany), 750 μ L Biomix A, 750 μ L Biomix B and 5 μ L BirA. The mixture was incubated overnight at RT. The biotinylated FcRn was dialyzed against 20 mM sodium dihydrogen phosphate buffer comprising 150 mM NaCl, pH 7.5 at 4°C overnight to remove uncoupled biotin. For coupling to streptavidin sepharose, 1 g streptavidin-sepharose was added to the biotinylated and dialysed FcRn and incubated at 4°C overnight. The FcRn-derivatized sepharose was packed in a 1 mL XK column and the FcRn column was then equilibrated with 20 mM 2-(N-morpholine)-ethanesulfonic acid (MES) sodium salt buffer containing 140 mM NaCl, pH 5.5.

3.4.2.3. FcRn affinity chromatography using a pH gradient

The pH gradient FcRn affinity chromatography was conducted using the prepared FcRn-column on a Summit HPLC-system. The elution peaks were monitored at 280 nm. Each sample contained 30 μ g mAb per injection and was prepared in 20 mM MES sodium salt, 140 mM NaCl, pH 5.5. Antibodies were eluted by a linear pH gradient ranging from pH 5.5 to 8.8 within 120 min using 20 mM MES sodium salt, 140 mM NaCl, pH 5.5, and 20 mM TRIS, 140 mM NaCl, pH 8.8, as eluents and a flow rate of 0.5 mL/min. FcRn column chromatography shows binding at acidic pH (pH 5.5– 6.0) and release at higher pH values. For complete elution of the antibodies, the pH was increased in the gradient up to pH 8.8. The chromatograms were integrated using the Chromeleon software. The experiments were performed at RT. The elution profile was obtained by continuous measurement of the absorbance at 280 nm. The time taken for an analyte peak to reach the detector after sample injection was called the retention time. The FcRn affinity chromatograms of all mAbs were intensity-normalized for clarity. To determine the elution pH at particular retention times, samples were collected every 5 min and the pH was measured

offline. The nearly linear range was fitted using a 4-parameter fit (fit $y = A \times x^3 + B \times x^2 + C \times x + D$) of the “XLfit4” software. (Figure 3-8). The retention times were measured and the elution pHs were calculated on the basis of the 4-parameter fit.

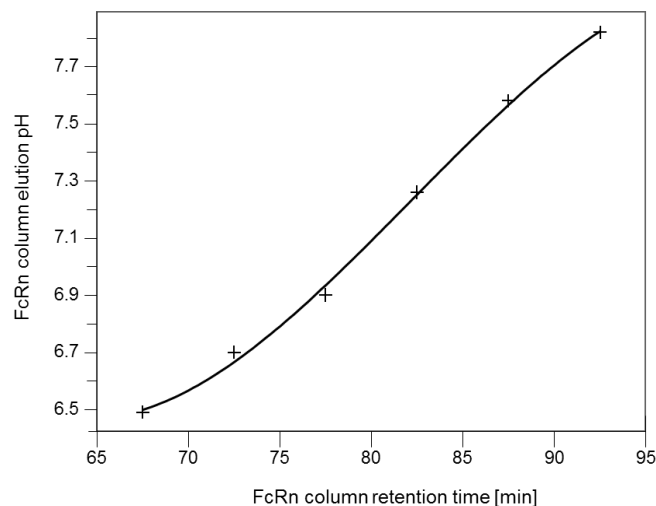


Figure 3-8: FcRn column elution pH plotted against the retention time

Samples were collected every 5 min and the pH was measured offline. Data was fitted using a 4-parameter fit (fit $y = A \times x^3 + B \times x^2 + C \times x + D$).

3.4.2.4. FcRn affinity chromatography under high ionic strength conditions

Higher ionic strength conditions were used to analyze charge-mediated effects on FcRn-mAb interaction. Therefore, the FcRn affinity chromatography was conducted as described above, but using buffers supplemented with different NaCl concentrations. Buffers were used containing 20 mM MES sodium salt, pH 5.5, and 20 mM TRIS, pH 8.8, each comprising 140 mM, 170 mM, 200 mM, 250 mM, 300 mM or 400 mM NaCl.

3.4.2.5. FcRn affinity chromatography using a salt gradient

The salt gradient FcRn affinity chromatography analyzes charge-mediated FcRn-IgG interactions at constant pH. The salt gradient FcRn affinity chromatography was conducted using the prepared FcRn-column on a Summit HPLC-system. The samples were prepared in 10 mM MES sodium salt, pH 7.8. Each sample contained 30 µg mAb per injection. Antibodies were eluted by a linear salt gradient from 0 mM to 250 mM NaCl within 60 min using 10 mM MES sodium salt, pH 7.8, and 10 mM

MES sodium salt, 250 mM NaCl, pH 7.8, as eluents and a flow rate of 0.5 mL/min. The chromatograms were integrated using the Chromeleon software. The elution profile was obtained by continuous measurement of the absorbance at 280 nm.

3.5. *In vivo* PK study

To analyze if different FcRn-mAb interactions have an influence on PK, *in vivo* studies in human FcRn transgenic and FcRn knockout mice were performed. The PK studies were conducted in human FcRn transgenic mice with Briakinumab, Ustekinumab, mAb 8 and mAb 9 and in FcRn knockout mice with Briakinumab, Ustekinumab and mAb 9. All animal experiments were kindly performed by the department of LMR Discovery (Roche Diagnostics GmbH, Mannheim, Germany, Site Penzberg). The studies were approved by the Government of Upper Bavaria, Germany (permit number 55.2-1-54-2532.2-28-10) and performed in an AAALAC accredited animal facility according to the European Union Normative for Care and Use of Experimental Animals. Mouse husbandry was carried out under specific pathogen free conditions and the animals were housed in standard cages having free access to food and water during the whole study period.

3.5.1. Mice

B6.Cg-Fcgrt<tm1Dcr>Tg(FCGRT)276Dcr mice deficient in mouse FcRn α -chain gene, but hemizygous transgenic for a human FcRn α -chain gene (muFcRn-/-huFcRn tg +/-, line 276) were used for the PK studies. Mice were obtained from the Jackson Laboratory (Bar Harbor, ME, USA) (female, age 4-10 weeks, weight 17-22 g at time of dosing).

B6.129X1-Fcgrt<tm1Dcr>/DcrJ mice are homozygous FcRn α -chain knockout mice (muFcRn -/-). These mice cannot express mouse FcRn. A detailed description of the mouse strain is provided by Roopenian et al. (2003) and Roopenian et al. (2010). Mice were obtained from the Jackson Laboratory (Bar Harbor, ME, USA) (female, age 4-10 weeks, weight 15-21 g at time of dosing).

3.5.2. Study design

Treatment: A single dose of antibody was injected i.v. via the lateral tail vein at a dose level of 10 mg/kg and a dose volume of 10 mL/kg.

Blood sampling: Blood was collected via the retro bulbar venous plexus from each

animal for the determination of the compound levels. Each mouse was subjected twice to retro-orbital bleeding, performed under light anesthesia with Isoflurane™; a third blood sample was collected at the time of euthanasia. Blood was collected into serum tubes using hematocrit capillaries. After 2 h incubation at RT, samples were centrifuged for 3 min at 9,300 g at 4°C to obtain serum. After centrifugation, serum samples were stored frozen at -80°C until analysis. Blood sampling was performed according to a schedule to ensure that the weekly collected blood volume did not exceed 7.5% of the mice blood volume (Diehl et al. 2001). Furthermore blood can only be collected via the retro bulbar venous plexus triply per mouse, once from the right eye, once from the left eye and a third time at the time of euthanasia (Hack et al. 2013). Because of these animal welfare guidelines it was not possible to collect blood from each mouse at each of the 9 time points to achieve single-animal kinetics. Therefore the mice were divided into 3 groups of 6 mice each to cover 9 serum collection time points in total (Table 3-1 and Table 3-2)

Table 3-1: Blood sampling schedule- human FcRn transgenic mice

Mice were divided in 3 groups with 6 mice each to cover 9 blood sampling time points indicated as (X) over a study period of 4 weeks.

Time after treatment (h) / (d)	Group 1						Group 2						Group 3					
	M 1	M 2	M 3	M 4	M 5	M 6	M 1	M 2	M 3	M 4	M 5	M 6	M 1	M 2	M 3	M 4	M 5	M 6
0.08 / 0	X	X	X	X	X	X												
2 / 0							X	X	X	X	X	X						
8 / 0													X	X	X	X	X	X
24 / 1	X	X	X	X	X	X												
48 / 2							X	X	X	X	X	X						
168 / 7													X	X	X	X	X	X
336 / 14	X	X	X	X	X	X												
504 / 21							X	X	X	X	X	X						
672 / 28													X	X	X	X	X	X

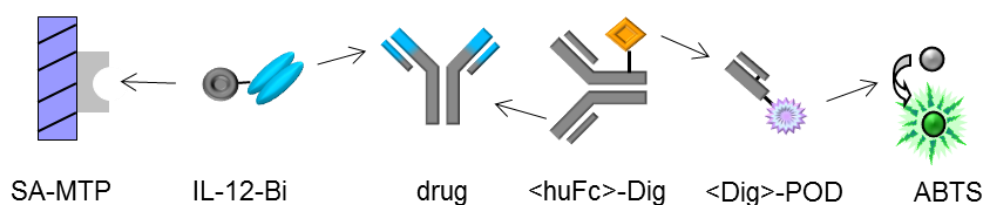
Table 3-2: Blood sampling schedule- FcRn knockout mice

Mice were divided in 3 groups with 6 mice each to cover 9 blood sampling time points indicated as (X) over a study period of 2 weeks.

Time after treatment (h) / (d)	Group 1						Group 2						Group 3					
	M 1	M 2	M 3	M 4	M 5	M 6	M 1	M 2	M 3	M 4	M 5	M 6	M 1	M 2	M 3	M 4	M 5	M 6
0.08 / 0	X	X	X	X	X	X												
2 / 0							X	X	X	X	X	X						
8 / 0													X	X	X	X	X	X
24 / 1	X	X	X	X	X	X												
48 / 2							X	X	X	X	X	X						
168 / 7													X	X	X	X	X	X
192 / 8	X	X	X	X	X	X												
216 / 9							X	X	X	X	X	X						
336 / 14													X	X	X	X	X	X

3.5.3. Determination of human antibody serum concentrations

Concentrations of Ustekinumab, Briakinumab, mAb 8 and mAb 9 in murine serum were determined by a specific ELISA.

**Figure 3-9: ELISA-Design for mAb detection in human serum samples**

Streptavidin-coated MTPs were coated with biotinylated capture reagent (IL-12-Bi). Afterwards serum samples and calibration standard were added at various dilutions. Bound human antibodies were detected by subsequent incubation with digoxigenin-labeled detection antibody (<huFc>-Dig), followed by an incubation with anti-digoxigenin Fab fragments conjugated to horseradish peroxidase (<Dig>-POD). ABTS was used as HRP substrate to form a colored reaction product. Absorbance of the resulting reaction product was read at 405 nm with a reference wavelength at 490 nm and the serum concentrations were calibrated against reference standard using a 4-parameter fit.

Preparation: All serum samples, positive and negative control samples were analyzed in duplicates. 5 samples per MTP were analyzed. All dilutions were made

in assay buffer (Universal buffer for ELISA). Reagents and buffers were raised to RT before usage. Incubation steps were performed under agitation at 500 rpm at RT and were followed by 3 washing steps using 300 μ L wash buffer (PBS, 0.05% Tween20) per well.

Capture reagent: A streptavidin-coated MTP was coated with 100 μ L biotinylated IL-12-solution (IL-12-Bi, concentration 100 ng/mL) per well and incubated for 60 min.

Sample-Preparation: The calibration standard stock solution (Briakinumab, Ustekinumab, mAb 8 or mAb 9, depending on the study) was serially 1:2 diluted starting at 12 ng/mL. The resulting calibrator concentrations were 12, 6, 3, 1.5, 0.75, 0.38, 0.19 and 0 ng/mL. Serum samples of the first five sampling time points (0.08 h till 48 h) were diluted 1:5000 and the later time points (168 h till 672 h) were diluted 1:500 and afterwards serially 1:2 diluted.

Sample-application: 100 μ L of each calibration standard dilution was added to column 1 and 2 on the coated MTP (Table 3-3). 100 μ L of the sample dilutions as well as of positive and negative control samples were added to each well and incubated for 60 min.

Table 3-3: MTP allocation

5 samples per MTP were analyzed.

	1	2	3	4	5	6	7	8	9	10	11	12
	calibration standard		Sample 1		Sample 2		Sample 3		Sample 4		Sample 5	
A	12 ng/mL											
B	6 ng/mL											
C	3 ng/mL											
D	1.5 ng/mL											
E	0.8 ng/mL											
F	0.4 ng/mL											
G	0.2 ng/mL											
H	0 ng/mL											

First detection reagent: A volume of 100 µL of digoxigenin-labeled antibody (50 ng/mL <huFc>-Dig) that binds to the Fc region of human IgGs was added to each well and incubated for 60 min.

Second detection reagent: 100 µL of anti-digoxigenin Fab fragments conjugated to horseradish peroxidase (15mU/mL <Dig>-POD) were added per well and incubated for 60 min.

Substrate reaction: A volume of 100 µL substrate solution ABTS was added to the MTP to each well and the extinction was measured at 405 nm with a reference wavelength of 490 nm. Measurement was stopped when the highest calibration standard concentration reached an OD of 2.0.

Calculation: The standard calibration curve was calculated using a 4-parameter fit (Wiener-Rodbard equation $= A + \frac{B}{(1+C \times x^D)}$) of the “XLfit4” software. Sample concentrations were calculated from the calibration curve.

Acceptance criteria: The standard calibration curve must consist of at least 5 values. The absorbance of the lowest calibration standard should be below 0.1 OD. For sample analysis at least two dilutions of the sample should be within the linear range of the standard calibration curve.

Accuracy: The accuracy of the ELISA was determined to be $\pm 20\%$ according to Roche internal guidelines.

3.5.4. Pharmacokinetic analysis

Blood level curves: Mean serum concentrations and standard deviations were calculated for each sampling time point.

Calculation of PK parameters: The pharmacokinetic parameters were calculated using WinNonlin™ version 5.3 (Pharsight, USA). Non-compartmental analysis with the following settings was used: NCA Model 201, i.v. bolus-input for plasma data. The same method has been used by Ling et al. (2009). Pharmacokinetic analysis of antibodies is mostly calculated by non-compartmental analysis because antibodies

remain nearly exclusively in the central compartment. Distribution volume (V_d), area under the curve (AUC), clearance (Cl) and terminal half-life ($T_{1/2}$) were calculated.

Briefly, $AUC_{0-\infty}$ values were calculated by logarithmic trapezoidal method due to non-linear decrease of the antibodies and extrapolated to infinity using the apparent terminal rate constant λ_z , with extrapolation from the observed concentration at the last time point.

Plasma clearance was calculated as dose rate (D) divided by $AUC_{0-\infty}$. The apparent terminal half-life ($T_{1/2}$) was derived from the equation $T_{1/2} = \ln 2 / \lambda_z$.

3.5.5. Statistical analysis

Outlier test: Outliers in serum concentration analysis were detected using the Nalimov outlier test and were excluded from further analysis.

Statistical significance test: The Tukey's honest significance test (Tukey's HSD test) was used as statistical test for analysis of statistically significant differences in the terminal half-life.

3.5.6. Detection of drug/ADA immune complexes

The study samples of the *in vivo* studies in human FcRn transgenic mice and in FcRn knockout mice were tested for the existence of anti-drug antibodies (ADAs). An immune complex assay in the ELISA format was used which was based on transformation of free ADAs to immune complexes by pre-incubation with excess of drug (Figure 3-10). The assay design was modified from Stubenrauch et al. (2012). Chemical conjugates of polyclonal human IgG and monoclonal murine IgG were prepared as described by Stubenrauch et al. (2010) and used as calibration standard and quality control samples (QCs) in the immune complex assay.

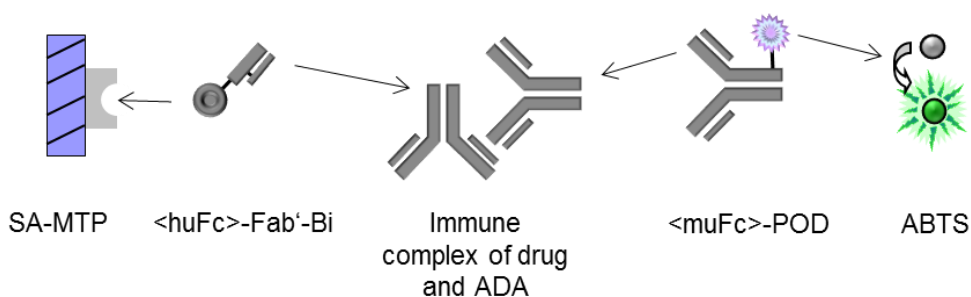


Figure 3-10: ELISA-Design for detection of drug/ADA immune complexes

Samples and QCs were preincubated in assay buffer and assay buffer containing the antibody. Streptavidin-coated MTPs were coated with biotinylated capture reagent (<huFc>-Fab'-Bi). Afterwards serum samples and calibration standard were added at various dilutions. Bound drug/ADA immune complexes were detected by subsequent incubation with POD-labeled detection antibody (<muFc>-POD). ABTS was used as HRP substrate to form a colored reaction product. Absorbance of the resulting reaction product was read at 405 nm with a reference wavelength at 490 nm and the serum concentrations were calibrated against calibration standard using a 3-parameter fit.

Preparation: All serum samples, calibration standards, positive and negative control samples were analyzed in duplicates. Per MTP, 16 samples were analyzed. Reagents and buffers were raised to RT before usage. All dilutions were made in assay buffer (Universal buffer for ELISA). Incubation steps of the streptavidin-coated MTP were performed under agitation at 500 rpm at RT and were followed by 3 washing steps using 300 μ L wash buffer (PBS, 0.05% Tween20) per well.

Preincubation: The samples, positive QC (calibration standard) and negative QC (mouse pool serum, MPS) were incubated with assay buffer and with assay buffer containing the antibody at 260 ng/mL for 1 h in a separate preincubation MTP (1:50 dilution to obtain 2% mouse serum content) under agitation at 500 rpm at RT.

Capture reagent: A streptavidin-coated MTP was coated with 100 μ L biotinylated <huFc>-Fab'-Bi-solution (concentration 1000 ng/mL) per well and incubated for 30 min.

Calibration standard preparation: The calibration standard stock solution (chemical conjugates of huIgG and muIgG) was diluted in a first step to 200 ng/mL and then serially 1:2 further diluted in assay buffer containing 2% MPS. Resulting calibrator concentrations in 2% MPS were 200, 100, 50, 25, 12.5, 6.25, 3.13 and 0 ng/mL.

Sample application: 100 μ L of each calibration standard dilution was added to column 1 and 2 on the coated MTP (Table 3-4). 100 μ L of each sample as well as of positive and negative control samples were added to each well and incubated for 60 min.

Table 3-4: MTP allocation for the drug/ADA immune complex assay

Per MTP, 16 samples were analyzed in buffer and in buffer containing drug.

	1	2	3	4	5	6	7	8	9	10	11	12
	In 2% MPS		In drug-buffer				In buffer					
	calibration standard		Sample		Sample		QC	Sample		Sample		QC
A	200 ng/mL		1		9		blank	1		9		blank
B	100 ng/mL		2		10			2		10		
C	50 ng/mL		3		11			3		11		
D	25 ng/mL		4		12			4		12		
E	12.5 ng/mL		5		13		Pos.	5		13		Pos.
F	6.25 ng/mL		6		14		contr.	6		14		contr.
G	3.13 ng/mL		7		15		Neg.	7		15		Neg.
H	0 ng/mL		8		16		contr.	8		16		contr.

Detection reagent: A volume of 100 μ L of POD-labeled antibody (0.4 μ g/mL <muFc>-POD) that binds to the Fc region of mouse IgGs was added to each well and incubated for 60 min.

Substrate reaction: 100 μ L substrate solution ABTS was added to the MTP per well and the extinction was measured at 405 nm with a reference wavelength of 490 nm. Measurement was stopped when the highest calibration standard concentration reached an OD of 2.0.

Calculation: The obtained data was used for generating the standard calibration curve and calculation of the drug/ADA immune complex concentrations of each sample. The standard calibration curve was calculated using a 3-parameter fit

(equation $y = A \times x^2 + B \times x + C$) of the “XLfit4” software and the sample concentrations were calibrated against the absorbance-concentration curves of the calibration standard.

Acceptance criteria: The standard calibration curve must consist of at least 5 values. The absorbance of the lowest reference standard concentration should be below 0.1 OD. Samples were classified moderate ADA-positive when the signal was threefold higher than the signal of the predose sample. Samples were classified severe ADA-positive when the signal was tenfold higher than the signal of the predose sample.

Accuracy: The accuracy of the ELISA was determined to be $\pm 20\%$.

3.6. Second model antibody system

The transferability of the previous results was being tested using a second antibody system. Bevacizumab was chosen as second model antibody because the charge distribution of Bevacizumab showed no striking positively or negatively charged regions.

Bevacizumab and a Bevacizumab-variant with additional positively charged regions in the V_L domain were produced. Both antibodies were kindly provided by the department of LMR Discovery (Roche Diagnostics GmbH, Mannheim, Germany, Site Penzberg). Briefly, synthetic genes were produced for Bevacizumab (Geneart, Life technologies, USA) and Bevacizumab-variant was produced by site-directed mutagenesis to mutate specific amino acids. The purification process was identical to the Briakinumab/Ustekinumab model system and was kindly performed by the department of Biochemical & Analyticals Research (Roche Diagnostics GmbH, Mannheim, Germany, Site Penzberg).

The biochemical characterization included measurement of protein concentration, size and MW. The methods were performed as described in 3.2.1, 3.2.2 and 3.2.3.

The functional characterization consisted of analysis of the affinity to human vascular endothelial growth factor (VEGF). For quantitative determination of the antibodies bound to VEGF, a specific ELISA was performed.

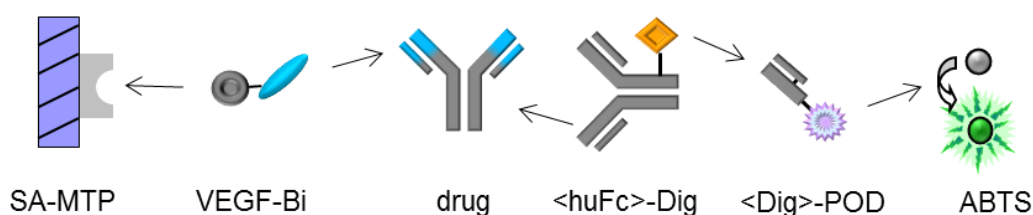


Figure 3-11: ELISA-Design for Bevacizumab detection

Streptavidin-coated MTPs were coated with biotinylated capture reagent (VEGF-Bi). Afterwards antibodies were added at various dilutions. Bound human antibodies were detected by subsequent incubation with digoxigenin-labeled detection antibody (<huFc>-Dig), followed by an incubation with anti-digoxigenin Fab fragments conjugated to horseradish peroxidase (<Dig>-POD). ABTS was used as HRP substrate to form a colored reaction product. Absorbance of the resulting reaction product was read at 405 nm with a reference wavelength at 490 nm.

Preparation: All reagents and buffers were raised to RT before usage. All dilutions were made in assay buffer (Universal buffer for ELISA). Incubation steps were performed under agitation at 500 rpm at RT and were followed by 3 washing steps using 300 μ L wash buffer (PBS, 0.05% Tween20) each.

Capture reagent: A streptavidin-coated MTP was coated with 100 μ L biotinylated VEGF-solution (VEGF-Bi, concentration 500 ng/mL) per well and incubated for 60 min.

Samples: The antibody stock solutions were serially 1:2 diluted starting at 25 ng/mL. The resulting concentrations were 25, 12.5, 6.25, 3.13, 1.56, 0.78, 0.39 and 0 ng/mL. 100 μ L of each antibody dilution as well as of positive and negative control samples were added to each well and incubated for 60 min. All samples were analyzed in duplicates.

First detection reagent: A volume of 100 μ L of digoxigenin-labeled antibody (50 ng/mL <huFc>-Dig) that binds to the Fc region of human IgGs was added to each well and incubated for 60 min.

Second detection reagent: 100 μ L of anti-digoxigenin Fab fragments conjugated to horseradish peroxidase (25 mU/mL <Dig>-POD) were added to each well and incubated for 60 min.

Substrate reaction: 100 μ L of substrate solution ABTS was added to the MTP to

each well and the extinction was measured at 405 nm with a reference wavelength of 490 nm. At an absorbance of 2.0 OD the measurement was stopped.

Calculation: Using a 4-parameter fit (Wiener-Rodbard equation $= A + \frac{B}{(1+C \times x^D)}$) of the “XLfit4” software the concentration-OD-curves were calculated and compared to each other.

4. Results

Abstract

To investigate the Fab influence on FcRn-mAb interaction, variants of Briakinumab and Ustekinumab with cross-over mutations and modified charge distribution in the Fab region were analyzed. Using different biochemical methods, it was elucidated that the main difference between the mAbs is the charge distribution in the Fv domain. Analysis of the FcRn-mAb interactions revealed that an increased extent of positively charged regions in the Fv domain resulted in slower dissociation from the FcRn. Differences in FcRn-mAb dissociation correlated with *in vivo* terminal half-lives in human FcRn transgenic mice, but not in FcRn knockout mice. Using a second model antibody indicated that the charge distribution in the Fv domain influences FcRn-mAb dissociation in general.

4.1. Production

Briakinumab and Ustekinumab are two fully human monoclonal IgG1 antibodies. The sequence alignments of the HC and of the LC of both antibodies are shown in Figure 4-1.

Heavy chain

Briakinumab	<i>QVQLV</i> ESGGG	<i>VVQPG</i> RSLE <i>LI</i>	<i>SCAASG</i> FTFS	<i>SYGM</i> H WVRQA	<i>PGKGL</i> E WVAF	<i>IRYDGS</i> N <i>KYY</i>
Ustekinumab	<i>EVQLV</i> QSGAE	<i>VKKPG</i> ESLKI	<i>SCKGS</i> GSYFT	<i>TYWL</i> GWVRQM	<i>PGKGL</i> D WIGI	<i>MSPVDS</i> D <i>IRY</i>

Briakinumab	<i>ADS</i> V <i>KGRFTI</i>	<i>SRD</i> N <i>SKNTLY</i>	<i>LQMNS</i> L RAED	<i>TAVYY</i> C <i>KT..</i>	<i>..HGSH</i> D <i>NWNG</i>	<i>QGT</i> M <i>VTVSSA</i>
Ustekinumab	<i>SPS</i> F <i>QGQVTM</i>	<i>SVDK</i> S <i>ITITAY</i>	<i>LQWNS</i> L KASD	<i>TAMYY</i> C ARRR	<i>PGQGY</i> F <i>DFWNG</i>	<i>QGT</i> L <i>VTVSSS</i>

Briakinumab	<i>STKGPS</i> V <i>FPL</i>	<i>APSSK</i> S <i>STSGG</i>	<i>TAALG</i> C <i>LVKD</i>	<i>YFPEP</i> V <i>TVSW</i>	<i>NSGALT</i> S <i>GVH</i>	<i>TFFAVL</i> Q <i>SSG</i>
Ustekinumab	<i>STKGPS</i> V <i>FPL</i>	<i>APSSK</i> S <i>STSGG</i>	<i>TAALG</i> C <i>LVKD</i>	<i>YFPEP</i> V <i>TVSW</i>	<i>NSGALT</i> S <i>GVH</i>	<i>TFFAVL</i> Q <i>SSG</i>

Briakinumab	<i>LYSLSS</i> V <i>VTV</i>	<i>PSSSL</i> G <i>TQTY</i>	<i>ICNVN</i> H <i>KPSN</i>	<i>TKVDK</i> K <i>VEPK</i>	<i>SCDKT</i> H <i>TCP</i>	<i>CPAPEL</i> L <i>LGGP</i>
Ustekinumab	<i>LYSLSS</i> V <i>VTV</i>	<i>PSSSL</i> G <i>TQTY</i>	<i>ICNVN</i> H <i>KPSN</i>	<i>TKVDK</i> K <i>VEPK</i>	<i>SCDKT</i> H <i>TCP</i>	<i>CPAPEL</i> L <i>LGGP</i>
####						
Briakinumab	<i>SVFLF</i> P <i>PKPK</i>	<i>DTLMI</i> S <i>RTPE</i>	<i>VTCV</i> V <i>VDVSH</i>	<i>EDPEV</i> K <i>FNWY</i>	<i>VDGVE</i> V <i>HNAK</i>	<i>TKPRE</i> E <i>QYNS</i>
Ustekinumab	<i>SVFLF</i> P <i>PKPK</i>	<i>DTLMI</i> S <i>RTPE</i>	<i>VTCV</i> V <i>VDVSH</i>	<i>EDPEV</i> K <i>FNWY</i>	<i>VDGVE</i> V <i>HNAK</i>	<i>TKPRE</i> E <i>QYNS</i>
###						
Briakinumab	<i>TYRVV</i> S <i>VLTV</i>	<i>LHQD</i> W <i>LNGKE</i>	<i>YKCKV</i> S <i>NKAL</i>	<i>PAPIE</i> K <i>TISK</i>	<i>AKGQ</i> P <i>REPQV</i>	<i>YTLPP</i> S <i>REEM</i>
Ustekinumab	<i>TYRVV</i> S <i>VLTV</i>	<i>LHQD</i> W <i>LNGKE</i>	<i>YKCKV</i> S <i>NKAL</i>	<i>PAPIE</i> K <i>TISK</i>	<i>AKGQ</i> P <i>REPQV</i>	<i>YTLPP</i> S <i>RDEL</i>

Briakinumab	<i>TKNQV</i> S <i>LTCL</i>	<i>VKGFY</i> P <i>SDIA</i>	<i>VEWES</i> N <i>GQPE</i>	<i>NNYKT</i> T <i>PPVL</i>	<i>DSG</i> S <i>FFLYS</i>	<i>KLTVD</i> K <i>SRWQ</i>
Ustekinumab	<i>TKNQV</i> S <i>LTCL</i>	<i>VKGFY</i> P <i>SDIA</i>	<i>VEWES</i> N <i>GQPE</i>	<i>NNYKT</i> T <i>PPVL</i>	<i>DSG</i> S <i>FFLYS</i>	<i>KLTVD</i> K <i>SRWQ</i>
###						
Briakinumab	<i>QGNVF</i> S <i>C</i> S <i>V</i> M	<i>HEALH</i> N <i>H</i> Y <i>TQ</i>	<i>KSLSL</i> S <i>R</i> G <i>K</i>			
Ustekinumab	<i>QGNVF</i> S <i>C</i> S <i>V</i> M	<i>HEALH</i> N <i>H</i> Y <i>TQ</i>	<i>KSLSL</i> S <i>P</i> G <i>K</i>			

Light chain

Briakinumab	<i>QSV</i> L <i>TQPP</i> .S	<i>VSGAP</i> G <i>QRVT</i>	<i>ISCS</i> G <i>RSNI</i>	<i>GSNTV</i> K <i>WYQQ</i>	<i>LPGTAP</i> K <i>LLI</i>	<i>YYNDQ</i> R <i>PSGV</i>
Ustekinumab	<i>DIQ</i> M <i>TQSP</i> SS	<i>LSASV</i> G <i>DRVT</i>	<i>ITCRAS</i> Q <i>G.I</i>	<i>SS.WLAW</i> Y <i>QQ</i>	<i>KPEKAP</i> K <i>SLI</i>	<i>YAASSL</i> Q <i>SGV</i>

Briakinumab	<i>PDRFS</i> G <i>SKSG</i>	<i>TSASL</i> A <i>ITGL</i>	<i>QAEDE</i> A <i>DYYC</i>	<i>QSYDR</i> Y <i>THPA</i>	<i>LLFGT</i> G <i>TKVT</i>	<i>VLGQ</i> P <i>KAAPS</i>
Ustekinumab	<i>PSRFS</i> G <i>SGSG</i>	<i>TDFTL</i> T <i>ISSL</i>	<i>QPEDF</i> A <i>TYYC</i>	<i>QQYNI</i> Y <i>PT.</i>	<i>..FGQ</i> G <i>TKLE</i>	<i>I.KRTV</i> A <i>APS</i>

Briakinumab	<i>VT</i> L <i>FPPS</i> EE	<i>LQANK</i> A <i>T</i> L <i>V</i> C	<i>LISDF</i> Y <i>PGAV</i>	<i>TVAWK</i> A <i>DSSP</i>	<i>IKAG</i> .. <i>VETT</i>	<i>TPSKQ</i> S <i>NNKY</i>
Ustekinumab	<i>VF</i> L <i>FPPS</i> EE	<i>LKSGT</i> A <i>S</i> V V C	<i>LLNNF</i> Y <i>P</i> R E A	<i>KVQWK</i> V <i>D</i> N .A	<i>LQSGN</i> S <i>QESV</i>	<i>TEQDS</i> K <i>DSTY</i>

Briakinumab	<i>AASSY</i> L <i>SL</i> TP	<i>EQW</i> K <i>SH</i> SY S	<i>CQVTH</i> E <i>G</i> ..S	<i>TVEKT</i> V <i>APTE</i>	<i>CS</i>	
Ustekinumab	<i>SLSS</i> T <i>L</i> SK	<i>ADY</i> E <i>KH</i> V Y A	<i>CEVTH</i> Q <i>GLSS</i>	<i>PVTKS</i> F <i>N</i> R G E	<i>C.</i>	

Figure 4-1: Alignment of Briakinumab and Ustekinumab













Identical and similar amino acids are shown in cyan and dark blue, respectively; V_H and V_L domains are shown in italics; CDRs are marked with an asterisk (*); Single amino acid residues mutated to alanines for mAb 7-10 are highlighted in red; a hash (#) denotes amino acids in close proximity (≤ 4 Å) to the FcRn in the published FcRn-Fc structure (PDB 4N0U (Oganessian et al. 2014)).

Systematically engineered variants of Briakinumab and Ustekinumab with cross-over exchanges and modified charge distributions in the Fab region were produced and are summarized in Table 4-1. Briefly, structural parts like Fv domains, LCs and CDRs were exchanged between Briakinumab and Ustekinumab: mAb 1- 6. Three and five basic amino acids in the V_H domain of Briakinumab were mutated to alanines that resulted in mAb 7 and mAb 8, respectively. MAb 9 is a Briakinumab-variant with three basic amino acids in the V_L domain mutated to alanines. MAb 10 is a Briakinumab-variant with three basic amino acids in the V_L domain and five basic amino acids in the V_H domain mutated to alanines.

After expression and purification the final antibody yield was at least of 4 mg and of 20 mg for antibodies selected to take part in the *in vivo* studies. After purification using protein A chromatography and SEC, all antibodies seemed to be produced correctly which was further tested in the biochemical and functional characterization.

Table 4-1: Systematically engineered variants of Briakinumab and Ustekinumab

Antibodies conducting PK studies are colorcoded; Briakinumab (orange), Ustekinumab (green), mAb 8 (magenta) and mAb 9 (blue). Mutation of basic amino acids is illustrated by blue dots; mutation of three amino acids corresponds to 1 blue dot, of five amino acids corresponds to 2 blue dots. An asterisk (*) marks mutated amino acid residues according to the EU numbering of Kabat.

Name	Description	
Briakinumab	Briakinumab wild type	
Ustekinumab	Ustekinumab wild type	
mAb 1	Ustekinumab Fv + Briakinumab constant domains	
mAb 2	Briakinumab Fv + Ustekinumab constant domains	
mAb 3	Ustekinumab HC + Briakinumab LC	
mAb 4	Briakinumab HC + Ustekinumab LC	
mAb 5	Ustekinumab CDRs on Briakinumab	
mAb 6	Briakinumab CDRs on Ustekinumab	
mAb 7	Briakinumab R19 ^{HC} A, K64 ^{HC} A, R83 ^{HC} A*	
mAb 8	Briakinumab R16 ^{HC} A, R19 ^{HC} A, K57 ^{HC} A, K64 ^{HC} A, R83 ^{HC} A*	
mAb 9	Briakinumab R27 ^{LC} A, R55 ^{LC} A, R94 ^{LC} A*	
mAb 10	Briakinumab R16 ^{HC} A, R19 ^{HC} A, K57 ^{HC} A, K64 ^{HC} A, R83 ^{HC} A, R27 ^{LC} A, R55 ^{LC} A, R94 ^{LC} A*	

4.2. Biochemical characterization

Antibodies were biochemically characterized to test if antibodies were produced correctly and to find differences between Briakinumab and Ustekinumab that could explain the reported differences in PK. The biochemical characterization of Briakinumab and Ustekinumab is shown in detail. Summarized results of the biochemical characterization of all mAbs are presented in Table 4-2 and Table 4-10.

4.2.1. Determination of mAb concentration

The protein concentration of Briakinumab and Ustekinumab samples used in this work was determined at 2.36 and 2.67 mg/mL, respectively. The concentrations of all mAbs are summarized in Table 4-2.

4.2.2. Determination of mAb molecular weight by CE-SDS

Briakinumab and Ustekinumab have molecular weights of about 155 kDa as measured by CE-SDS which is comparable with the theoretical molecular weight calculated by the protein sequence of 143 and 146 kDa, respectively (Figure 4-2). Reduced HCs have nearly identical molecular weights of about 58-59 kDa and the LCs vary between ~33 kDa of Briakinumab and ~26 kDa of Ustekinumab due to different LC-isotypes. The theoretical MWs for HCs and LCs of both antibodies are 49 and 23 kDa, respectively, and are in agreement with the determined MWs. Reduced HCs and LCs show in total a higher molecular weight than the non-reduced antibodies which could be caused by sterical effects of the free disulfide strands.

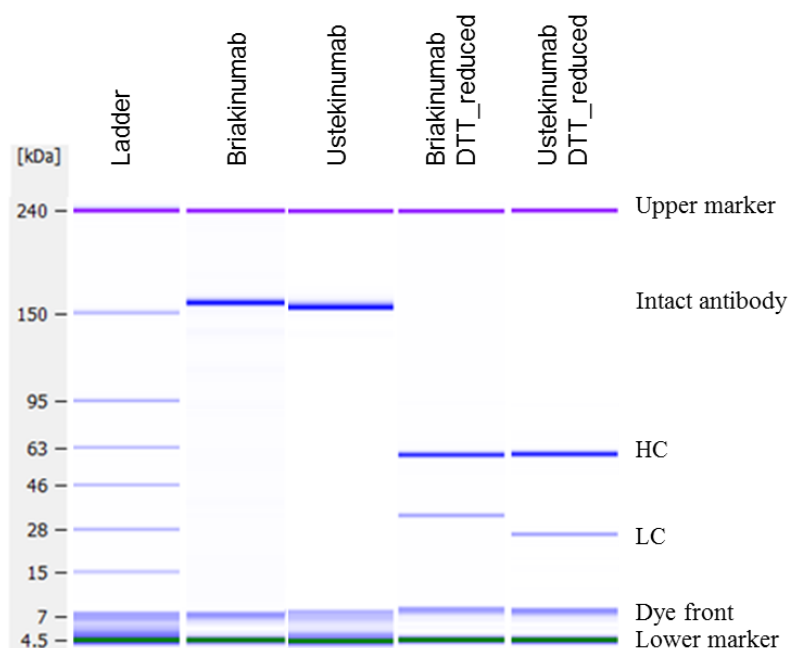


Figure 4-2: Purity and molecular weight

Gel-like images of the intact mAbs and of HCs and LCs after DTT-reduction.

The purity of the intact antibody of Briakinumab and Ustekinumab is 92 and 84%, respectively. The occurred impurities of both mAbs are mainly a single LC and a combination of two heavy chains and one light chain. This can also be confirmed by the ratio of Briakinumab's intact HCs and LCs of 67 and 33%, respectively. The HC ratio is twice as high as the LC ratio which is due to the higher MW of the HC and a therefore higher fluorescence intensity in the electropherogram. Also, Ustekinumab's HCs and LCs have intact chains of 64 and 32%, respectively. Therefore the ratio of minor forms being neither intact HC nor LC is 0 and 4% for Briakinumab and Ustekinumab, respectively.

The MW distribution of all mAbs is summarized in Table 4-2. The MW of each mAb is in agreement with the theoretical value and the purity of the MW species is also high.

4.2.3. Determination of mAb size by SEC

Briakinumab and Ustekinumab show monomer contents of at least 99%. The content of aggregates and LMWs is very small ($< 1\%$). Briakinumab shows a slightly longer retention time (Figure 4-3) which might indicate an interaction with the column matrix or a slightly smaller hydrodynamic radius.

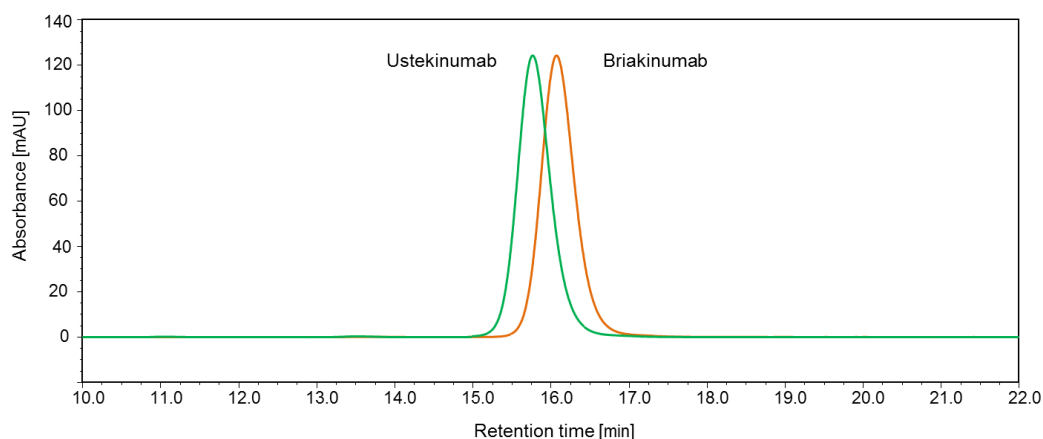


Figure 4-3: SEC chromatogram

Sample peaks are normalized to Briakinumab's main peak.

The monomer content of all mAbs is summarized in Table 4-2. The content of aggregates and LMWs is very small ($< 3\%$).

4.2.4. Determination of mAb hydrophobicity

Hydrophobicity of proteins is not an absolute molecule property and depends on numerous factors including protein sequence and structure. To classify antibodies with respect to potential hydrophobic interactions, hydrophobicity was determined relative to two low and high hydrophobic antibodies. These low and high hydrophobic reference samples (RS) were defined as 0 and 100% hydrophobic, respectively. Briakinumab elutes 2.2 min after Ustekinumab (Figure 4-4) indicating a slightly higher hydrophobicity, but according to this hydrophobicity scale, Briakinumab and Ustekinumab are both low hydrophobic.

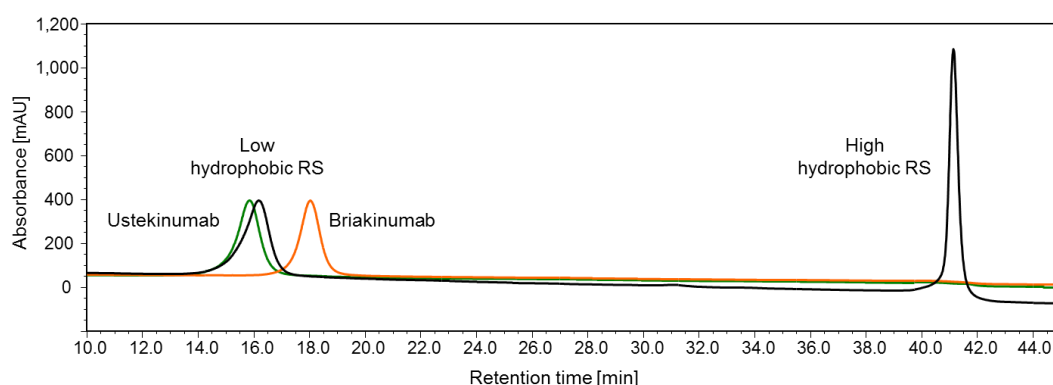


Figure 4-4: HIC chromatogram

Low and high hydrophobic RS define the hydrophobic range. Sample peaks are normalized to the low hydrophobic RS peak.

Table 4-2 summarizes the hydrophobic profile of all mAbs. Variants with cross-over exchanges show a relative hydrophobicity of $\leq 13\%$. Antibodies with mutation of three basic amino acids to alanines in the V_H and V_L domains have relative hydrophobic values of 13 and 16%, respectively. Mutation of five basic amino acids in the V_H domain results in 24% hydrophobicity. The hydrophobicity is increased to 34% by mutation of three and five basic amino acids in V_L and V_H domains, respectively.

Table 4-2: Overview biochemical characterization of all mAbs

The concentration is given as the average of 3 measurements. Monomer contents are determined by integration of the SEC chromatogram. Purity of antibody species is determined by CE-SDS of the intact mAbs and after DTT-reduction. The hydrophobicity is presented relative to low and high hydrophobic RS.

Sample	Conc. [mg/mL]	SEC [%]	CE-SDS [%]			Hydro- phobicity [%]
		Monomer content	Intact mAb	HC	LC	
Briakinumab	2.36	99.9	92	67	33	7
Ustekinumab	2.67	99.0	84	64	32	-1
mAb 1	2.32	99.4	74	66	31	-6
mAb 2	1.66	98.1	91	64	32	8
mAb 3	2.14	99.3	80	66	28	8
mAb 4	2.10	99.8	82	64	32	-4
mAb 5	3.03	99.5	90	70	30	13
mAb 6	0.40	97.1	95	66	32	12
mAb 7	2.90	97.2	85	65	33	13
mAb 8	3.10	98.9	85	64	34	24
mAb 9	3.15	99.1	80	70	29	16
mAb 10	4.08	98.6	88	70	28	34

4.2.5. Analysis of stressed mAbs

Stress tests were performed to analyze the protein stability and evaluate the tendency to aggregate formation. The concentrations of the samples before and after 6 freeze-thaw cycles are nearly identical (Table 4-3). The monomer content and MW of the stressed samples are comparable to the ones of the unstressed samples (compare with 4.2.2 and 4.2.3), therefore Briakinumab and Ustekinumab are resistant to freeze-thaw stress.

Table 4-3: Protein concentration, size and MW after freeze-thaw stress

Protein concentration was measured before and after freeze-thaw stress and is given as the average of 3 measurements. Monomer contents are determined by integration of the SEC chromatogram. Purity of antibody species is determined by CE-SDS of the intact mAbs and after DTT-reduction.

Sample	Concentration [mg/mL]		SEC [%]	CE-SDS [%]		
	Cycle 0	Cycle 6	Monomer content	Intact mAb	HC	LC
Briakinumab	1.0	0.99	99.7	90	65	35
Ustekinumab	1.0	0.95	98.7	82	66	34

The protein concentration, size and MW of the samples after accelerated temperature stress are comparable to the ones of the unstressed samples (compare with 4.2.2 and 4.2.3) indicating that both mAbs have a stable protein structure in different buffers and under different temperature conditions. Therefore both mAbs are resistant to storage-temperature stress.

Table 4-4: Protein concentration, size and MW after storage-temperature stress

Protein concentration, size and MW distribution were measured after incubation under different buffer and temperature conditions for 7 days. Protein concentration is given as the average of 3 measurements. Monomer contents are determined by integration of the SEC chromatogram. Purity of antibody species is determined by CE-SDS of the intact mAbs and after DTT-reduction.

Sample	Storage condition		Conc. [mg/mL]	SEC [%]	CE-SDS [%]		
	Buffer	Temp. [°C]		Monomer content	Intact mAb	HC	LC
Briakinumab	His/NaCl, pH 6.0	- 80	0.98	99.8	84	62	32
	His/NaCl, pH 6.0	37	0.94	99.7	84	65	32
	PBS, pH 7.4	- 80	0.99	99.8	80	64	31
	PBS, pH 7.4	37	0.97	99.5	77	61	31
Ustekinumab	His/NaCl, pH 6.0	- 80	0.96	99.6	85	68	31
	His/NaCl, pH 6.0	37	0.90	99.4	85	65	28
	PBS, pH 7.4	- 80	0.99	99.3	82	68	30
	PBS, pH 7.4	37	0.93	99.4	82	68	30

The monomer contents of both mAbs were still $\geq 99\%$, therefore no significant aggregate formation was observed due to freeze-thaw or storage-temperature stress. Both stress-tests showed that Briakinumab and Ustekinumab are unaffected by temperature and storage conditions, thereby demonstrating high protein stability.

4.2.6. Determination of mAb isoelectric point

The isoelectric points of Briakinumab and Ustekinumab are given in Table 4-5. Calculated and measured pIs are in good agreement; therefore the pIs of the mAb variants were subsequently calculated only.

Table 4-5: Isoelectric points of Briakinumab and Ustekinumab

The isoelectric points were measured and calculated using cIEF and GPMW, respectively.

Sample	Measured pI	Calculated pI
Briakinumab	9.6	9.7
Ustekinumab	9.3	9.4

The isoelectric points of variants with cross-over exchanges (mAb 1-6) range between pI 9.4 and 9.6. MAbs with mutated basic amino acids to alanines range between 9.0 and 9.4 illustrating that smaller positively charged regions slightly reduce the pI. To sum up, all mAbs are in a narrow pI-range between 9.0 and 9.7 (Table 4-6).

In addition to the isoelectric points, the net charges of the Fv domains at lysosomal pH 6.0 and at physiological pH 7.4 were calculated and summarized in Table 4-6. Due to cross-over exchanges and modified charge distribution, the net charges of the respective domains are affected. For example, mAbs with less basic amino acids in the V_H have reduced net charges in this domain.

Table 4-6: Net charges of all mAbs

The isoelectric points were calculated assuming all cysteines are involved in disulfide bridges. The net charge [e^-] of V_H, V_L and Fv domains at pH 6.0 and pH 7.4 were calculated assuming all cysteines are involved in disulfide bridges.

	calc. pI (IgG)	q (V _L) pH 6	q (V _L) pH 7.4	q (V _H) pH 6	q (V _H) pH 7.4	q (Fv) pH 6.0	q (Fv) pH 7.4
Briakinumab	9.7	3.8	3.0	6.4	4.3	10.2	7.3
Ustekinumab	9.4	2.1	1.9	3.1	2.9	5.2	4.9
mAb 1	9.5	2.1	1.9	3.1	2.9	5.2	4.9
mAb 2	9.4	3.8	3.0	6.4	4.3	10.2	7.3
mAb 3	9.5	3.8	3.0	3.1	2.9	6.9	6.0
mAb 4	9.5	2.1	1.9	6.4	4.3	8.4	6.2
mAb 5	9.6	2.1	1.9	4.1	3.9	6.1	5.9
mAb 6	9.4	3.9	3.0	5.4	3.3	9.2	6.3
mAb 7	9.4	3.8	3.0	3.4	1.3	7.2	4.3
mAb 8	9.3	3.8	3.0	1.4	-0.7	5.2	2.3
mAb 9	9.4	0.8	0.0	6.4	4.3	7.2	4.3
mAb 10	9.0	0.8	0.0	1.4	-0.7	2.2	-0.6

4.2.7. Charge distribution analysis

The charge distribution in the Fv domain of all mAbs as well as of the FcRn was calculated using a 3D model and expert software by Dr. Hubert Kettenberger (Biochemical & Analyticals Research, Roche Diagnostics GmbH, Mannheim, Germany, Site Penzberg).

Using the published crystal structure of Ustekinumab (Luo et al. 2010) and a homology model of Briakinumab, it was observed that Briakinumab exhibits a non-uniform charge distribution at physiological pH of 7.4. Briakinumab shows a large positively charged region on the Fab region which is absent in Ustekinumab (Figure 4-5). This positively charged region spans the V_H and the V_L domains.

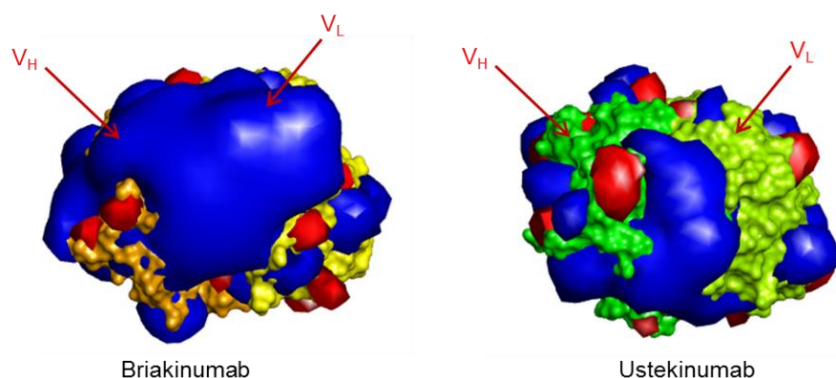


Figure 4-5: Charge distribution of Briakinumab and Ustekinumab

Isopotential surfaces of the proteins protonated at pH 7.4 and contoured at $2 k_B T/e$; blue: positive; red: negative. The view focuses on the CDRs. Briakinumab: Light and heavy chains are shown in yellow and orange, respectively. Ustekinumab: Light and heavy chains are colored in light and dark green, respectively.

Isopotential surfaces of all mAbs are shown in Figure 4-6. The charge distribution is strongly affected by cross-over exchanges. MAb 1 and mAb 4 both containing Ustekinumab's V_L domain show a smaller positively charged region in the Fab than mAb 2 and mAb 3 bearing Briakinumab's V_L domain. MAb 7 and mAb 8, which have basic amino acids in the V_H domain mutated to alanines, show a smaller positively charged region in this domain. MAb 9 which has basic amino acids in the V_L domain mutated to alanines illustrates a smaller positively charged region in this area. MAb 10 that has basic amino acids in V_H and V_L domains mutated to alanines shows smaller positively charged regions in the Fv domain.

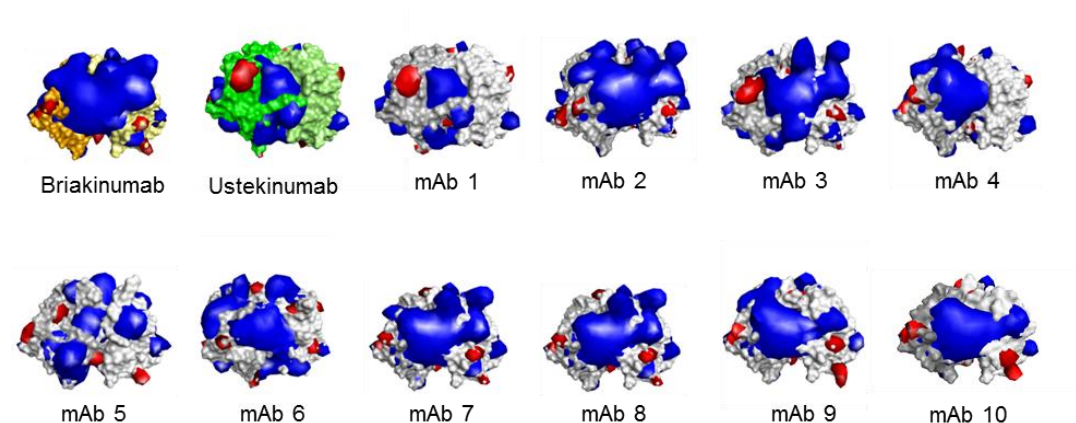


Figure 4-6: Charge distribution of all mAbs

Isopotential surfaces of the proteins protonated at pH 7.4 and contoured at $2 k_B T/e$; blue: positive; red: negative. The light and heavy chains are shown in light and dark grey, respectively. The view focuses on the CDRs.

Using the recently published crystal structure of human FcRn (Oganesyan et al. 2014), it was observed that FcRn possesses an extended negatively charged region on one side of the receptor at physiological pH of 7.4. On the other receptor side, positively charged regions were observed (Figure 4-7) which are not involved in cognate Fc binding.

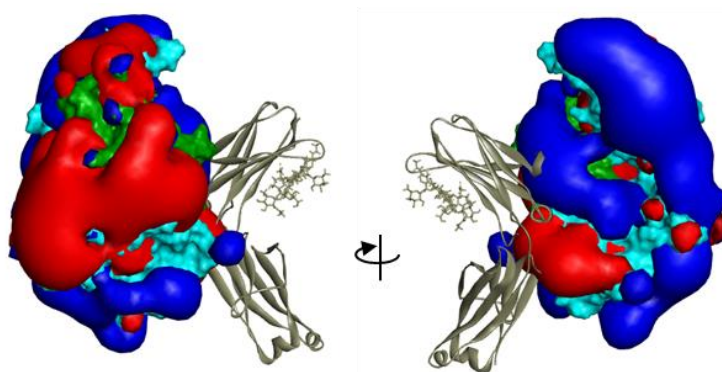


Figure 4-7: Charge distribution of the FcRn

Isopotential surface at pH 7.4 of a human FcRn (cyan) in complex with human β_2 microglobulin (green) contoured at $1 k_B T/e$; blue: positive; red: negative. A different contour level ($1 k_B T/e$ instead of $2 k_B T/e$) is used for clarity. Views of the left and right image are related by a rotation about a vertical axis. The Fc domain is shown as ribbons for clarity and was not considered in isopotential calculation.

4.2.8. IdeS cleavage

The IdeS cleavage was controlled by CE-SDS and analytical SEC. The IdeS-cleaved antibodies have molecular weights of about 108 kDa and 38 kDa (Figure 4-8) which corresponds to the $F(ab')_2$ part (literature data 110 kDa) and the Fc fragments (literature data 31 kDa), respectively (Loomes et al. 1993; von Pawel-Rammingen et al. 2002). The absence of mAb bands indicates complete cleavage. The Fc fragment is detected as a faint band which is typical for glycoproteins on CE-SDS.

Intact $F(ab')_2$ part and Fc monomers of Briakinumab show high purity of 61 and 32%, respectively. Ustekinumab's $F(ab')_2$ part and Fc monomers have pure fragments of 64 and 31%, respectively. Therefore the ratio of minor forms being neither intact $F(ab')_2$ nor Fc monomer is small with 7 and 5% for Briakinumab and Ustekinumab, respectively.

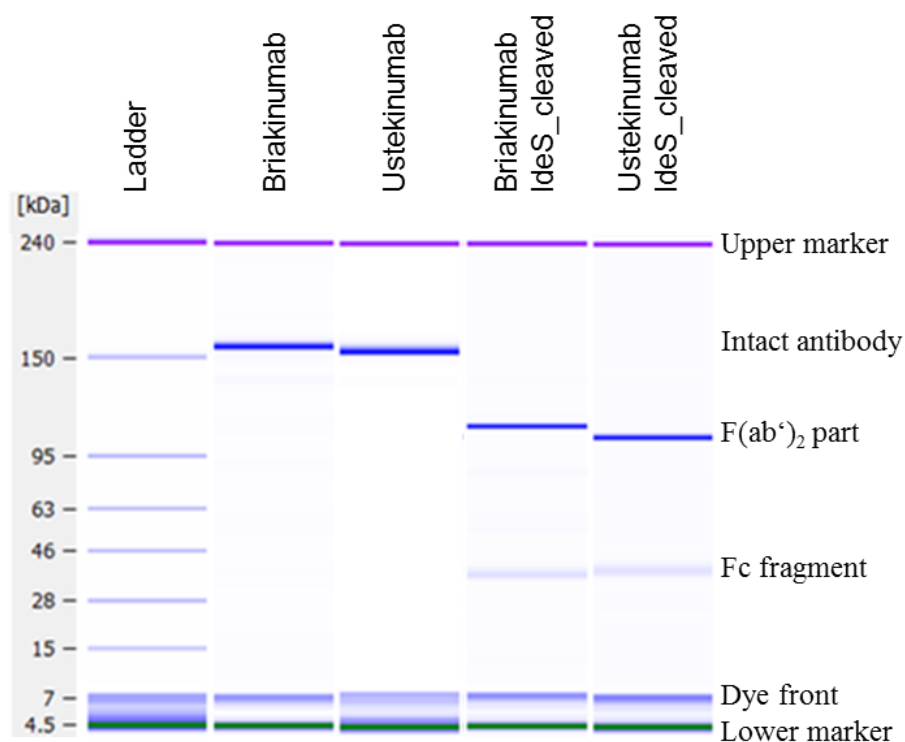


Figure 4-8: Molecular weight of IdeS-cleaved mAbs

Gel-like images of the intact mAbs and after IdeS-cleavage into $F(ab')_2$ and Fc fragments.

These observations were further confirmed by the SEC-results which also provide two fractions at about 110 kDa and 33 kDa and no residual intact antibody. Briakinumab's F(ab')₂ part shows a slightly longer retention time which might indicate an interaction with the column matrix or a slightly smaller hydrodynamic range (Figure 4-9).

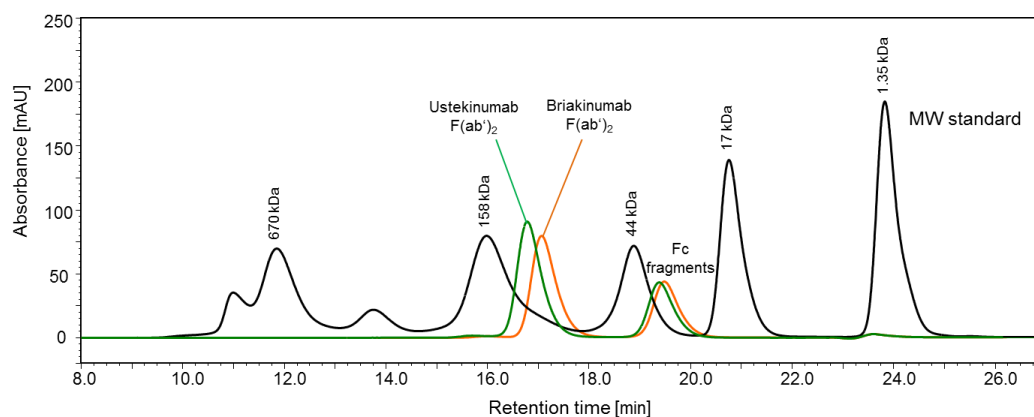


Figure 4-9: Apparent molecular weight of Briakinumab and Ustekinumab after IdeS cleavage.

Sample peaks are normalized to Briakinumab's Fc fragment peak.

The cleavage was therefore successful, the F(ab')₂ region and the Fc fragments were tested for FcRn interactions (4.4.2.2).

4.3. Functional characterization

The functional characterization includes analysis of the interaction with the target (human IL-12) to test if Briakinumab and Ustekinumab were produced correctly and the target binding is still functional. The mAb variants were modified in the Fab region and it is tested if these modifications alter the target binding. Furthermore the interaction of the antibodies used in the mouse PK study with mouse IL-12/-23 are analyzed to exclude target-mediated clearance effects in the mouse study. In addition, binding levels to mouse Fcγ receptor I (muFcγRI) are measured because stronger binding to mouse FcγRI could lead to a faster decrease in a PK study due to faster uptake into antigen presenting cells.

4.3.1. Interaction with human IL-12

Briakinumab, Ustekinumab and the variants have structural differences in the Fab region that can influence IL-12 binding, therefore the results of all mAbs are presented in detail.

4.3.1.1. ELISA

The absorbance-concentration curves of the variants with cross-over exchanges (mAb 1-6) and with modified charge distribution (mAb 7-10) are shown in Figure 4-10 and Figure 4-11, respectively. The concentration of each mAb was calculated using the fit of the Briakinumab calibration curve to obtain IL-12 binding relative to Briakinumab (Briakinumab = 100%). Binding differences of $\leq 30\%$ were assessed to show similar binding to IL-12 as Briakinumab, differences of $\geq 30\%$ indicate reduced binding to IL-12. Briakinumab, Ustekinumab and mAbs with exchanged Fv domains (mAb 1 and mAb 2) show similar IL-12 binding profiles. The binding of Briakinumab, Ustekinumab and mAb 2 ranges in a 20% window and of mAb 1 in a 30% window. MAbs with exchanged LCs (mAb 3 and mAb 4) and mAbs with exchanged CDRs (mAb 5 and mAb 6) do not bind to IL-12.

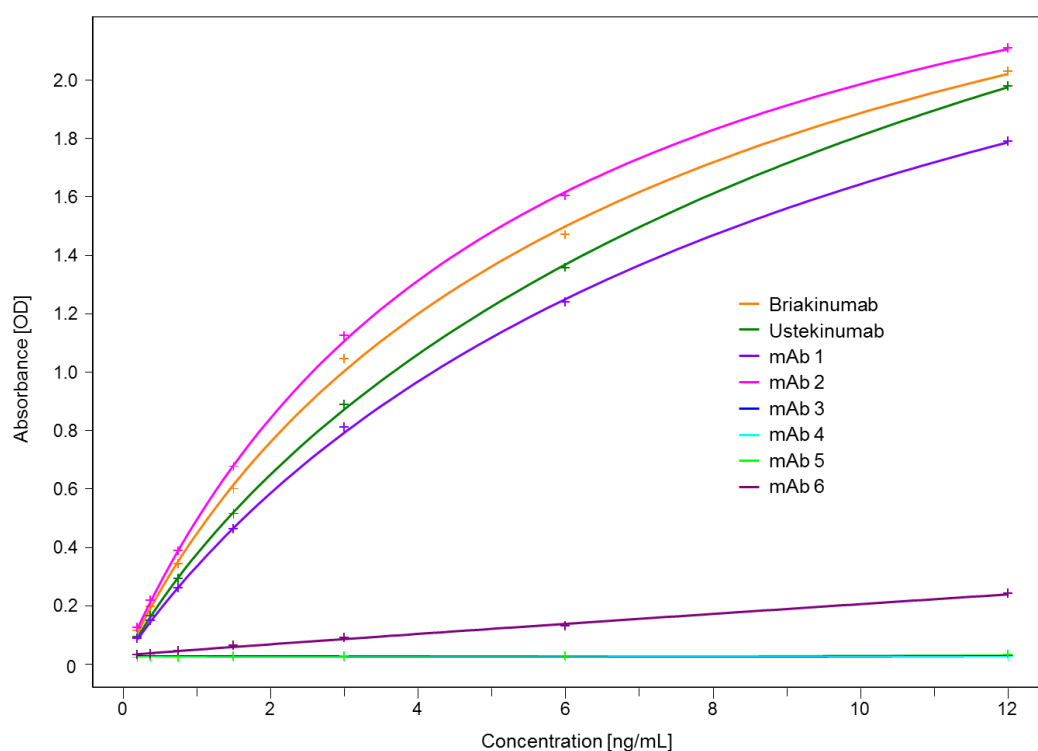


Figure 4-10: IL-12 interaction of Briakinumab, Ustekinumab and mAb 1-6

The absorbance-concentration curves of Briakinumab, Ustekinumab and mAbs with cross-over exchanges. The absorbance-concentration curves of mAb 3-5 overlap.

Briakinumab variants with modified charge distribution (mAb 7–9) bind IL-12 in a range of 30% relative to Briakinumab indicating similar IL-12 binding. Only mAb 10 shows reduced IL-12 binding with 63% binding compared to Briakinumab.

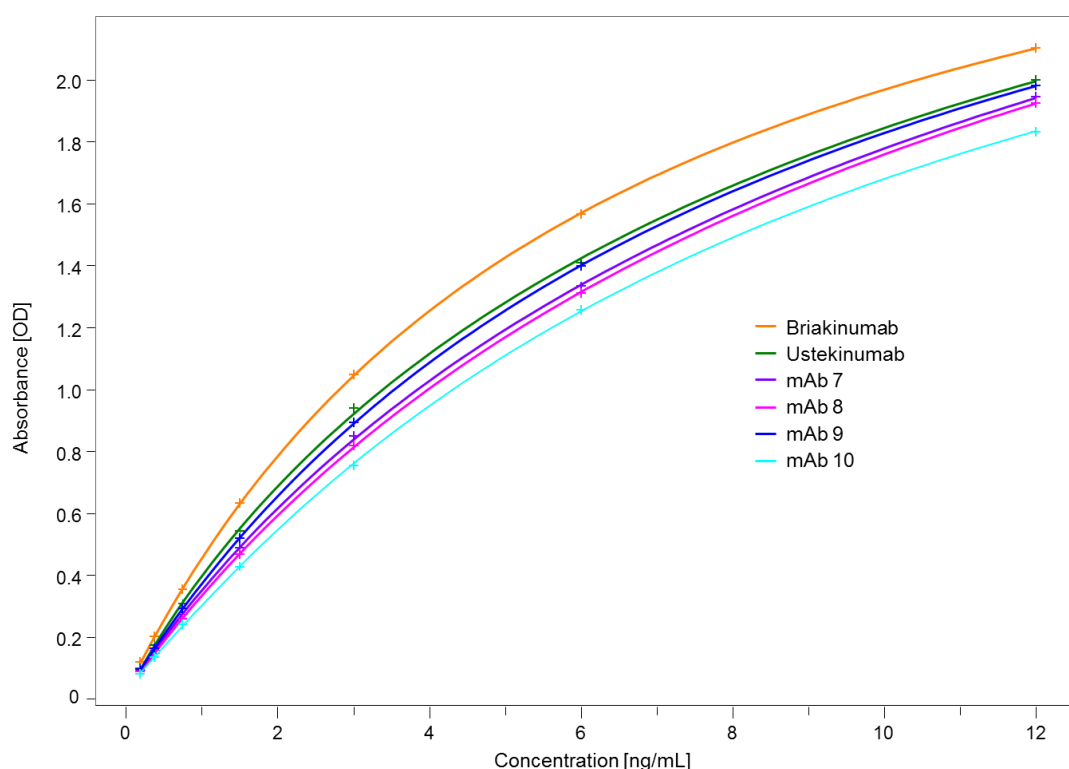


Figure 4-11: IL-12 interaction of Briakinumab, Ustekinumab and mAb 7-10

The absorbance-concentration curves of Briakinumab, Ustekinumab and mAb 7-10.

4.3.1.2. SPR

SPR was used to confirm the results of the target specific ELISA. Ustekinumab and Briakinumab have nearly identical association rate constants (k_a) (k_a (Briakinumab) = 8×10^5 1/Ms vs. k_a (Ustekinumab) = 9×10^5 1/Ms). The dissociation of IL-12 and the mAbs is very slow (Figure 4-12), therefore calculation of the dissociation rate constant (k_d) and subsequently of the equilibrium dissociation constant (K_D) may differ from the actual values. Despite the limitation of the method in this setting, the calculated values can give a general impression and can be used to confirm the ELISA results. Briakinumab and Ustekinumab bind IL-12 with high affinity and the K_D is in a low nM-range (K_D (Briakinumab) = 0.07 nM vs. K_D (Ustekinumab) = 0.2 nM). The measured affinity of Briakinumab with k_a , k_d and K_D values of 8×10^5 1/Ms, 6×10^{-5} 1/s and 70 pM, respectively, are in agreement with literature data (k_a = 5×10^5 1/Ms, k_d = 5.1×10^{-5} 1/s, K_D = 100 pM) (Ding et al. 2008). The high affinity of Ustekinumab to IL-12 is also described in literature (Weber and Kean 2009).

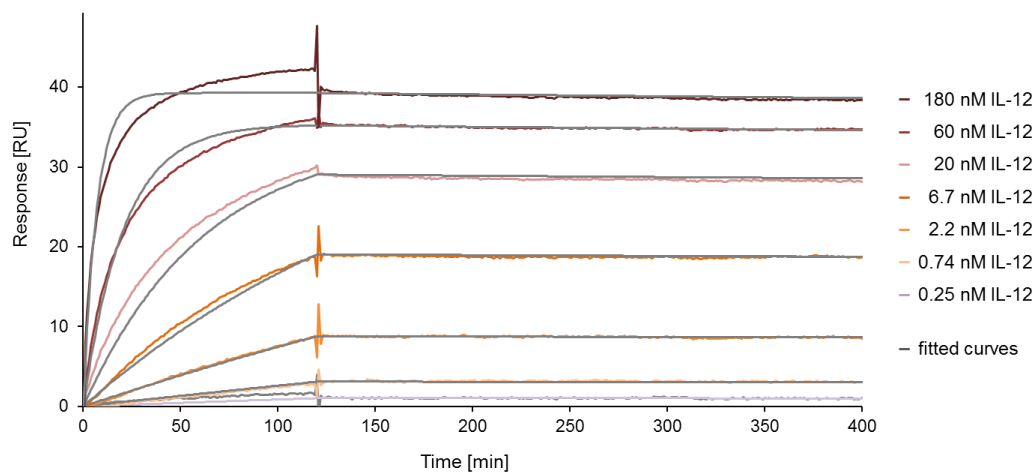


Figure 4-12: SPR sensorgrams (concentration series) of Briakinumab binding to IL-12.

Sensorgrams were fitted to a steady state affinity model; fitted curves are shown in dark grey. IL-12 association and dissociation was detected in a rising concentration series.

Table 4-7 summarizes the calculated kinetic parameters of the target interaction. MAbs with exchanged Fv domains (mAb 1 and mAb 2) and mAbs with modified charge distributions (mAb 7-10) have affinities to IL-12 similar to Briakinumab and Ustekinumab. MAb 3 and mAb 5 do not bind to IL-12 and mAb 4 and mAb 6 show very weak binding to IL-12. The data is in agreement with the ELISA results.

Table 4-7: SPR parameters of mAbs and IL-12

K_D , k_a and k_d were calculated using steady state affinity.

Sample	k_a [1/Ms]	k_d [1/s]	K_D [nM]
Ustekinumab	9.0×10^5	1.8×10^{-4}	0.20
Briakinumab	8.0×10^5	6.0×10^{-5}	0.07
mAb 1	1.7×10^6	4.1×10^{-4}	0.24
mAb 2	1.2×10^6	3.0×10^{-4}	0.25
mAb 3	no binding	no binding	no binding
mAb 4	1.2×10^7	2.3	191
mAb 5	no binding	no binding	no binding
mAb 6	2.0×10^6	1.9×10^{-2}	9.62
mAb 7	1.0×10^6	7.9×10^{-5}	0.08
mAb 8	1.2×10^6	9.1×10^{-5}	0.07
mAb 9	8.8×10^6	1.3×10^{-4}	0.01
mAb 10	1.4×10^7	1.3×10^{-4}	0.01

4.3.2. Interaction with IL-12 and IL-23 of different species

The binding levels of the mAbs used in the *in vivo* study (Briakinumab, Ustekinumab, mAb 8 and mAb 9) to recombinant human IL-12, human IL-23, mouse IL-12 and mouse IL-23 were analyzed. The approach to determine binding levels can be used if a general evaluation is sufficient information, because binding levels do not provide information about the binding kinetics. All mAbs showed RU binding levels to human IL-12 and human IL-23, but hardly any to mouse IL-12 and mouse IL-23. This finding is in accordance with literature data (Luo et al. 2010; Traczewski and Rudnicka 2012) and confirms that target-mediated clearance effects can be excluded when performing a mouse PK study.

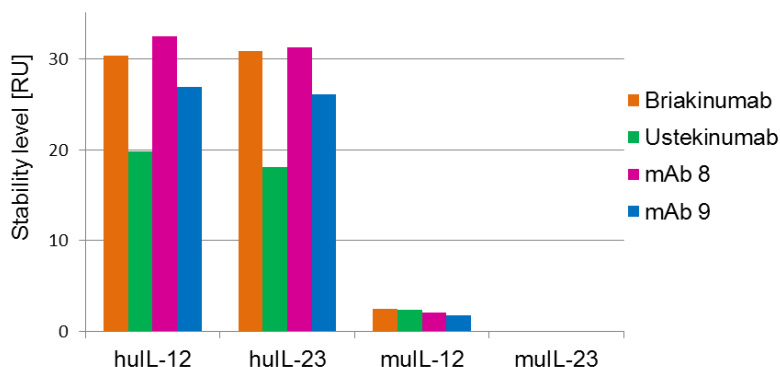


Figure 4-13: Binding levels to IL-12/-23 of different species

Binding levels to recombinant human IL-12, human IL-23, mouse IL-12 and mouse IL-23.

4.3.3. Interaction with mouse FcγRI

The binding levels of the mAbs studied in the *in vivo* experiments (Briakinumab, Ustekinumab, mAb 8 and mAb 9) to muFcγRI were determined. Briakinumab showed higher binding levels than Ustekinumab, mAb 8 and mAb 9. Higher binding levels may indicate a stronger interaction with mouse FcγRI resulting in faster uptake into antigen presenting cells and subsequently in a faster serum concentration decrease in a PK study. To better analyze this interaction more appropriate tools would be needed to get stronger data.

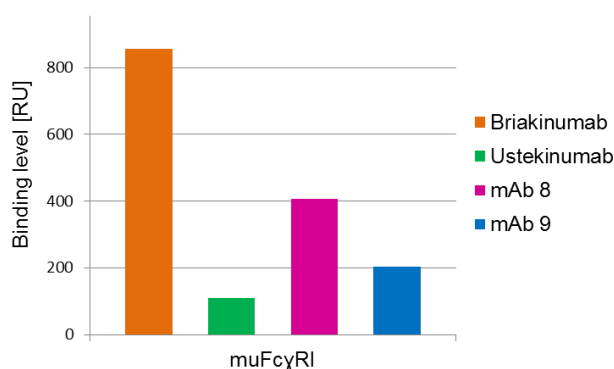


Figure 4-14: Binding levels to muFcγRI.

Binding levels of the antibodies used in the *in vivo* study to mouse FcγRI.

4.4. FcRn-mAb interaction

The FcRn-mAb interaction is studied to elucidate the contribution of the FcRn-IgG interaction on PK. The interaction consists of two parts, which were analyzed separately. The FcRn-mAb interaction analyzed at pH 6.0 provides information about the affinity and at higher pH values about the dissociation of the FcRn-mAb complex.

4.4.1. FcRn-mAb affinity at pH 6.0

The K_D was calculated relative to Ustekinumab (Ustekinumab = 1.0). From the K_D values, the affinity of the mAbs to FcRn was assessed to be similar to the Ustekinumab-FcRn affinity if differences were smaller than one decimal power to the Ustekinumab-FcRn K_D . K_D s were rated as different if K_D differences were bigger than one decimal power to the Ustekinumab-FcRn K_D . The FcRn affinities at pH 6.0 fell in a narrow range for all mAbs. Briakinumab had a relative K_D of 0.2 and the variants ranged between Briakinumab and Ustekinumab except for mAb 10 that had a relative K_D of 1.1 (Table 4-8).

Table 4-8: Relative K_D s of all mAbs to FcRn

Relative K_D values (Ustekinumab = 1) are presented as the mean ($n = 3$) \pm standard deviation.

Sample	rel. K_D
Ustekinumab	1
Briakinumab	0.2 \pm 0.07
mAb 1	1.0 \pm 0.22
mAb 2	0.3 \pm 0.19
mAb 3	0.2 \pm 0.06
mAb 4	0.5 \pm 0.08
mAb 5	0.9 \pm 0.16
mAb 6	0.4 \pm 0.17
mAb 7	0.2 \pm 0.03
mAb 8	0.4 \pm 0.07
mAb 9	0.4 \pm 0.04
mAb 10	1.1 \pm 0.09

4.4.2. FcRn-mAb dissociation

The dissociation of FcRn and the mAbs was analyzed by SPR and FcRn affinity chromatography.

4.4.2.1. FcRn-mAb dissociation using SPR

K_D values were evaluated as follows: K_D values below 1 μ M were assessed to show moderate affinity, between 1-5 μ M to show weak affinity and above 5 μ M to show no binding to FcRn. Briakinumab and Ustekinumab showed similar affinities at pH 6.0. Ustekinumab showed very weak affinity at pH 6.6 and no affinity at pH 6.8. In contrast, Briakinumab showed a moderate affinity up to pH 6.8, weak affinity at pH 7.0 and no binding at pH 7.2 (Table 4-9).

Table 4-9: K_D of Briakinumab and Ustekinumab to FcRn

K_{DS} were calculated using buffers with increasing pH values. K_D values higher than 5 μM were classified as no binding.

	Briakinumab K_D [μM]	Ustekinumab K_D [μM]
pH 6.0	0.09	0.39
pH 6.4	0.10	1.00
pH 6.6	0.36	3.10
pH 6.8	0.60	no binding
pH 7.0	4.20	no binding
pH 7.2	no binding	no binding

4.4.2.2. FcRn affinity chromatography using a pH gradient

For analysis of the FcRn-mAb dissociation at physiological pH the FcRn affinity chromatography was used because SPR does not provide precise information about the dissociation pH. The FcRn affinity chromatography closely mimics physiological conditions for the dissociation between FcRn and IgGs. The principle is shown in Figure 4-15. The method describes a chromatography method that uses a column packed with high concentration of FcRn. Antibodies bind at acidic pH of 5-6 to the FcRn and afterwards elute from the FcRn column due to increasing pH. Therefore the FcRn affinity chromatography gives precise information about the pH dependency of the FcRn-IgG dissociation.

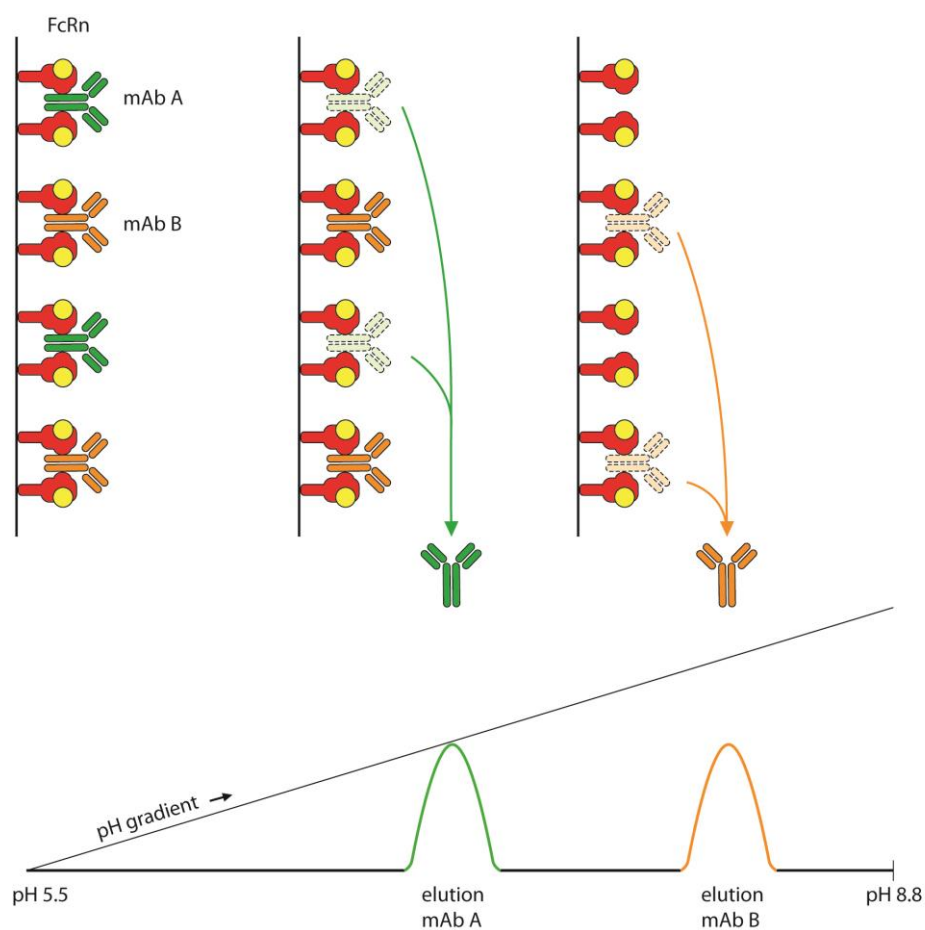


Figure 4-15: Principle FcRn affinity chromatography

IgGs bind to the FcRn at pH 5.5 and are eluted by a linear pH gradient from pH 5.5 to 8.8. Retention times and elution pHs can be measured.

Briakinumab and Ustekinumab showed striking retention time differences. Briakinumab eluted after 93.7 min, whereas Ustekinumab eluted after 84.4 min (Figure 4-16). These retention times correspond to elution pHs of 7.9 and 7.4 for Briakinumab and Ustekinumab, respectively. These differences in FcRn-mAb dissociation are in agreement with the SPR results (4.4.2.1). Using both methods, the interaction between Briakinumab and FcRn seems to be stronger at higher pH values than between Ustekinumab and FcRn.

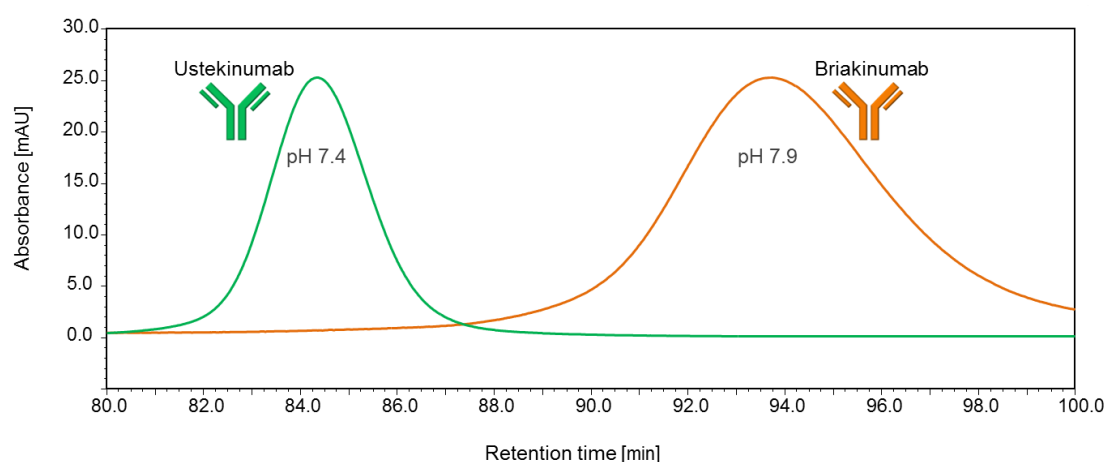


Figure 4-16: FcRn column chromatogram of Briakinumab and Ustekinumab
Sample peaks are normalized to Briakinumab's main peak.

To investigate whether the retention time differences of Briakinumab and Ustekinumab are influenced by the Fab region, both antibodies were cleaved using IdeS. The $F(ab')_2$ region did not bind to FcRn and eluted in the first minutes after injection indicating that the Fc region is indispensable for the interaction with FcRn. The cleaved Fc regions of Briakinumab and Ustekinumab eluted after 85.6 min (elution pH of 7.5) and 85.2 min (elution pH 7.4), respectively (Figure 4-17). The nearly identical retention times of the IdeS-cleaved Fc regions of Briakinumab and Ustekinumab indicate the negligible role of the Fc region in this setting and point toward the role of the Fab region on FcRn-mAb dissociation.

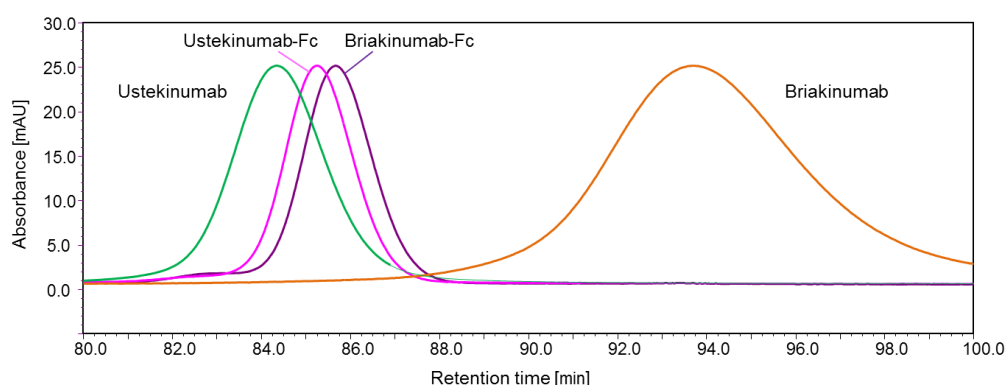


Figure 4-17: FcRn column chromatogram of IdeS-cleaved Fc regions
Sample peaks are normalized to Briakinumab's main peak.

To further elucidate which structural elements of the Fab region are mainly

influencing FcRn column retention times, the antibody variants mAb 1 and mAb 2 were analyzed for FcRn column binding (Figure 4-18). MAb 1, which bears the Fv domain of Ustekinumab on the constant parts of Briakinumab, had the same FcRn column retention time as Ustekinumab. MAb 2, containing the Fv domain of Briakinumab on the Ustekinumab constant domains, eluted close to Briakinumab indicating that the Fv domain influences the interaction with FcRn.

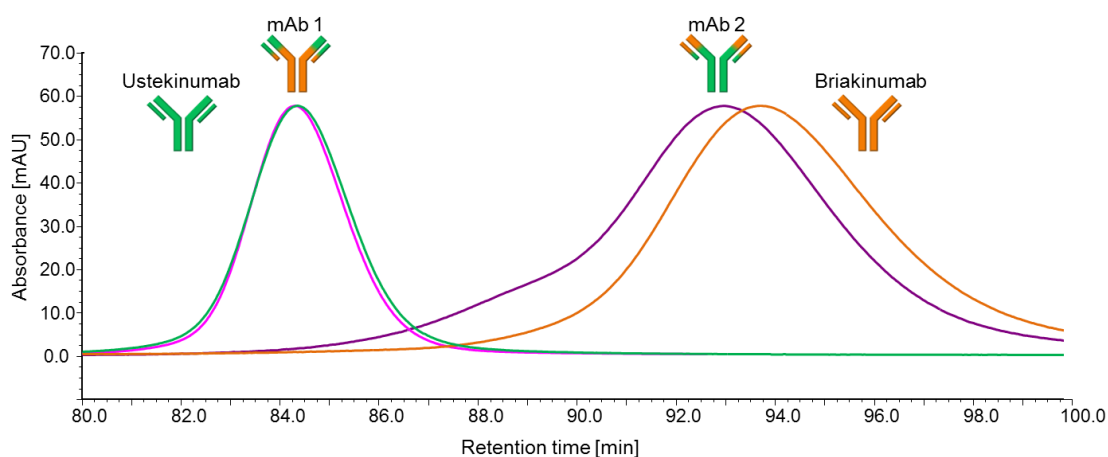


Figure 4-18: FcRn column chromatogram of Fv-exchanged variants

Sample peaks are normalized to Briakinumab's main peak.

The influence of the LCs was analyzed using mAb 3 and mAb 4. MAb 3, comprising the HCs of Ustekinumab and the LCs of Briakinumab, eluted close to Briakinumab (Figure 4-19). MAb 4, containing Ustekinumab LCs and Briakinumab HCs, eluted close to Ustekinumab revealing the strong impact of the LC on FcRn-mAb interaction.

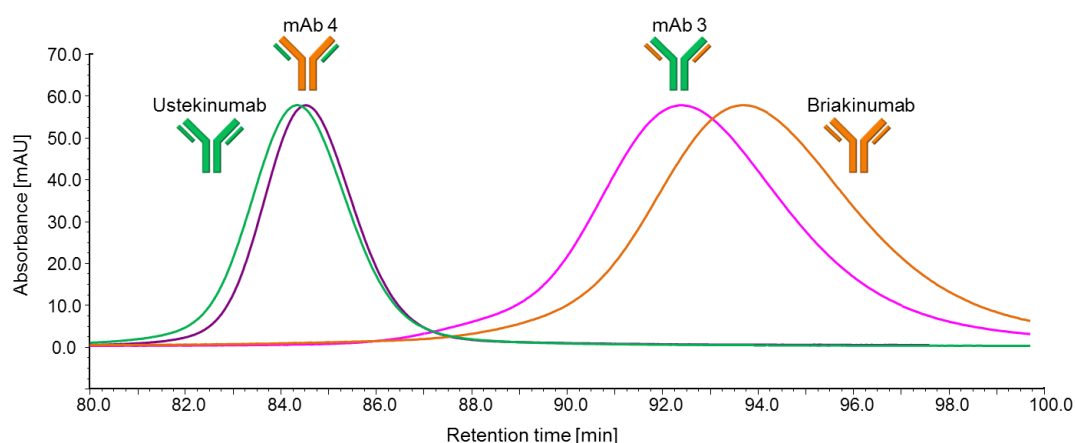


Figure 4-19: FcRn column chromatogram of LC-exchanged variants

Sample peaks are normalized to Briakinumab's main peak.

To study the influence of the CDRs on FcRn dissociation, mAb 5 and mAb 6 were tested for FcRn column interaction (Figure 4-20). MAb 5, that has Ustekinumab CDRs grafted on Briakinumab, has a retention time shift close to the retention time of Ustekinumab. The opposite was not observed to the same extent. MAb 6, Briakinumab CDRs on Ustekinumab, described an elution profile which was still close to that of Ustekinumab.

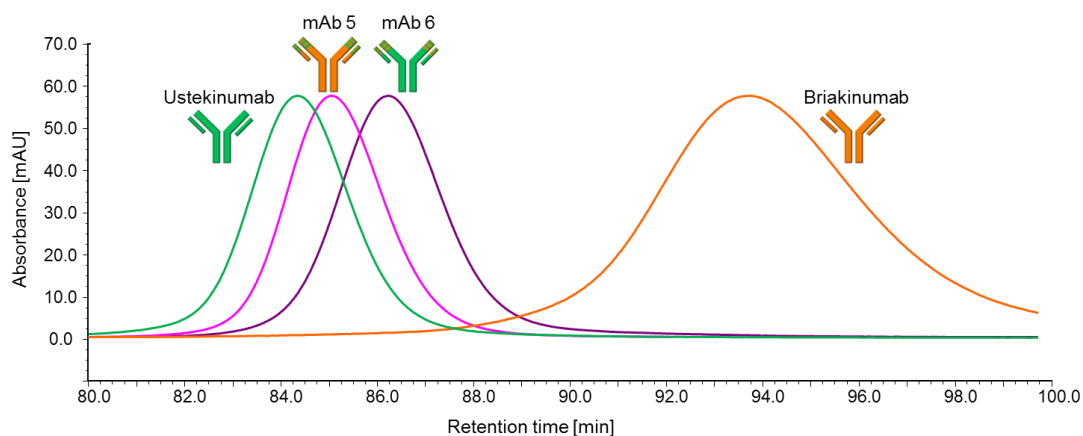


Figure 4-20: FcRn column chromatogram of CDRs-exchanged variants

Sample peaks are normalized to Briakinumab's main peak.

The results so far suggested that the light chain CDRs of Briakinumab have the main influence on FcRn column retention times. To confirm this hypothesis the FcRn-mAb interaction was analyzed using mAbs bound to their target. By binding to the target, the CDRs of the mAbs are shielded, thereby repressing the influence of the

CDRs on the FcRn-mAb interaction. Briakinumab as well as Ustekinumab bind human IL-12 with high affinity, therefore the mAb-IL-12 complex is supposed to be very stable.

Ustekinumab and Ustekinumab-IL-12 complex have identical FcRn column retention times of 82.8 minutes (Figure 4-21). Ustekinumab-IL-12 complex shows a fronting before the main peak, but the main peak retention time is identical to unbound Ustekinumab.

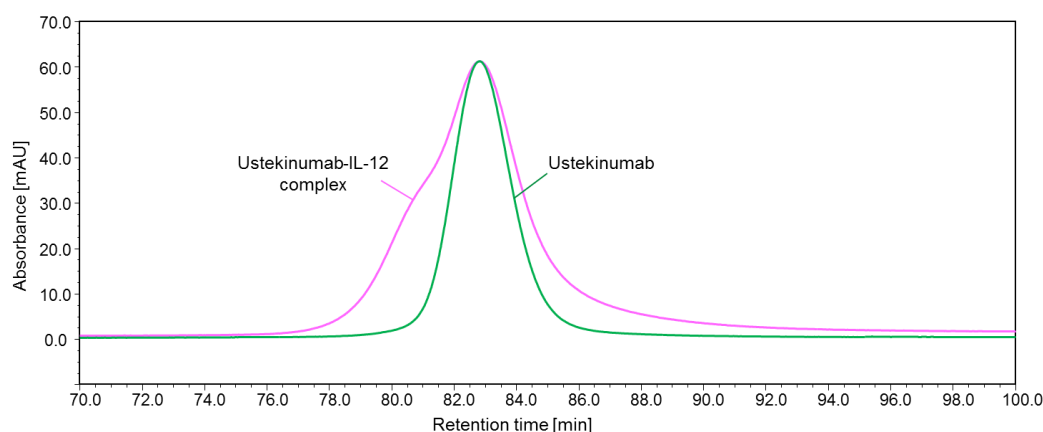


Figure 4-21: FcRn column chromatogram of Ustekinumab-IL-12 complex
Sample peaks are normalized to Ustekinumab's main peak.

The Briakinumab-IL-12 complex assembled using an excess of Briakinumab shows three fractions with different FcRn column retention times. The main peak has the same retention time as Briakinumab of about 93 min (Figure 4-22). Therefore it was assumed that the main fraction is probably unbound Briakinumab. Prepeak 1 and prepeak 2 elute at 85 min and 80 min, respectively. Prepeak 1 could be a fraction including Briakinumab with one bound IL-12, by which the CDRs of one Fab-arm are shielded while the other one remains unshielded. Prepeak 2 could be a fraction including Briakinumab with two bound IL-12, by which CDRs of both Fab-arms are shielded.

This assignment was further confirmed by the FcRn column profile of the Briakinumab-IL-12 complex assembled using an IL-12 excess. The IL-12 excess shifts the balance towards a complex of two IL-12 molecules binding to one Briakinumab molecule. The FcRn column retention times are nearly identical to the

ones of the prepeak 2 of the Briakinumab-IL-12 complex consisting of Briakinumab-excess, therefore prepeak 2 presents most likely Briakinumab bound to two IL-12 molecules.

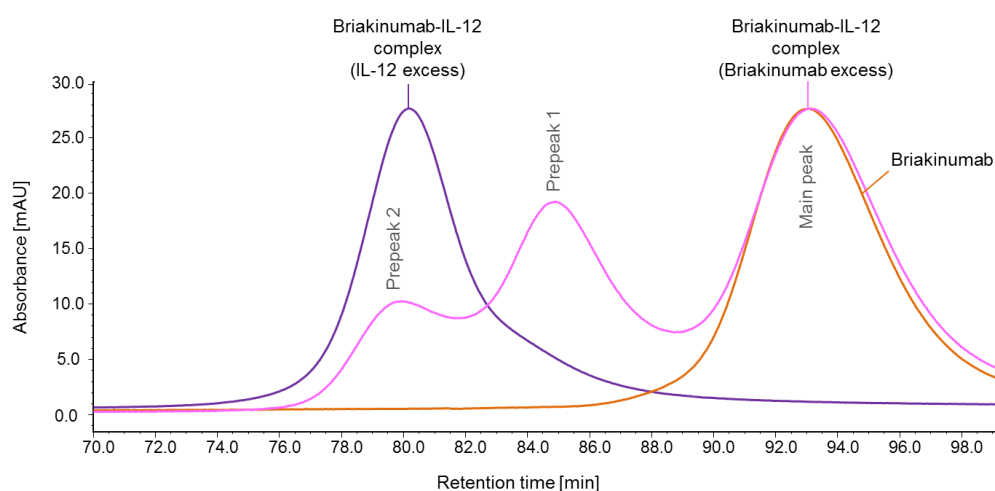


Figure 4-22: FcRn column chromatogram of Briakinumab-IL-12 complex

Sample peaks are normalized to the main peak of Briakinumab-IL-12 complex assembled using IL-12 excess.

By binding to the target and thereby shielding the CDRs of the antibodies the Briakinumab-FcRn interaction is more affected than the Ustekinumab-FcRn interaction. Shielding the CDRs of Ustekinumab does not influence the interaction with FcRn. In contrast, repressing the influence of the CDRs on the FcRn-Briakinumab interaction, by binding to the target, results in faster dissociation from the FcRn.

To study the nature of the FcRn-mAb interaction further, the FcRn column retention times were measured in the presence of increasing salt concentrations in both eluents of the pH gradient system. Charge-mediated interactions are thereby weakened, whereas hydrophobic interactions are strengthened under high ionic strength conditions. The FcRn column retention time of Ustekinumab remained essentially unaffected by higher salt concentrations (Figure 4-23). In contrast, the retention time of Briakinumab was shortened in the presence of salt in a manner roughly proportional to the inverse square root of the ionic strength (Figure 4-24) as suggested by the Debye-Hückel law of charge screening (Israelachvili 1985). In

conclusion, a significant part of the excessive FcRn-Briakinumab interaction seems to be charge-mediated.

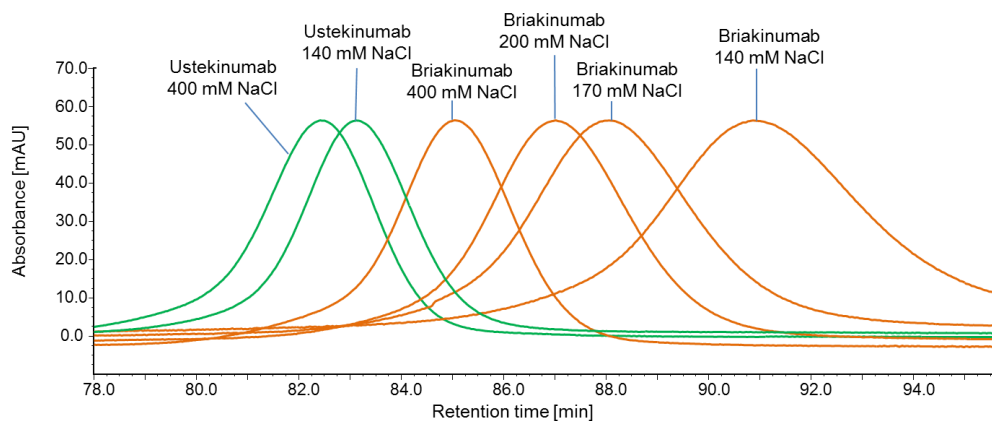


Figure 4-23: FcRn column chromatogram under higher ionic strength conditions

Sample peaks are normalized to the main peak of Briakinumab using 140 mM NaCl.

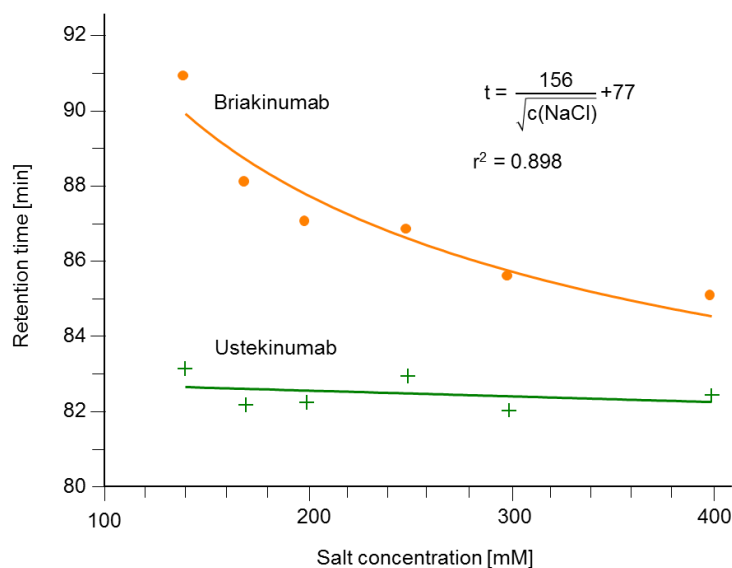


Figure 4-24: Salt-dependent FcRn-mAb interaction of Briakinumab and Ustekinumab

Retention times are plotted against the salt concentration. A regression line is generated for Ustekinumab's data. Briakinumab's data are fitted to an inverse square root function with $1/\sqrt{c(\text{NaCl})}$ ($r^2 = 0.898$).

To further study the charge-mediated FcRn-mAb interaction, Briakinumab variants with smaller positively charged regions in the V_H and V_L domain were analyzed for FcRn-mAb dissociation behavior.

FcRn column retention times seemed to be mainly influenced by the V_L domain. It needed to be studied if the large positively charged region in the V_H domain of Briakinumab (Figure 4-5) has also an influence on FcRn-mAb dissociation. Therefore the FcRn-mAb dissociation was analyzed using two variants of Briakinumab with smaller positively charged regions in the V_H domain, mAb 7 and mAb 8. Both mAbs showed shorter retention times compared to Briakinumab (Figure 4-25). This confirms the hypothesis that a Briakinumab-variant with smaller positively charged region dissociates faster from FcRn than Briakinumab. The differences in retention time are not as large as with exchanged LCs or Fv domains, but they nevertheless seem to influence FcRn-mAb interaction. MAb 7 with three mutated amino acids and mAb 8 with five mutated amino acids showed nearly identical retention times of 90.4 and 90.1 min, respectively, indicating that additional mutation of R16^{HC}A and R57^{HC}A does not influence FcRn-mAb dissociation.

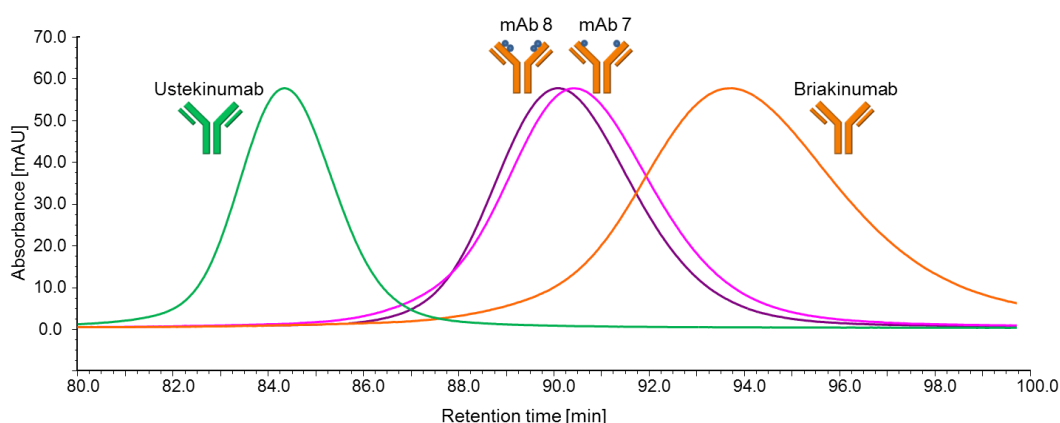


Figure 4-25: FcRn column chromatogram of Briakinumab-variants with modified charge distribution in the V_H domain

Sample peaks are normalized to Briakinumab's main peak.

The influence of charged regions in the V_L on FcRn-mAb interaction was analyzed using the variants with smaller positively charged regions in the V_L domain. A strong retention time shift from Briakinumab in the direction of Ustekinumab was observed

for mAb 9, that is a Briakinumab-variant with three positively charged residues in the V_L domain mutated to alanines (Figure 4-26). Additional mutation of 5 basic amino acids in the V_H domain of Briakinumab (mAb 10) shortened FcRn column retention times even more, so that mAb 10 had almost the same retention time as Ustekinumab.

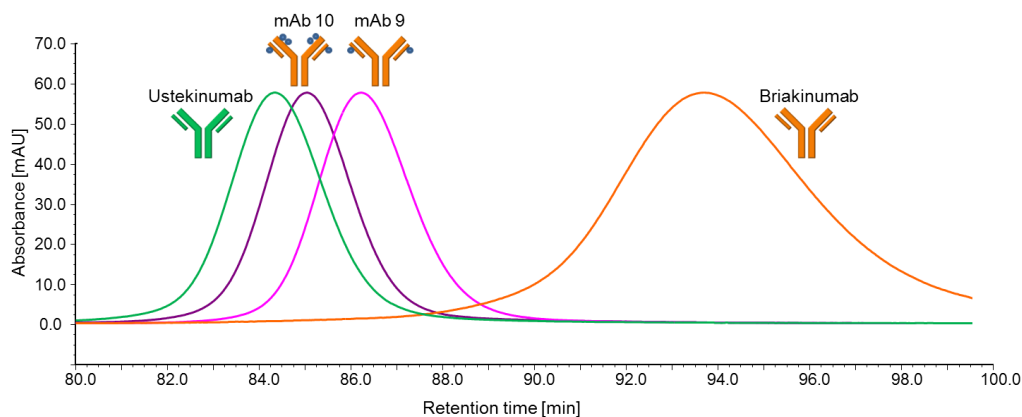


Figure 4-26: FcRn column chromatogram of Briakinumab-variants with modified charge distribution in the V_H and V_L domain


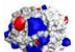
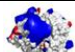
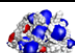
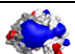
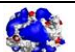

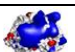
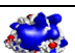
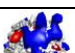
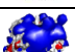
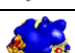
Sample peaks are normalized to Briakinumab's main peak.

In summary, FcRn affinity chromatography of the engineered variants showed that antibodies with the same Fv domain and the same LC elute at nearly identical FcRn column retention times. Furthermore, grafting Ustekinumab CDRs on Briakinumab (mAb 5) shifts the retention time close to that of Ustekinumab. Combining these results leads to the conclusion that the light chain variable domain (V_L), and for Briakinumab especially the light chain CDRs, provide the main influence on the FcRn-mAb interaction.

FcRn column retention times were compared with net charges of the Fv domains at pH 6.0 or pH 7.4, hydrophobicity, isoelectric points and the extent of charged regions in the Fv structures (Table 4-10) to find the parameter that mainly influences FcRn-mAb dissociation.

Table 4-10: FcRn affinities, calculated net charges and hydrophobicity

Antibodies are sorted according to the FcRn column retention times. Isopotential surfaces of the proteins protonated at pH 7.4 and contoured at $2 k_B T/e$. The K_D was normalized to the K_D of Ustekinumab. Relative K_D values (Ustekinumab = 1) are presented as the mean ($n=3$) \pm standard deviation. The net charge [e^-] of V_H , V_L and Fv domains at pH 6.0 and pH 7.4 were calculated assuming all cysteines are involved in disulfide bridges. The hydrophobicity is presented relative to low and high hydrophobic RS.

		Ret.Time [min]	rel. K_D	calc. pI (IgG)	q (V_L) pH 6	q (V_L) pH 7.4	q (V_H) pH 6	q (V_H) pH 7.4	q (Fv) pH 6.0	q (Fv) pH 7.4	Hydro- phobicity [%]
Ustekinumab		84.3	1.0	9.4	2.1	1.9	3.1	2.9	5.2	4.9	-1
mAb 1		84.3	1.0 ± 0.22	9.5	2.1	1.9	3.1	2.9	5.2	4.9	-6
mAb 4		84.5	0.5 ± 0.08	9.5	2.1	1.9	6.4	4.3	8.4	6.2	-4
mAb 5		85.1	0.9 ± 0.16	9.6	2.1	1.9	4.1	3.9	6.1	5.9	13
mAb 10		85.1	1.1 ± 0.09	9.0	0.8	0.0	1.4	-0.7	2.2	-0.6	34
mAb 6		86.2	0.4 ± 0.17	9.4	3.9	3.0	5.4	3.3	9.2	6.3	12
mAb 9		86.2	0.4 ± 0.04	9.4	0.8	0.0	6.4	4.3	7.2	4.3	16
mAb 8		90.1	0.4 ± 0.07	9.3	3.8	3.0	1.4	-0.7	5.2	2.3	24
mAb 7		90.4	0.2 ± 0.03	9.4	3.8	3.0	3.4	1.3	7.2	4.3	13
mAb 3		92.4	0.2 ± 0.06	9.5	3.8	3.0	3.1	2.9	6.9	6.0	8
mAb 2		93.0	0.3 ± 0.19	9.4	3.8	3.0	6.4	4.3	10.2	7.3	8
Briakinumab		93.7	0.2 ± 0.07	9.7	3.8	3.0	6.4	4.3	10.2	7.3	7

FcRn column retention times did not correlate with the hydrophobicity or the isoelectric points or the net charges of the Fv domains at lysosomal pH 6.0 or physiological pH 7.4. Instead it was observed that FcRn column retention times increased with the extent of positively charged regions on the Fv structures, especially around the V_L domain. Figure 4-27 summarizes the pH-dependent FcRn-mAb interaction of all mAbs and the corresponding charge distributions in the Fv domain.

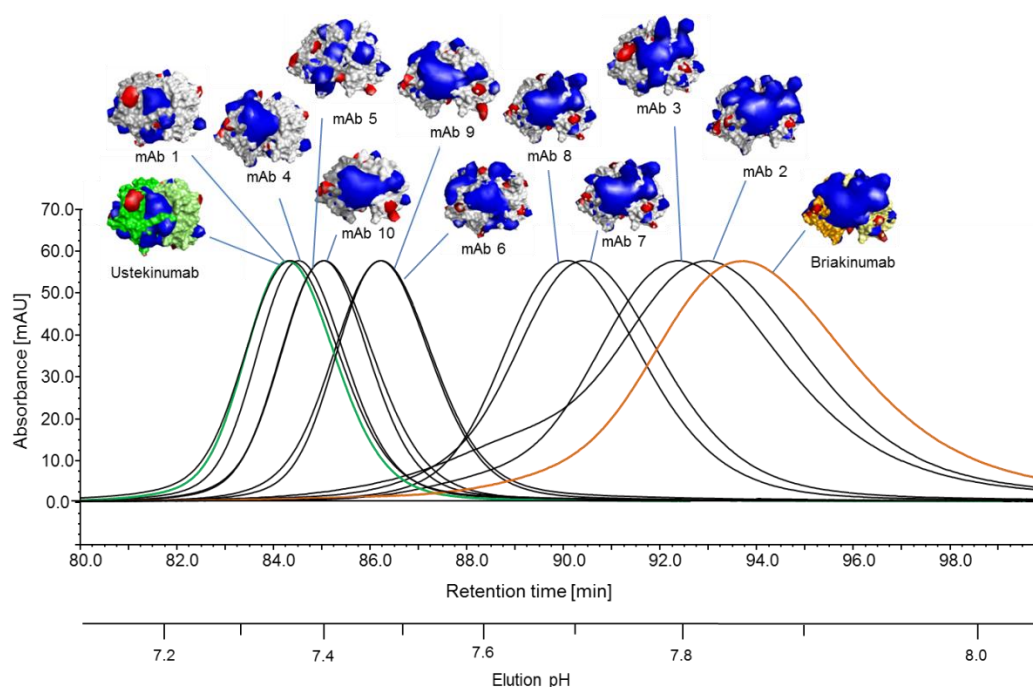


Figure 4-27: pH-dependent FcRn-mAb interaction of all mAbs

A molecular surface representation of the structural models, protonated at pH 7.4, was superimposed with isopotential surfaces contoured at $2 k_B T/e$. A second horizontal axis indicates the elution pH, interpolated from offline pH measurements. Sample peaks are normalized to Briakinumab's main peak.

4.4.2.3. FcRn affinity chromatography using a salt gradient

Based on the previous findings that the FcRn-mAb interaction seems to be charge-mediated, a method was developed to analyze charge-mediated interactions within one run. For this purpose, the pH-gradient FcRn affinity chromatography method was modified. The FcRn column was used but a salt gradient from 0 to 250 mM NaCl at pH 7.8 instead of a pH-gradient was used. Antibodies with larger charged regions should need higher salt concentrations to dissociate from the FcRn and have an increased retention time. The elution order of the mAbs is nearly identical using pH-gradient and salt-gradient FcRn affinity chromatography (Figure 4-28). Except mAb 10 has a different elution profile with reduced FcRn column retention times using salt gradient instead of pH gradient. The peak pattern of mAb 10 has also a non-uniform form which indicates that the sample may include fractions with different FcRn binding. This phenomenon could not be elucidated, but in general antibodies with larger positively charged regions in the Fv domain need higher salt

concentrations to dissociate from the FcRn. This finding also confirms the charge-mediated FcRn-mAb interaction.

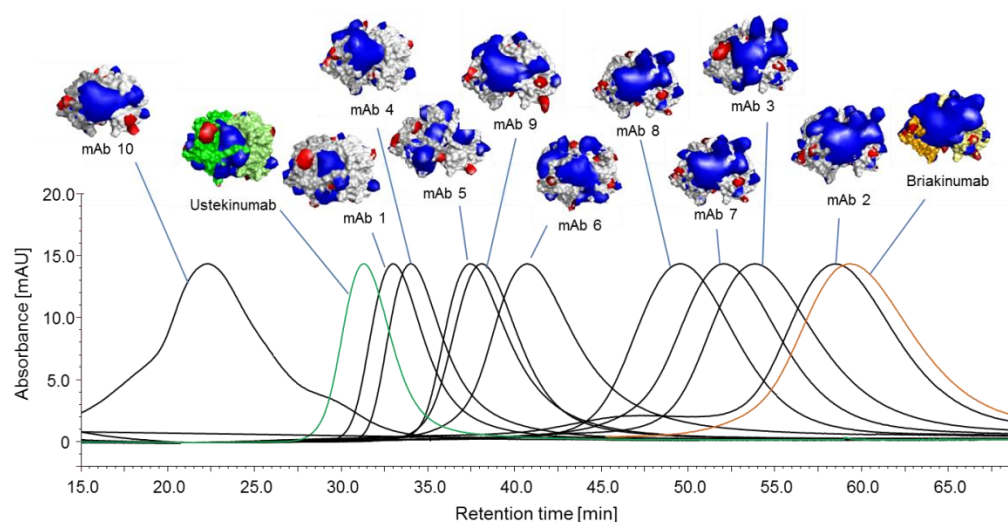


Figure 4-28: Salt-dependent FcRn-mAb interaction of all mAbs

A molecular surface representation of the structural models, protonated at pH 7.4, was superimposed with isopotential surfaces contoured at $2 k_B T/e$. Sample peaks are normalized to Briakinumab's main peak.

4.5. *In vivo* studies

To analyze if different FcRn-mAb interactions have an influence on PK, *in vivo* studies in human FcRn transgenic and FcRn knockout mice were performed.

4.5.1. *In vivo* study in human FcRn transgenic mice

To assess whether the effect of modified charged regions in the variable domains on FcRn-mAb interaction translates into modulated *in vivo* PK properties, PK studies in human FcRn transgenic mice were conducted. Briakinumab, Ustekinumab, together with Briakinumab-variants with modified charge distribution in the V_H (mAb 8) and V_L domain (mAb 9), were tested. These four antibodies were chosen because the elution pHs were equally distributed between pH 7.4 and 7.9 (Figure 4-29). Additionally, mAb 8 and mAb 9 are Briakinumab-variants with modified charge distribution in the V_H and V_L domain, respectively, therefore the effect of different charge distributions in the Fv domain on PK can be investigated.

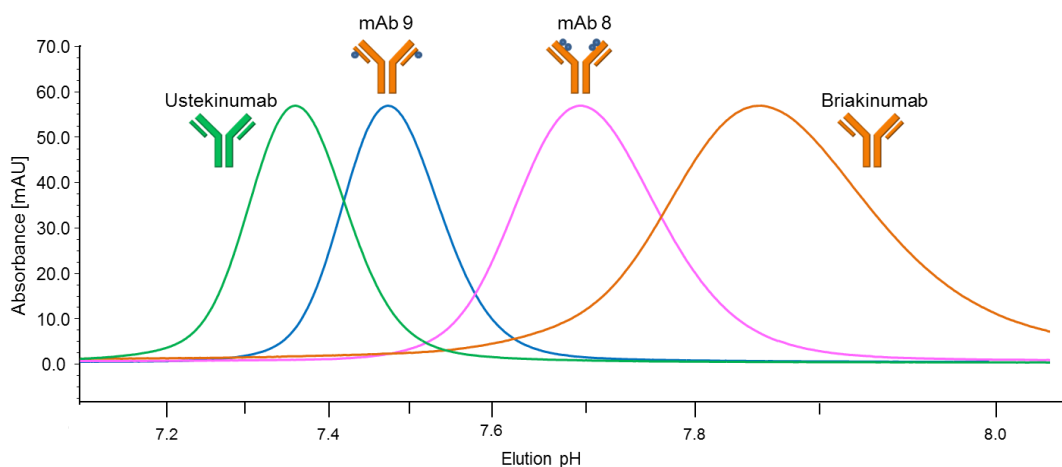


Figure 4-29: FcRn column chromatogram of antibodies used in mouse PK study

Ustekinumab, mAb 9, mAb 8 and Briakinumab have elution pHs of 7.4, 7.5, 7.7 and 7.9, respectively. Sample peaks are normalized to Briakinumab's main peak.

After i.v. administration of 10 mg/kg antibody, the typical kinetic profile for an IgG1 was observed (Figure 4-30), which is divided into alpha and beta phases (Roopenian et al. 2010). The alpha phase occurs rapidly (in the first 24 hours) and shows mainly the distribution process until the administered antibody reaches equilibrium. The beta

phase demonstrates the log-linear serum concentration-time relationship in the following days where elimination processes occur. The kinetic profiles show that Briakinumab has a different alpha phase with faster distribution compared to the alpha phases of Ustekinumab, mAb 8 and mAb 9. Ustekinumab, mAb 8 and mAb 9 are comparable within the first 24 hours.

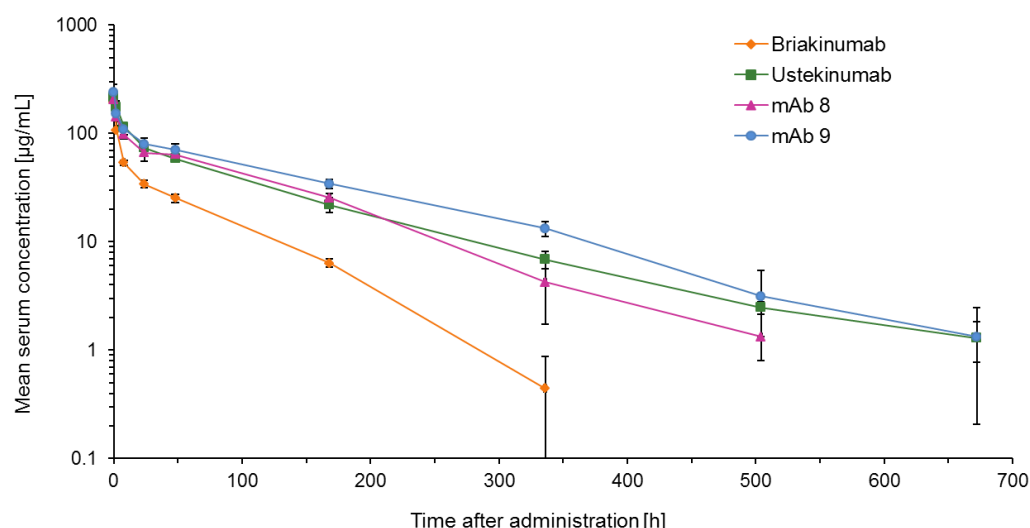


Figure 4-30: Blood level curves in human FcRn transgenic mice

Antibodies were administered as a single i.v. bolus injection of 10 mg/kg to 6 animals per group. Data points represent the mean \pm standard deviation.

The following PK parameters were calculated and summarized in Table 4-11: area under the curve (AUC_{0-inf}), clearance (Cl), volume of distribution at steady state (V_{ss}) and the terminal half-life ($T_{1/2}$).

Table 4-11: PK parameters in human FcRn transgenic mice

PK parameters were calculated after administration of 10 mg/kg to 6 animals per group. PK data represent the mean \pm standard deviation.

Sample	AUC_{0-inf} [h*mg/mL]	Cl [mL/min/kg]	V_{ss} [L/kg]	$T_{1/2}$ [h]
Briakinumab	4.3 ± 0.2	0.0394 ± 0.001	0.162 ± 0.015	48 ± 9
Ustekinumab	12.2 ± 0.9	0.0137 ± 0.001	0.116 ± 0.006	137 ± 48
mAb 8	11.5 ± 0.8	0.0146 ± 0.001	0.101 ± 0.013	78 ± 22
mAb 9	16.0 ± 0.9	0.0104 ± 0.001	0.099 ± 0.011	109 ± 13

AUC_{0-inf} and clearance are influenced by distribution and elimination processes. Due

to Briakinumab's different alpha phase AUC_{0-inf} and Cl differ between Briakinumab and the other mAbs. Briakinumab has also a bigger V_{SS} than the other mAbs.

The focus of this work was to elucidate the influence of the Fv domain on FcRn-mediated IgG-recycling, therefore the terminal half-life was examined, which is exclusively calculated in the elimination phase where FcRn-mediated IgG-recycling dominates (Roopenian et al. 2010). The order by $T_{1/2}$ is the following: Briakinumab < mAb 8 < mAb 9 < Ustekinumab.

The terminal half-lives were compared with the isoelectric points and the hydrophobicity of the mAbs. Neither isoelectric points nor the hydrophobicity correlate with the terminal half-life *in vivo* (Figure 4-31) indicating that these parameters do not mainly influence the terminal half-life. In contrast, the terminal half-lives of the four antibodies correlate linearly with the *in vitro* FcRn column elution pHs (Figure 4-32). Higher FcRn column elution pHs result in shorter terminal half-lives. A Pearson correlation factor of 0.9924 confirms an existing correlation between terminal half-life *in vivo* and FcRn column elution pH *in vitro*.

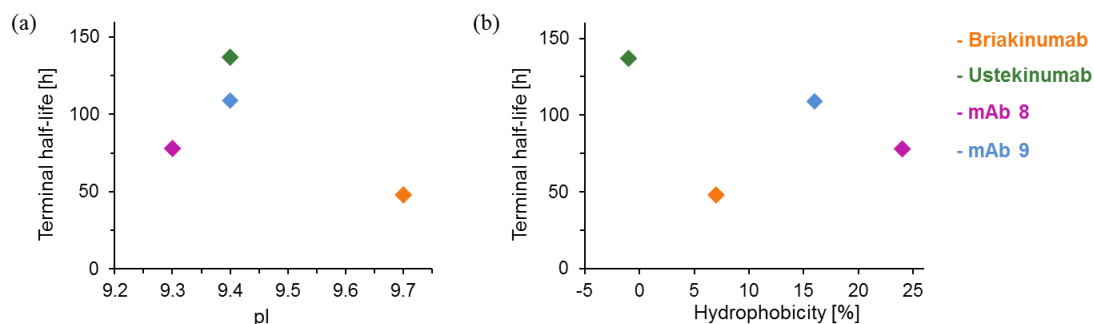


Figure 4-31: Correlation between terminal half-life and isoelectric point or hydrophobicity

Terminal half-lives are plotted against (a) isoelectric points and (b) hydrophobicity.

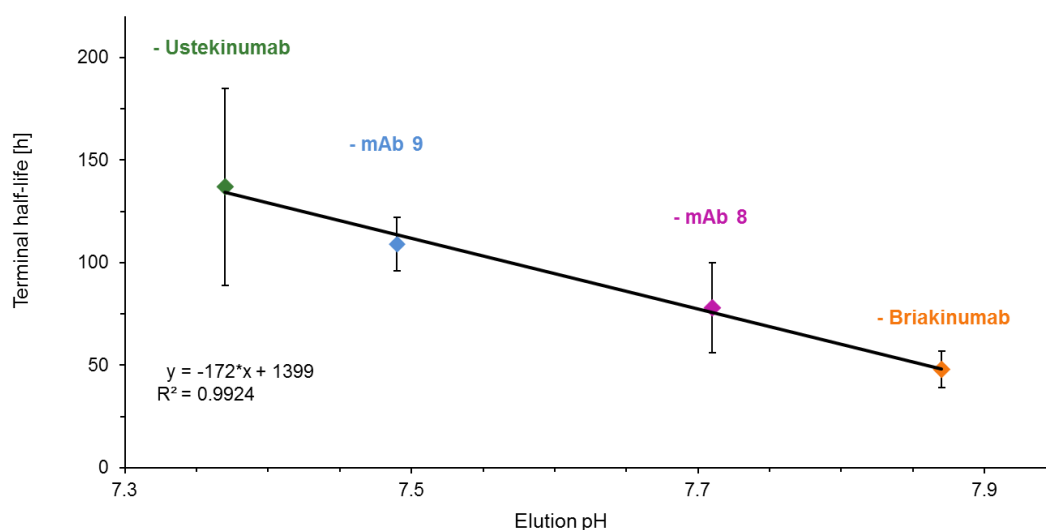


Figure 4-32: Correlation between *in vivo* terminal half-life and FcRn column elution pH

Terminal half-lives are plotted against the corresponding elution pHs. A regression line is generated and the correlation factor R^2 is calculated.

A statistical analysis of the terminal half-lives was calculated using the Tukey HSD Test. A statistically significant difference could be detected between the terminal half-lives of Briakinumab and Ustekinumab, Briakinumab and mAb 9 as well as Ustekinumab and mAb 8.

PK can also be influenced by anti-drug antibodies (ADAs), therefore serum samples were tested for the existence of ADAs by detection of drug/ADA immune complexes. After i.v. administration of 10 mg/kg Briakinumab in human FcRn transgenic mice Briakinumab/ADA immune complexes were first detected after about 336 hours (14 days, Table 4-12).

Table 4-12: ADA-positive samples after Briakinumab administration in human FcRn transgenic mice

Serum concentrations of each sampling time point after i.v. administration of 10 mg/kg Briakinumab. ADA-positive samples are illustrated as * and ** describing formation of moderate and severe drug/ADA immune complexes, respectively. (B.l.q. = below limit of quantification)

Time [h/d]	M 1 [µg/mL]	M 2 [µg/mL]	M 3 [µg/mL]	M 4 [µg/mL]	M 5 [µg/mL]	M 6 [µg/mL]
0.08	201	174	188	192	214	194
2	109	105	106	105	110	110
8	50	53	53	54	56	58
24/ 1	37	32	30	34	35	35
48/ 2	27	23	24	27	24	28
168/ 7	6.2	5.4	6.7	6.7 *	6.4	6.8
336/ 14	0.4	1.0 *	0.1 **	0.2 **	0.7 *	0.1**
504/ 21	b.l.q.	b.l.q.**	b.l.q.**	b.l.q.**	b.l.q.**	b.l.q.**
672/ 28	b.l.q.	b.l.q.**	b.l.q.	b.l.q.**	b.l.q.**	b.l.q.**

After administration of mAb 8 and mAb 9 drug/ADA immune complexes were also detected after about 336 hours (14 days, Table 7-3 and Table 7-4). The concentration-time curves show no rapid decrease due to ADA formation, therefore the influence on PK is assessed to be neglected.

In contrast, administration of Ustekinumab did not cause formation of Ustekinumab/ADA immune complexes in human FcRn transgenic mice (Table 7-2).

4.5.2. *In vivo* study in FcRn knockout mice

To confirm that differences in the terminal half-lives in human FcRn transgenic mice were caused by different FcRn-mAb interactions, a second *in vivo* study in FcRn knockout mice was conducted. In order to reduce the number of mice used in this study, only three antibodies were used: Briakinumab, Ustekinumab and mAb 9.

After i.v. administration of 10 mg/kg antibody the clearance of all antibodies is much faster in FcRn knockout mice than in human FcRn transgenic mice due to missing FcRn-mediated IgG-recycling. Division in alpha and beta phase is not clearly

definable because antibodies are eliminated very fast. It can be demonstrated that Briakinumab has a different pharmacokinetic behavior with faster distribution in the first hours after administration compared to Ustekinumab and mAb 9 (Figure 4-33). These findings were also observed in human FcRn transgenic mice indicating that the distribution process in the first hours after administration is not FcRn-mediated.

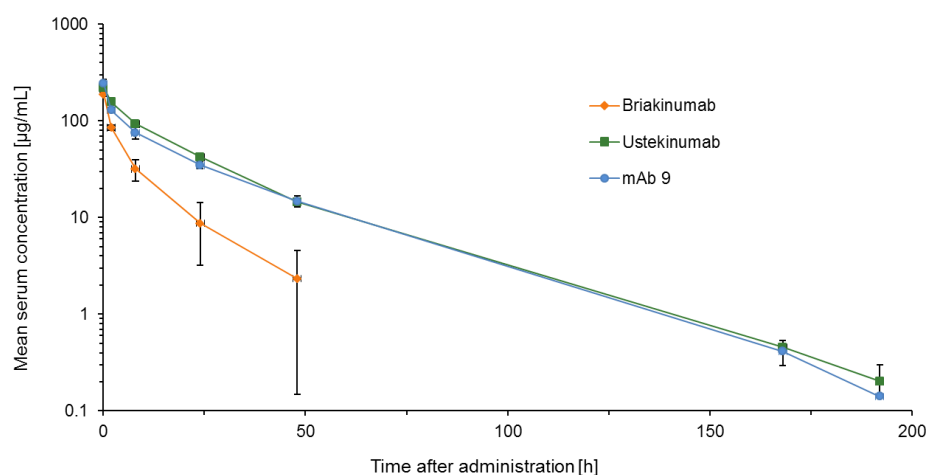


Figure 4-33: Blood level curves in FcRn knockout mice

Antibodies were administered as a single i.v. bolus injection of 10 mg/kg to 6 animals per group. Data points represent the mean \pm standard deviation.

The following PK parameters were calculated and summarized Table 4-13: AUC_{0-inf} , Cl , V_{ss} and $T_{1/2}$.

Table 4-13: PK parameters in FcRn knockout mice

PK parameters were calculated after administration of 10 mg/kg to 6 animals per group. PK data represent the mean \pm standard deviation.

Sample	AUC_{0-inf} [h*mg/mL]	Cl [mL/min/kg]	V_{ss} [L/kg]	$T_{1/2}$ [h]
Briakinumab	1.0 ± 0.1	0.163 ± 0.008	0.113 ± 0.004	10.6 ± 0.6
Ustekinumab	3.3 ± 0.1	0.051 ± 0.002	0.077 ± 0.004	22.8 ± 1.1
mAb 9	2.9 ± 0.1	0.059 ± 0.003	0.093 ± 0.005	23.2 ± 1.2

Ustekinumab and mAb 9 are comparable regarding AUC_{0-inf} , Cl , V_{ss} and $T_{1/2}$. Briakinumab has a smaller AUC_{0-inf} , faster Cl and smaller $T_{1/2}$ than Ustekinumab and mAb 9. The calculation of $T_{1/2}$ might differ from the actual value, because time points after 3 and 4 days would have been needed to calculate $T_{1/2}$ more precisely.

The statistical analysis of the terminal half-lives was calculated using the Tukey HSD Test. A statistical significance could be detected between the terminal half-lives of Briakinumab and Ustekinumab and of Briakinumab and mAb 9.

The formation of ADAs was tested by detection of drug/ADA immune complexes. In FcRn knockout mice administration of 10 mg/kg Briakinumab resulted in formation of Briakinumab/ADA immune complexes after about 168-192 hours (7-8 days, Table 4-14).

Table 4-14: ADA-positive samples after Briakinumab administration in FcRn knockout mice

Serum concentrations of each sampling time point after i.v. administration of 10 mg/kg Briakinumab in FcRn knockout mice. ADA-positive samples are illustrated as * and ** describing formation of moderate and severe drug/ADA immune complexes, respectively.

Time [h/d]	M 1 [µg/mL]	M 2 [µg/mL]	M 3 [µg/mL]	M 4 [µg/mL]	M 5 [µg/mL]	M 6 [µg/mL]
0.08	192	181	200	187	186	178
2	86	79	74	91	89	91
8	31	32	36	31	29	33
24/ 1	6.7	12	7.9	11	6.9	8.0
48/ 2	1.8	2.3	2.7	2.6	2.4	2.2
168/ 7	b.l.q.	b.l.q.	b.l.q. **	b.l.q.	b.l.q. **	b.l.q.
192/ 8	b.l.q. *	b.l.q. *	b.l.q. **	b.l.q. *	b.l.q. **	b.l.q. **
216/ 9	b.l.q. *	b.l.q.	b.l.q. **	b.l.q. **	b.l.q. *	b.l.q. **
336/ 14	b.l.q.	b.l.q. **	b.l.q. *	b.l.q. **	b.l.q. **	b.l.q. *

After administration of mAb 9, drug/ADA immune complexes were also first detected after about 168 hours (7 days, Table 7-7). After administration of Ustekinumab, no Ustekinumab/ADA complexes were detected in FcRn knockout mice (Table 7-6). The concentration-time curves of Briakinumab and mAb 9 show no rapid decrease due to ADA formation. Ustekinumab and mAb 9 have very similar concentration-time curves indicating that ADA formation after mAb 9 administration does not influence PK.

4.6. Second model antibody

The transferability of the results from the Briakinumab-Ustekinumab model antibodies was tested using a second antibody: Bevacizumab.

A Bevacizumab-variant was produced with three amino acids in the CDRs mutated to lysines in the V_L domain to generate a variant with additional positively charged regions. Figure 4-34 presents the sequence alignment of the light chains.

Bevacizumab	DIQMTQSPSS	LSASVGDRVT	ITCSASQDIS	NYLNWYQQKP	GKAPKVLITYF	TSSLHSGVPS
Bevacizumab-variant	DIQMTQSPSS	LSASVGDRVT	ITCSASQKIS	NYLNWYQQKP	GKAPKVLITYF	TSSKHSGVPS
***** *						
Bevacizumab	RFSGSGSGTD	FTLTISSLQP	EDFATYYCQQ	YSTVPWTFGQ	GTKVEIKRTV	AAPSVFIFPP
Bevacizumab-variant	RFSGSGSGTD	FTLTISSLQP	EDFATYYCQQ	YSKVPWTFGQ	GTKVEIKRTV	AAPSVFIFPP
** *****						
Bevacizumab	SDEQLKSGTA	SVVCLLNIFY	PREAKVQWKV	DNALQSGNSQ	ESVTEQDSKD	STYLSSTLT
Bevacizumab-variant	SDEQLKSGTA	SVVCLLNIFY	PREAKVQWKV	DNALQSGNSQ	ESVTEQDSKD	STYLSSTLT
Bevacizumab	LSKADYEKHK	VYACEVTHQG	LSSPVTKSFN	RGEEVQLVES	GGGLVQPGGS	LRLSCAASGY
Bevacizumab-variant	LSKADYEKHK	VYACEVTHQG	LSSPVTKSFN	RGEEVQLVES	GGGLVQPGGS	LRLSCAASGY
Bevacizumab	TFTNYGMNWV	RQAPGKGLEW	VGWINTYTGE	PTYAADFKRR	FTFSLDTSKS	TAYLQMNSLR
Bevacizumab-variant	TFTNYGMNWV	RQAPGKGLEW	VGWINTYTGE	PTYAADFKRR	FTFSLDTSKS	TAYLQMNSLR
Bevacizumab	AEDTAVYYCA	KYPHYYGSSH	WYFDVWGQGT	LVTVSSASTK	GPSVFPLAPS	GTAALGCLVK
Bevacizumab-variant	AEDTAVYYCA	KYPHYYGSSH	WYFDVWGQGT	LVTVSSASTK	GPSVFPLAPS	GTAALGCLVK
Bevacizumab	DYFPEPVTVS	WNSGALTSGV	HTFPAVLQSS	GLYSLSSVVT	VPSSSLGTQT	YICNVNHKPS
Bevacizumab-variant	DYFPEPVTVS	WNSGALTSGV	HTFPAVLQSS	GLYSLSSVVT	VPSSSLGTQT	YICNVNHKPS
Bevacizumab	NTKVDKKVEP	K				
Bevacizumab-variant	NTKVDKKVEP	K				



Figure 4-34: LC-alignment of Bevacizumab and Bevacizumab-variant

Identical amino acids are shown in cyan; V_L domains are shown in italics; CDRs are marked with an asterisk (*).

The heavy chains are identical for Bevacizumab and Bevacizumab-variant (Table 4-15).

Table 4-15: Bevacizumab and Bevacizumab-variant with additional positively charged regions in the V_L domain

Mutation of three amino acids in the CDRs to lysines is illustrated as 1 blue dot. An asterisk (*) marks mutated amino acid residues according to the EU numbering of Kabat.

Name	Description	
Bevacizumab	Bevacizumab wild type	
Bevacizumab-variant	Bevacizumab D27 ^{LC} K, L54 ^{LC} K, T93 ^{LC} K*	

4.6.1. Biochemical characterization

The biochemical characterization included measurement of protein concentration, size and MW distribution. The results are summarized in Table 4-16.

Table 4-16: Overview biochemical characterization of Bevacizumab and Bevacizumab-variant

The concentration is given as the average of 3 measurements. Monomer contents are determined by integration of the SEC-chromatogram. Purity of antibody species is determined by CE-SDS of the intact mAbs and after DTT-reduction.

Sample	Conc. [mg/mL]	SEC [%]	CE-SDS [%]		
			Intact mAb	HC	LC
Bevacizumab	2.40	99.7	93	70	30
Bevacizumab-variant	2.10	99.6	97	69	31

Bevacizumab and Bevacizumab-variant show high monomer contents of at least 99%. The intact mAbs, cleaved HCs and LCs show MWs of about 156-161, 60 and 26-27 kDa, respectively (Figure 4-35). The purity of the intact mAbs and chains is very high (Table 4-16).

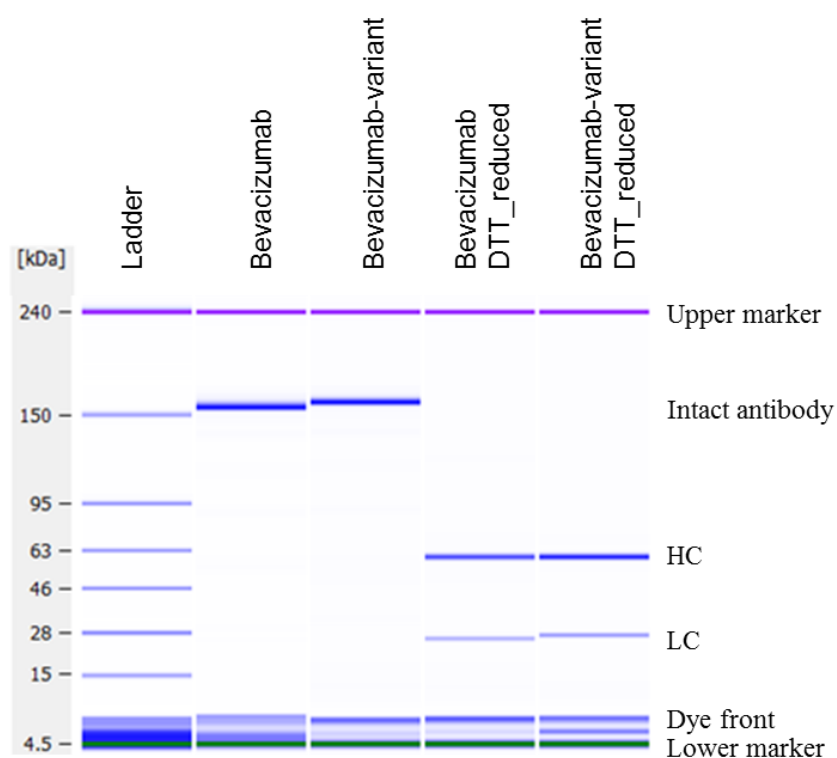


Figure 4-35: Molecular weight of Bevacizumab and Bevacizumab-variant and DTT-reduced mAbs

Gel-like images of the intact mAbs and after DTT-reduction into HCs and LCs.

4.6.1.1. Charge distribution analysis

The charge distribution of Bevacizumab revealed no striking positively or negatively charged regions in the Fv domain. By mutation of two neutral (L54, T93) and one acidic amino acid residue (D27) to basic lysines, a larger positively charged region in the V_L domain was created (Figure 4-36).

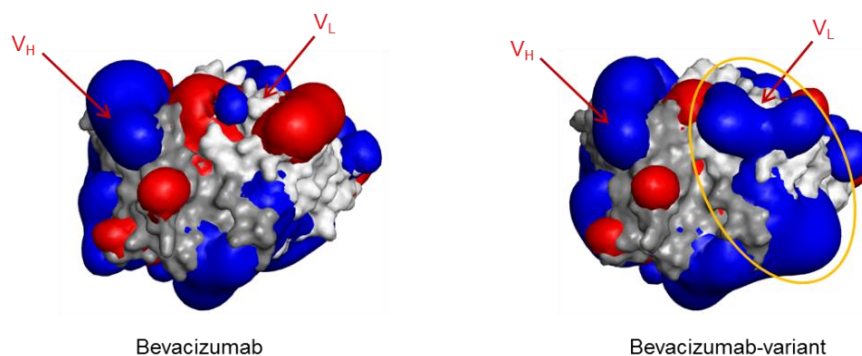


Figure 4-36: Charge distribution of Bevacizumab and Bevacizumab-variant

Isopotential surfaces of the proteins protonated at pH 7.4 and contoured at $1 k_B T/e$; blue: positive; red: negative. A different contour level ($1 k_B T/e$ instead of $2 k_B T/e$) is used for clarity. Orange oval highlights the region of increased positive charge. The light and heavy chains are shown in light and dark grey, respectively. The view focuses on the CDRs.

4.6.2. Functional characterization

The functional characterization consisted of a target binding ELISA.

The Bevacizumab and the Bevacizumab-variant with additional positively charged residues in the Fv domain both bind to VEGF. The binding of the Bevacizumab-variant is slightly reduced to 90% which ranges in the assay deviation (Figure 4-37).

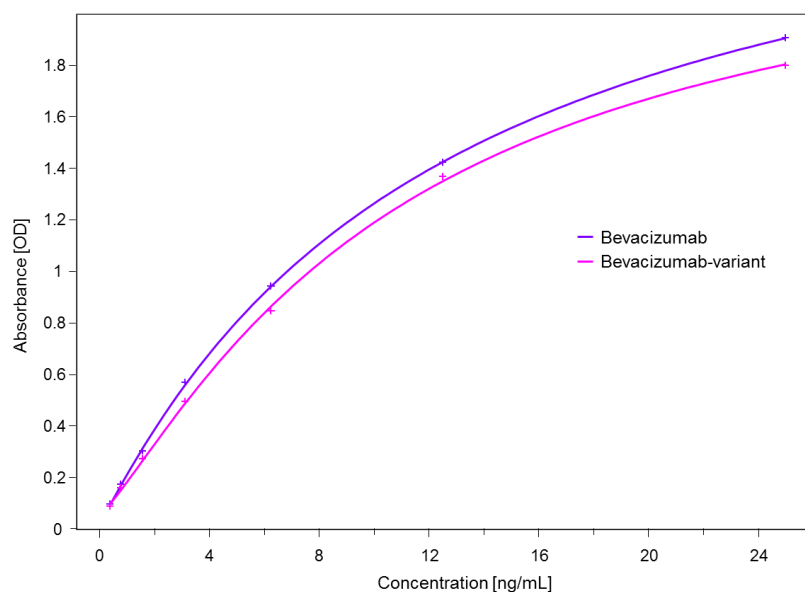


Figure 4-37: VEGF binding of Bevacizumab and Bevacizumab-variant

The absorbance-concentration curves of Bevacizumab and Bevacizumab-variant are similar indicating comparable VEGF affinities.

4.6.3. FcRn-mAb dissociation

Bevacizumab and Bevacizumab-variant showed FcRn column retention time differences of 2.2 min (Figure 4-38). Bevacizumab eluted at an elution pH of 7.4 and Bevacizumab-variant at pH 7.6. The higher elution pH of the Bevacizumab-variant confirms that additional positively charged regions in the Fv domain result in mAb-FcRn dissociation at higher pH values.

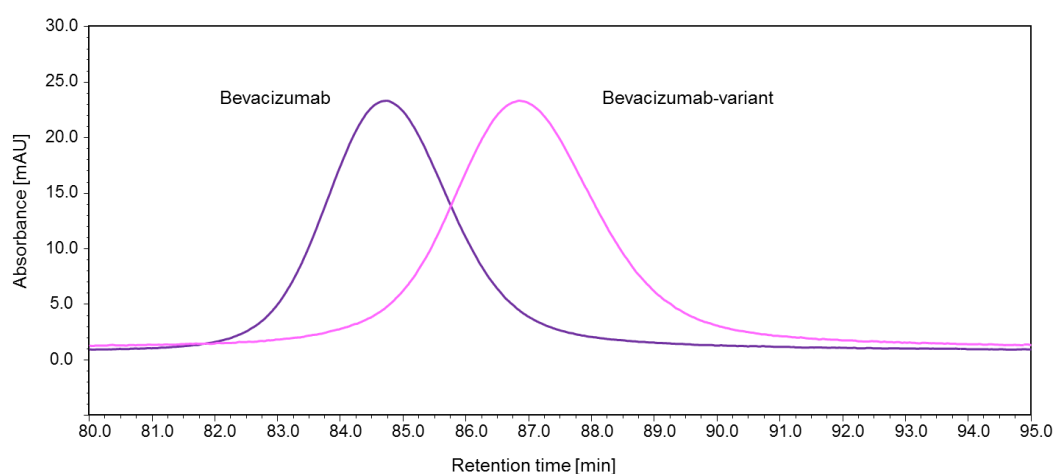


Figure 4-38: FcRn column chromatogram of Bevacizumab and Bevacizumab-variant

Sample peaks are normalized to Bevacizumab's main peak.

5. Discussion

The discussion addresses the question if the Fab region influences FcRn-dependent PK. Briakinumab and Ustekinumab are a very good model system to investigate the influence of the Fab region on PK, because both antibodies have nearly identical Fc sequences and the same target specificity but different terminal half-lives in humans (Gandhi et al. 2010). To investigate the reasons for different PK profiles, factors influencing PK, like target affinity, presence of aggregates and isoelectric points, are analyzed and discussed. Another approach is to study if differences in PK can occur due to differences in the interaction with FcRn. To better understand the influence of the Fab region on PK, systematically engineered variants of Briakinumab and Ustekinumab with cross-over exchanges and modified charge distribution in the Fab region are produced to localize the influencing structural element of the Fab region and to analyze if the interaction is charge-mediated. Finally, the transferability of the findings to other antibodies is discussed.

5.1. Biochemical characterization

The aim of the biochemical characterization was to find differences between Briakinumab and Ustekinumab that might explain the reported differences in the PK behavior in humans (Lima et al. 2009; Zhu et al. 2009).

First, antibodies were tested for their tendency to form aggregates, because the formation of protein aggregates can effect PK in a direct way due to FcγR interactions or indirectly via immunogenic reactions (Putnam et al. 2010). IgG dimers were found to activate immune cells (macrophages and neutrophils) through FcγR triggering (Bleeker et al. 2001). This can result in a higher rate of phagocytosis and increased clearance. High aggregate contents are also reported to induce immunogenic reactions (Putnam et al. 2010). Protein aggregates have a high molecular weight, contain repetitive epitopes and can therefore mimic viruses or bacteria. By binding and cross-linking of B-cell receptors, the formation of ADAs is induced. Formation of drug/ADA immune complexes can subsequently induce a quick elimination of the drug (Brinks et al. 2011). The focus of this work was on soluble aggregates which were analyzed by SEC. In future experiments it would also be interesting to study aggregate formation in more detail, e.g. by analysis of subvisible protein particles. SEC chromatograms of Briakinumab and Ustekinumab show that the content of soluble aggregates is low (< 3%) with the majority of MWs being dimers (Figure 4-3). Furthermore both antibodies are resistant to freeze-thaw and storage-temperature stress. There was hardly any aggregate formation in the stressed samples (Table 4-3 and Table 4-4), so the tendency to form aggregates is for both antibodies relative low. In conclusion, differences in PK are probably not influenced by the presence of soluble aggregates.

Second, the question was raised if differences in hydrophobicity cause differences in PK. Hydrophobicity is defined as the tendency to repel water (Chandler 2005). The antibody structure is folded so that hydrophobic amino acids are clustered together and form a hydrophobic core within the protein. A high content of hydrophobic amino acid residues on the protein surface can be one factor for increased tendency of protein aggregation (Haverick et al. 2014; Joubert et al. 2011). Measured by HIC,

Briakinumab is slightly more hydrophobic than Ustekinumab, but compared to high and low hydrophobic reference samples they are both in a low hydrophobic range (Figure 4-4).

Third, differences in the isoelectric point (pI) were discussed as reason for PK differences. The isoelectric point describes the pH at which antibodies carry no electrical net charge (Boswell et al. 2010). Previous studies have discussed pI differences to be a driving force for altered PK by affecting the electrostatic interaction between the antibody and negatively charged groups on the surface of endothelial cells (Khawli et al. 2002; Khawli et al. 2010; Putnam et al. 2010). For example, Igawa et al. (2010) observed that IgG4 antibodies with lower isoelectric points due to engineering in the variable region have a lower rate of fluid-phase pinocytosis and in turn a reduced elimination rate. Here, Ustekinumab has a lower isoelectric point and longer terminal half-life than Briakinumab which could be due to a lower rate of fluid-phase pinocytosis. On the other hand, mAb 8, having a lower pI than Ustekinumab and mAb 9, has a shorter terminal half-life which differs from Igawa's et al. (2010) observation. Furthermore, Boswell et al. (2010) proposed the pI differences needed to be at least of one unit to influence PK. In contrast, the pIs of Briakinumab and Ustekinumab vary between 9.4 and 9.7 (Table 4-5). Therefore, the influence on fluid-phase pinocytosis is assumed to be minimal.

Finally, the charge distribution was analyzed to look for striking positively or negatively charged regions. Isopotential surfaces were calculated from the crystal structure (Ustekinumab) or homology models (Briakinumab and all variants) and illustrate a modeled charge distribution. The calculated size of the charged regions at pH 7.4 does not correlate with the net charge of the V_H, V_L or Fv domain at pH 7.4 (Table 4-10). Position and size of the charged regions can therefore only be visual rated and not be classified by a specific value. It was observed that Briakinumab has a large positively charged region in the Fab which is absent in Ustekinumab. The location of the positively charged region spreads across the V_H and the V_L domains (Figure 4-5). The variants of Briakinumab and Ustekinumab have also differences in the charge distribution due to cross-over exchanges and mutations in the Fv domain.

On the other hand, FcRn possesses an extended negatively charged region (Figure 4-7) which is not involved in cognate Fc binding.

Thus, the hypothesis was proposed that positively charged regions in the Fv domain interact with negatively charged regions on the FcRn, thereby strengthening the FcRn-IgG interaction at physiological pH which in turn leads to less efficient IgG-recycling and shortened terminal half-lives *in vivo*.

5.2. Functional characterization

A functional characterization was performed to test if antibodies have different affinities to IL-12 and IL-23 of different species and to mouse FcγRI. Analysis of the interaction with the target (human IL-12) was performed to test if target binding is still functional, although antibody variants were modified in the Fab region. The cross-reactivity of the antibodies to mouse IL-12/-23 was analyzed to exclude target-mediated clearance effects in a mouse PK study. In addition, binding to mouse Fcγ receptor I (μFcγRI) was measured because stronger binding to mouse FcγRI could lead to a faster decrease of serum concentrations in a PK study due to faster uptake into antigen-presenting cells.

The affinity to human IL-12 was tested to confirm that functional active antibodies were produced. Briakinumab, Ustekinumab and mAbs with exchanged Fv domains (mAb 1 and 2) have nearly identical affinities to IL-12. In contrast, exchange of the LCs (mAb 3 and 4) and of the CDRs (mAb 5 and 6) results -as expected- in complete functional loss (Figure 4-10). Binding of Briakinumab and Ustekinumab to IL-12 is based on van der Waals forces and mainly on electrostatic interactions (Luo et al. 2010). Amino acid residues of the LCs and HCs form the CDRs. Both HC-CDRs and LC-CDRs are involved in the paratope and are therefore essential for target binding. The four variants with modified charge distributions in the Fv domain (mAb 7-10) still bind to IL-12, although the IL-12 affinity compared to Briakinumab is reduced (Figure 4-11). Therefore, it can be demonstrated that altering the charge distribution in the Fv domain of Briakinumab does not result in complete functional loss and that study samples of mAb 8 and mAb 9 can be analyzed using the target-specific ELISA.

Furthermore it was tested whether Briakinumab, Ustekinumab, mAb 8 and mAb 9 (mAbs used in the *in vivo* study) bind to mouse IL-12 and IL-23, because in the mouse study only target-independent clearance effects were addressed. It was reported that Briakinumab and Ustekinumab are not cross-reactive to mouse IL-12 (Luo et al. 2010; Traczewski and Rudnicka 2012); Ustekinumab does not bind mouse IL-12 because the murine p40-subunit differs in three amino acid residue clusters and especially one cluster (mouse: 40LDQSSEVL47 vs. human: 40SDQRHGVI47) is

essential for Ustekinumab binding (Luo et al. 2010). None of the four mAbs binds to mouse IL-12 and mouse IL-23, therefore target-dependent clearance effects can be excluded (Figure 4-13).

The binding to mouse FcγRI was analyzed because stronger binding to mouse FcγRI could lead to a faster decrease of serum concentrations in a PK study due to faster uptake of the antibody into antigen-presenting cells, followed by faster elimination in the alpha phase (Bleeker et al. 2001). Briakinumab and Ustekinumab show different binding levels to mouse FcγRI (Figure 4-14) suggesting that the Fab region could also influence the mouse FcγRI-IgG interaction. Therefore, Briakinumab's stronger binding to mouse FcγRI could result in a faster elimination in the first hours after administration due to a faster uptake into antigen-presenting cells and a faster elimination. The binding site of FcγRI is located at the lower hinge region of IgG (Burton and Woof 1992; Duncan et al. 1988) and the interaction between FcγRI and IgG is reported to be mainly influenced by the glycosylation of the Fc region (Jefferis 2009). The Fab region has not been described to influence the interaction with FcγRI, but it would be interesting to further study this interaction with more appropriate tools to get stronger data. Here, only binding levels were compared which is not sufficient for an accurate statement. In the beta phase FcRn-mediated recycling dominates, especially in human FcRn transgenic mice (Roopenian et al. 2010), therefore the influence of the mouse FcγRI-mAb interaction should be minimal in the beta phase.

5.3. FcRn-mAb interaction

The biochemical characterization of all antibodies showed no striking differences between Briakinumab, Ustekinumab and the variants, therefore the FcRn-mAb interaction was studied next to elucidate the contribution of the FcRn-IgG interaction on PK. The prolonged terminal half-life of IgG1 is predominantly mediated by the interaction with the FcRn (Ghetie and Ward 2000) which is strictly pH-dependent showing high affinity at pH 6.0 and negligible binding at pH 7.4 (Goebl et al. 2008; Ober et al. 2004b). This strict, pH-dependent bind-and-release mechanism is critical for IgG-recycling and any deviation of the binding characteristics at different pHs may strongly influence circulation half-lives of IgGs (Vaccaro et al. 2005). Therefore, the FcRn-mAb interaction was analyzed in two separate parts; the affinity at pH 6.0 and the dissociation at higher pH values.

At first the FcRn-mAb affinity at pH 6.0 was analyzed. The equilibrium dissociation constant K_D fell in a narrow range for all mAbs (Table 4-8) and the slight differences are considered to be negligible. It was reported that increased pH 6.0 binding can result in prolonged terminal half-lives (Suzuki et al. 2010). Briakinumab showed a slightly higher FcRn affinity at pH 6.0, although the terminal half-life of Briakinumab is shorter than of Ustekinumab, indicating that differences in PK are not caused by different FcRn affinities at pH 6.0.

Due to Briakinumab's and Ustekinumab's similar pH 6.0 affinities to FcRn, the second step was to analyze the pH-dependent FcRn-mAb dissociation. Using SPR and FcRn affinity chromatography, it was shown that the dissociation of the Briakinumab-FcRn complex is very different from the dissociation of the Ustekinumab-FcRn complex. Briakinumab and Ustekinumab showed striking retention time differences (Figure 4-16). Ustekinumab eluted at an elution pH of 7.4, whereas Briakinumab eluted at pH 7.9. These differences in FcRn-mAb dissociation were suspected to be a reason for the different terminal half-lives *in vivo* (Gandhi et al. 2010). Yeung et al. (2009) have described that efficient pH-dependent release of IgGs at pH 7.4 is essential for engineering antibodies with increased terminal half-lives. Briakinumab is released at higher pH values and therefore the dissociation at

the cell surface could be too slow resulting in only partial Briakinumab recycling to the systemic circulation. The hypothesis is that Briakinumab is transported back into the cell and finally being degraded after all. In contrast, Ustekinumab is released from the FcRn at physiological pH of 7.4 at the cell surface and is recycled back to the systemic circulation resulting in a prolonged terminal half-life.

In order to find the structural region that is responsible for different FcRn column retention times, the cleaved Fc fragments of Briakinumab and Ustekinumab were tested for FcRn-Fc dissociation. The F(ab')₂ region alone showed only very weak affinity to FcRn at pH 5.5 indicating that for the interaction with FcRn the Fc region is indispensable. Therefore modifications in the Fc region are reported to mainly influence FcRn-IgG binding and the Fab region to influence FcRn-IgG dissociation (Dall'Acqua et al. 2006; Petkova et al. 2006; Schlothauer et al. 2013). The nearly identical FcRn column retention times of the cleaved Fc fragments of Briakinumab and Ustekinumab (Figure 4-17) confirmed that the minor differences in the amino acid sequence of the Fc region do not influence FcRn-mAb dissociation. In conclusion, the Fab region has to be responsible for differences in FcRn column retention times of Briakinumab and Ustekinumab. The influence of the Fab region on FcRn interactions has recently been discussed (Schlothauer et al. 2013; Suzuki et al. 2010; Wang et al. 2011). Schlothauer et al. (2013) showed that IgGs with identical Fc regions differ in their dissociation from FcRn *in vitro* and Wang et al. (2011) indicated that IgGs with excessive binding to FcRn at pH 7.3 suffer from reduced terminal half-lives. However, it remained unknown which exact structural parts of the Fab region influence FcRn-mAb interaction and the underlying mechanism of this interaction.

The FcRn interaction of antibody variants with cross-over exchanges between Briakinumab and Ustekinumab was analyzed to obtain information on structural parts that mainly influence FcRn-IgG interaction. The analysis of this interaction revealed that mAbs with identical Fv domains and LCs elute at nearly identical FcRn column retention times (Figure 4-18 and Figure 4-19). Grafting Ustekinumab CDRs on Briakinumab shifts the retention times close to that of Ustekinumab. The other

way around, grafting Briakinumab CDRs on Ustekinumab presented an elution profile which was still close to Ustekinumab (Figure 4-20). The reason for this phenomenon could not be fully elucidated, but it was assumed that the FcRn interaction is affected by the different charge distribution in the Fv domain of Briakinumab and Ustekinumab. Briakinumab shows a large positively charged region on the Fv domain which is absent in Ustekinumab. Therefore the FcRn-mAb interaction is probably more affected by disrupting the large positively charged region of Briakinumab in the Fv domain than by creating a positively charged region which was significantly smaller. Combining the results of the structural analysis of the FcRn-mAb interaction leads to the conclusion that the Fv domain and especially the light chain variable domain (V_L) provides the main influence on the FcRn-mAb dissociation. This finding was unexpected because the Fv domain is distant from the cognate FcRn-binding site.

The extended positively charged regions in the Fv domain of Briakinumab lead to the hypothesis that the FcRn-mAb interaction is charge-mediated. To test this hypothesis, Briakinumab variants with smaller positively charged regions were analyzed for FcRn-mAb dissociation. Smaller positively charged regions located in the V_H domain resulted in a retention time shift in the direction of Ustekinumab (Figure 4-25). The retention time shift was not as pronounced as with exchanged LCs or Fv domains, but they nevertheless influence FcRn column dissociation. Smaller positively charged regions located in the V_L domain resulted in a big retention time shift in the direction of Ustekinumab (Figure 4-26) indicating that the major influence on FcRn-mAb interaction is specific located charge in the Fv domain.

To test this observation, FcRn column retention times of all antibodies were compared with the FcRn affinity at pH 6.0, hydrophobicity, isoelectric points, net charges of the Fv domains at pH 6.0 and pH 7.4 and with the extent of charged regions in the Fv structures (Table 4-10). Engineering antibodies to increase pH 6.0 binding to FcRn has been reported to simultaneously increase binding at pH 7.4 (Suzuki et al. 2010). In this study, differences in pH 6.0 affinity are too small to affect FcRn-mAb dissociation. Hydrophobicity could also affect FcRn-mAb

dissociation, because a high content of hydrophobic residues on the protein surface can increase the tendency of aggregation to minimize hydrophobic surfaces (Joubert et al. 2011). Therefore the dissociation tendency between FcRn and antibody could be reduced to cover hydrophobic antibody surfaces, but all mAbs are low hydrophobic and the FcRn retention times do not correlate with hydrophobicity. The isoelectric point is a parameter that describes the net charge of the whole antibody. The pI values range between 9.0 and 9.7 and do not correlate with FcRn column retention times indicating that the whole antibody net charge does not influence FcRn-mAb dissociation in this experiment. Furthermore there is no correlation between the net charges of the Fv domains at pH 6.0 and FcRn column retention times, because retention times describe the FcRn-mAb dissociation which occurs at higher pH values (Raghavan and Bjorkman 1996). Neither, do the net charges of the Fv domains at pH 7.4 seem to mainly influence FcRn-mAb dissociation. However, a closer look into FcRn column dissociations of all antibodies reveals that FcRn column retention times increased with the extent of positively charged regions on the Fv domains (Figure 4-27), especially around the light chain variable domains.

These findings demonstrate that specific charged regions in the Fv domain strongly influence FcRn-mAb dissociation. It was assumed that positively charged regions in the Fv domain could interact with negatively charged regions on FcRn. However, it remained unknown how the distal Fv domain interacts with the FcRn. To elucidate this interaction, Dr. Hubert Kettenberger (Biochemical & Analyticals Research, Roche Diagnostics GmbH, Mannheim, Germany, Site Penzberg) studied molecular dynamics simulations of the FcRn-mAb complexes. (The following findings were described by personal communication and are presented in the publication, “Charge-mediated Influence of the Antibody Variable Domain on FcRn-Dependent Pharmacokinetics”, which is currently under revision). Briefly, the dynamics of the FcRn-IgG complexes were studied over a period of 100 ns in explicit water and physiological ionic strength. During the course of the simulation, one of the two Fab regions approaches the tip of FcRn and persists in this conformation for the rest of the simulation time. The results of the simulation suggest that the conformational flexibility of the Fab arms allows them to readily assume conformations which can

stably interact with FcRn. The region on FcRn found to interact with the Fv domain has not been described before as being involved in IgG binding. Surprisingly, in the MD simulations not only Briakinumab but also Ustekinumab assumed a conformation with Fv domain and FcRn interacting with one another. However, the electrostatic contribution to the FcRn-Fv interaction was found to be about twice as high in Briakinumab as in Ustekinumab. In summary, the intrinsic flexibility of Fab arms in the FcRn-IgG complexes structurally allows a direct, stabilizing interaction of the Fv domain with the tip of FcRn.

The charge-mediated FcRn-mAb interaction was further confirmed by analyzing the dissociation under high ionic strength conditions. Briakinumab's shortened retention time under high ionic strength conditions indicates that the FcRn-Briakinumab interaction is charge-mediated (Figure 4-23). In addition, the FcRn affinity chromatography method was modified to analyze charge-mediated interactions within one run. For this purpose, a salt gradient was used instead of a pH-gradient. Antibodies that interact in a charge-mediated manner with the FcRn need higher salt concentrations to dissociate from the FcRn. The elution order of the mAbs was nearly the same using pH-gradient and salt-gradient FcRn affinity chromatography. This finding further confirms the charge-mediated nature of the FcRn-mAb interaction. The FcRn affinity chromatography using salt gradient elution presents a novel method to demonstrate differences in FcRn-mAb interaction caused by different charge distributions in the Fv domain.

5.4. *In vivo* studies

The *in vivo* studies are necessary to test if different FcRn-mAb dissociations affect pharmacokinetics. Pharmacokinetics describes the concentration-time process of the drug from application until elimination (Benet 1984).

To study the effect of different FcRn column dissociations, human FcRn transgenic mice were used because of the species-specific FcRn-IgG interaction (Roopenian et al. 2010). Murine FcRn binds IgG of several species, e.g. human, mouse, rabbit, guinea pig, bovine, sheep and rat IgG (Ober et al. 2001). On the contrary, human FcRn only binds human, rabbit and guinea pig IgG but not mouse IgG (Vaccaro et al. 2006; Zhou et al. 2005). Furthermore conventional mouse model systems do not reliably describe the pharmacokinetics of human antibodies, because these antibodies have an abnormally high affinity for mouse FcRn, resulting in an artificially prolonged serum persistence (Ober et al. 2001; Petkova et al. 2006; Ternant and Paintaud 2005).

After i.v. administration of 10 mg/kg antibody, the typical kinetic profile for an IgG1 can be seen (Figure 4-30), which is divided into alpha and beta phase (Roopenian et al. 2010). The division in alpha and beta phase is typical for IgGs if target-mediated drug disposition (TMDD) and immunogenicity can be excluded (Ghetie and Ward 2002). The profile of TMDD-mediated PK is non-linear and shows more than two phases (Mager 2006). TMDD can only occur if the human target is cross-reactive to the test animals target which occurs often in non-human primates and seldom in rodents (Mahmood and Green 2005; Mould and Green 2010). TMDD often results in increased clearance and is therefore also called target-mediated clearance (Gibiansky and Gibiansky 2009). The antibodies used in this study are not cross-reactive to the mouse target therefore target-mediated clearance effects can be excluded. In this study, the alpha phase occurs rapidly (in the first 24 hours) and shows mainly the distribution process until the administered antibody reaches equilibrium.

The kinetic profiles show that Briakinumab has a different alpha phase with faster distribution compared to the alpha phases of Ustekinumab, mAb 8 and mAb 9. This

fast serum concentration decrease in the first hours after administration of Briakinumab could be due to a higher affinity to mouse FcγRI (4.3.3) which could lead to a faster clearance. Ustekinumab, mAb 8 and mAb 9 are comparable within the first 24 hours.

A detailed characterization of absorption, distribution and elimination processes is achieved by PK parameters.

The distribution of mAbs is influenced by the rate of extravasation in tissue, the rate of distribution within tissue, the rate and extent of antibody binding in tissue, and the rates of elimination from tissue (Wang et al. 2008). The volume of distribution (V_d), also called the apparent volume of distribution, is defined as the theoretical volume in which the total amount of administered drug would need to be uniformly distributed to produce the desired blood concentration of a drug. Therefore higher V_d values indicate that the drug is more distributed in tissue. The volume of distribution at equilibrium (V_{ss}) is used to calculate the drug amount in the body under steady-state conditions, i.e. following drug i.v. infusion (Toutain and Bousquet-Melou 2004). V_{ss} after i.v. infusion differs only slightly from V_{ss} after i.v. injection, therefore V_{ss} was used to describe the volume of distribution in the conducted studies.

The volume of distribution of mAbs is reported to be in the order of 0.1 L/kg which is approximately equal to the extracellular fluid volume (Mould and Green 2010). Antibodies are mainly distributed in the blood and extracellular fluid and not in tissues due to their size and hydrophobicity (Ternant and Paintaud 2005; Toutain and Bousquet-Melou 2004). Ustekinumab, mAb 8 and mAb 9 have V_{ss} of about 0.1 L/kg (Table 4-11). This is in agreement with the V_{ss} of other IgGs (Mould and Green 2010). V_{ss} of Briakinumab is higher which indicates a higher distribution in tissues or a faster cellular uptake. The bigger V_{ss} can also be seen in the first hours of the concentration-time curves. To elucidate if Briakinumab shows higher unspecific binding to cell surfaces or has a faster cellular uptake, the working group of Dr. Olaf Mundigl (LMR Discovery, Roche Diagnostics GmbH, Mannheim, Germany, Site Penzberg) studied the uptake of Briakinumab and Ustekinumab in HeLa^{FcRn} cells

(The following findings were described by personal communication.). HeLa^{FcRn} cells are human epithelial cells of the cervical cancer that are transfected with human FcRn (Zhu et al. 2001). Briefly, Briakinumab and Ustekinumab were labeled with Alexa Fluor-488 and Alexa Fluor-594, respectively, according to the manufacturer's instructions (Alexa Fluor® 488 and 594 Protein Labeling Kit, Life Technologies, USA). Afterwards labeled antibodies were incubated at a concentration of 5 µg/mL with HeLa^{FcRn} cells at pH 6.0 and studied using confocal microscopy (Leica SP5, Leica Microsystems, Germany). The cells were observed over a period of 90 minutes. At the cell surface colocalisation of Briakinumab and Ustekinumab is observed indicating similar interactions with the cell membrane (Figure 5-1). Interestingly, the endosomes are divided in endosomes including only Briakinumab or only Ustekinumab. However, Briakinumab and Ustekinumab show similar interaction with the cell surface, therefore Briakinumab does not seem to have a faster cellular uptake due to positively charged regions in the Fv domain.

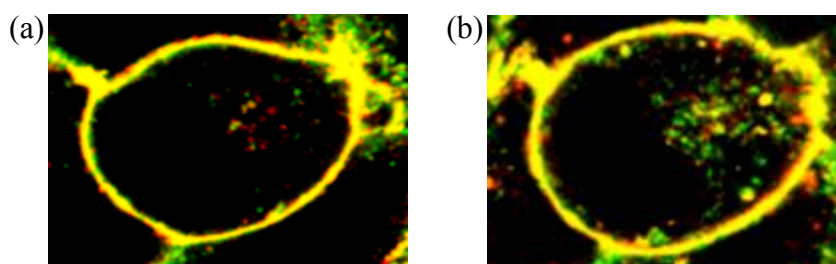


Figure 5-1: HeLa^{FcRn} cells incubated with Briakinumab and Ustekinumab
Confocal microscopy; (a) after 10 min and (b) after 25 min of incubation with Briakinumab (green) and Ustekinumab (red). Colocalisation is illustrated in yellow.

The bigger V_{ss} of Briakinumab could also be explained by the stronger interaction with mouse FcγRI (Figure 4-14). Briakinumab's stronger binding to mouse FcγRI could lead to a faster decrease of serum concentrations due to faster uptake of Briakinumab into antigen-presenting cells, followed by faster elimination in the alpha phase. However, as mentioned in 5.2, this interaction needs to be studied with more appropriate tools to get stronger data.

The area under the curve (AUC) represents the total drug exposure integrated over time and is an important parameter for both PK and PD analyses. The AUC is often

calculated from 0 hours to infinity (AUC_{0-inf}). Distribution and elimination processes can influence the AUC. Therefore, Briakinumab has a lower AUC_{0-inf} compared to Ustekinumab, mAb 8 and mAb 9 (Table 4-11) which is mainly caused by the fast serum concentration decrease within the first 24 hours.

Clearance describes the volume of plasma cleared of the drug per unit time and therefore represents a proportionality factor between the elimination rate and the serum concentration. Antibodies do not undergo renal elimination or metabolism by hepatic enzymes such as cytochrome P450 due to their high molecular weights. They are mainly cleared via proteolytic catabolism (Mould and Green 2010; Tabrizi et al. 2006).

Antibodies raised against membrane-associated antigens exhibit non-linear clearance because it is influenced by a specific, saturable target-mediated pathway and a non-specific linear clearance pathway mediated by the RES. The target-mediated clearance is dependent on several factors including the mAb-target affinity, the target concentration, distribution and internalization rate. High doses of antibody can saturate the target and reveal the linear clearance contribution (Mould and Green 2010; Tabrizi et al. 2006; Wang et al. 2008). For this reason the administration dose is often > 1 mg/kg in PK studies, because antibodies often show linear clearance at these dose levels (Ling et al. 2009).

In contrast, antibodies raised against soluble antigens, such as cytokines, generally exhibit dose-proportional, linear clearance after single-dose administration because clearance is only limited to catabolism (Lin et al. 1999; Tabrizi et al. 2006). The PK profile is characterized by a short distribution phase and a prolonged elimination half-life as a result of the non-specific clearance by the RES and the interaction with FcRn, respectively (Tabrizi et al. 2006). Antibodies bound to soluble antigens bind to FcRn and are internalized into cells, where antigen is degraded and intact antibody is recycled back to the circulation (Mould and Green 2010). When antibodies are administered at very high concentrations (2 g/kg), such as high-dose intravenous immunoglobulin (IVIG), IgG half-lives are shortened attributed to saturation of the FcRn salvage pathway (Bleeker et al. 2001).

The antibodies investigated in this study are directed against IL-12, which represents a soluble target (Gandhi et al. 2010). The clearance is therefore influenced by a short distribution phase and a prolonged elimination half-life due to the interaction with FcRn. Briakinumab has a higher clearance compared to Ustekinumab, mAb 8 and mAb 9 which is mainly caused by the fast concentration decrease in the first 24 hours. Zheng et al. (2012) have reported that antibodies with higher pI values (greater than ~9.0) tend to be associated with faster systemic clearance rates. Here, clearance did not correlate with the pI or the hydrophobicity or the charge calculated for the Fv domains which is in agreement with other reports (Hötzel et al. 2012). However, the focus of this work was to elucidate the influence of the Fv domain on FcRn-mediated IgG-recycling, therefore the terminal half-life was examined, which is exclusively calculated in the elimination phase where FcRn recycling dominates (Roopenian et al. 2010).

The terminal half-life is defined as the period of time required for a drug serum concentration in the elimination phase to be reduced to half of its value. It describes only elimination processes and is therefore the best parameter to describe the influence of the mAb-FcRn interaction on PK. Briakinumab and Ustekinumab show terminal half-lives of 48 and 136 hours, respectively (Table 4-11). These differences are also observed in humans with terminal half-lives of Briakinumab and Ustekinumab of 8 and 22 days, respectively (Gandhi et al. 2010). Variants with smaller positively charged regions in the Fv domain have longer terminal half-lives than Briakinumab. Interestingly, the terminal half-lives of the four antibodies correlate linearly with the *in vitro* FcRn column elution pH (Figure 4-32). The higher the FcRn elution pH, the shorter is the terminal half-life *in vivo*. The correlation between terminal half-lives and the FcRn column elution pHs confirms the importance of efficient FcRn-IgG dissociation at physiological pH. A similar finding has been observed for Fc-engineered IgG molecules with improved FcRn binding at both endosomal pH 6.0 and at physiological pH 7.4 which did not show prolonged half-life (Yeung et al. 2009). The FcRn-IgG complex is built in the endosomes at pH 6.0, therefore, less binding results in less IgG-recycling and faster clearance. During exocytosis the FcRn-IgG complex is released to the plasma membrane, where

dissociation of IgG and FcRn has to occur at a physiological pH of 7.4 within a short period of time (Prabhat et al. 2007). Consequently, dissociation at physiological pH is also important for a prolonged half-life (Prabhat et al. 2007; Vaccaro et al. 2005). In conclusion, these findings support the assumption that antibodies showing slower dissociation at higher pH values are transported back into the cell and are subsequently degraded instead of being released back to blood circulation.

The *in vivo* study in human FcRn knockout mice was conducted to confirm that differences in the terminal half-lives in human FcRn transgenic mice were caused by different FcRn-mAb interactions. The Three Rs (3Rs) describe guiding principles for a more ethical use of animals in research and comprise Replacement, Reduction and Refinement of test animals (Russell and Burch 1959). In order to reduce the animal number and follow the 3Rs guidelines only three antibodies conducted the knockout study: Briakinumab, Ustekinumab and mAb 9.

After i.v. administration of 10 mg/kg antibody, the clearance of all antibodies is much faster in FcRn knockout mice than in human FcRn transgenic mice (Figure 4-33) due to missing FcRn-mediated IgG-recycling (Junghans 1997; Roopenian et al. 2003; Ternant and Paintaud 2005). Especially Briakinumab is eliminated very fast, thereby preventing clear division in alpha and beta phase. Consequently, calculation of the terminal half-life is (most likely) inaccurate due to a missing beta phase.

Briakinumab has a different pharmacokinetic behavior with faster distribution in the first hours after administration compared to Ustekinumab and mAb 9. This finding was also observed in human FcRn transgenic mice which indicates that the distribution processes in the first hours after administration is not FcRn-mediated. Ustekinumab and mAb 9 have nearly identical terminal half-lives indicating that half-life differences in human FcRn transgenic mice were FcRn-mediated (Table 4-13). The study could have been improved if the sample collection time points were modified. Sample collections after 3 and 4 days would lead to a more precise terminal half-life calculation of Ustekinumab and mAb 9. Furthermore including mAb 8 into the study would be reasonable. MAb 8 shows the same distribution behavior in the alpha phase as Ustekinumab and mAb 9 and could therefore show the

same PK profile as Ustekinumab and mAb 9 in FcRn knockout mice. MAb 8 could consequently confirm that half-life differences in FcRn transgenic mice were FcRn-mediated because the terminal half-life difference between mAb 8 and Ustekinumab was even bigger than between Ustekinumab and mAb 9.

Immunogenic reactions can also influence blood levels by binding to the antibody (van Beers et al. 2010) that can be seen in a rapid decrease of the concentration-time curves after about six days (Roopenian et al. 2010). Immunogenicity is the ability to provoke an immune response. In the course of an immune response anti-drug antibodies (ADAs) can occur which can influence pharmacokinetics, efficacy and/or induce allergic reactions. ADAs can be classified in neutralizing antibodies and in binding (or non-neutralizing) antibodies (Casadevall et al. 2002). Neutralizing antibodies bind to the active site of the therapeutic protein and thereby inhibit its function resulting in diminished efficacy (Brinks et al. 2011; Putnam et al. 2010). Binding antibodies bind to the therapeutic protein and may change its PK but do not affect its intrinsic activity. Binding antibodies can result in faster clearance which can be recognized by a sharp bend in the concentration-time curve. There are factors advancing ADA development, like using antibodies of a different species (murine mAbs in human and vice versa) or multiple dose s.c. administration in contrast to single dose i.v. administration (Bertolotti-Ciarlet et al. 2009; Perini et al. 2001).

In both studies, after single dose i.v. administration of Briakinumab, mAb 8 and mAb 9 drug-ADA immune-complexes were detected (Table 4-12 and Table 4-14). The drug-ADA complexes were detected after about 7-14 days. The antibodies used in the studies were human antibodies, therefore the murine immune system identified the foreign antibodies and produced ADAs. The appearance of ADAs cannot be seen in the concentration-time curve. For example, Ustekinumab and mAb 9 have very similar concentration-time curves in the FcRn knockout study (Figure 4-33), although only after administration of mAb 9 ADAs can be detected. Therefore the influence of these ADAs on PK is expected to be negligible. It is not understood why Ustekinumab did not induce ADA formation, but it would be interesting to study this phenomenon.

5.5. Transferability to other mAbs

The Briakinumab-Ustekinumab model system showed that charged regions in the Fv domain, especially in the V_L domain, influence FcRn-IgG dissociation. A second model antibody system was used to show the transferability of these findings. Bevacizumab was chosen because the charge distribution showed no striking positively or negatively charged regions in the Fv domain and the terminal half-life is reported to be about 21 days. Bevacizumab was modified by mutation of three amino acids in the V_L domain into basic amino acids resulting in a Bevacizumab-variant that possessed a larger positively charged region in the V_L domain compared to the wild type (Figure 4-36). As expected, the Bevacizumab-variant eluted at a higher pH from the FcRn column than Bevacizumab (Figure 4-38). Therefore positively charged regions in the V_L domain resulted in FcRn-IgG dissociation at higher pH values for both model systems. The retention time shift was considered to be too small to result in statistically significant different terminal half-lives *in vivo*. Therefore this antibody pair was not tested in an *in vivo* PK study. The retention time shift could probably be further increased by enlarging the positively charged region all over the Fv domain which could then justify an *in vivo* study.

5.6. FcRn affinity column as analytical tool

FcRn plays a key role in regulating IgG homeostasis (Ghetie and Ward 2000), therefore analyzing the FcRn-IgG interaction is essential in predicting PK in drug development. The FcRn-IgG interaction consists of two parts that need to be analyzed separately: Binding at pH 6.0 and dissociation at higher pH values.

The FcRn affinity chromatography closely mimics physiological conditions for the dissociation of the FcRn-IgG complex. This method was shown to be a sensitive tool for analyzing differences in FcRn-IgG dissociation (Schlothauer et al. 2013). Structural differences in the Fab region and modified charged regions in the Fv domain resulted in altered FcRn column retention times. Furthermore, it is possible to separate species based on their FcRn binding properties using FcRn affinity chromatography.

Charge-mediated FcRn-IgG interactions can be precisely analyzed using two different methods; the FcRn affinity chromatography under high ionic strength conditions and the FcRn affinity chromatography using a salt gradient. The salt gradient FcRn affinity chromatography allows to analyze the influence of charged regions in the Fab within a single run.

In this work, the *in vitro* FcRn column elution pHs correlate linearly with the terminal half-lives of the four antibodies, thereby indicating the potential of FcRn affinity chromatography to predict Fab-mediated PK properties. Retention time shifts of ≥ 4 minutes resulted in statistically different terminal half-lives.

6. Final summary and conclusions

The **general aim** of this thesis was to elucidate the influence of the Fab region on interactions with FcRn as well as on FcRn-dependent pharmacokinetics. FcRn protects IgG from degradation and is responsible for the long half-life of IgG. Modulating the interaction between IgG and FcRn through protein engineering is an attractive method for modulating the PK of therapeutic antibodies. Modifications in the Fc region are known to affect FcRn-IgG interaction and a contribution of the Fab region has been reported. However, the underlying mechanism how the distal Fab region influences FcRn binding was hitherto only poorly understood.

To elucidate the influence of the Fab region on FcRn-IgG interactions, two IgG1 antibodies Briakinumab and Ustekinumab that have similar Fc regions but different terminal half-lives in human were used as a model system. Systematically engineered variants of both antibodies with cross-over exchanges and modified charge distributions were produced to investigate the influencing structural element of the Fab region and the mechanism that influences FcRn-IgG interactions.

Briefly, the work was divided in 5 parts. In part 1 and 2 the antibodies were biochemically and functionally characterized to test that antibodies were produced correctly and to find possible reasons explaining PK differences of Briakinumab and Ustekinumab. The third part analyzed the FcRn-IgG interaction to study if PK differences can be mediated by this interaction. Afterwards, in part 4, the effect of different FcRn-IgG dissociations on *in vivo* PK was investigated. Finally, the transferability of the previous results to a second model system was analyzed.

In **Part 1** the produced antibodies were biochemical characterized. Antibody size and molecular weight were in agreement with other IgG1 antibodies, therefore it was

concluded that all antibodies were produced correctly. Both antibodies were resistant to freeze-thaw and storage-temperature stress indicating high protein stability and a low tendency for protein aggregation. Furthermore, antibody net charges and hydrophobicity were in a narrow range for Briakinumab and Ustekinumab, which minimizes the occurrence of different absorption/unspecific binding processes. It was concluded that biochemical properties of Briakinumab, Ustekinumab and the variants cannot result in major PK differences.

Part 2 describes the functional characterization of the antibodies which includes affinity to the target (human IL-12 and IL-23) and affinity to mouse target (mouse IL-12 and mouse IL-23). Briakinumab, Ustekinumab and the variants, except variants with exchanged LCs and CDRs, bind their target with high affinity. Therefore, Briakinumab, Ustekinumab, variants with exchanged Fv domains and variants with modified charge distributions were still functional intact. Furthermore, it was confirmed that the four antibodies studied later in *in vivo* experiments were not cross-reactive to the mouse target and consequently target-mediated clearance effects could be excluded when performing an *in vivo* mouse study. Taken together, antibodies were functional intact except for antibodies with exchanged LCs or CDRs. Antibodies that conducted the PK studies showed high affinity to human IL-12 and no cross-reactivity to mouse IL-12/IL-23, therefore it was concluded that these antibodies should not show target-mediated clearance effects.

The *in vitro* interaction between FcRn and the antibodies was analyzed in **Part 3**. To gain a prolonged half-life due to FcRn-mediated IgG recycling, an antibody needs to have a strong affinity at endosomal pH of 6.0 and a fast dissociation at physiological pH of 7.4. Any deviation of this strict, pH-dependent bind-and-release mechanism is critical for IgG-recycling. Antibodies showed only slight differences in pH 6.0 affinity, therefore the Fab region seems to have negligible influence on pH 6.0 binding. In contrast, the dissociation between FcRn and the antibodies was strongly influenced by the Fab region.

Analysis of the cross-over variants revealed that the Fv domain, especially the V_L domain provides a slower-than-normal dissociation. Using the variants with modified

charge distribution, FcRn affinity chromatography under high ionic strength conditions and salt-gradient FcRn affinity chromatography, it was shown that the interaction between FcRn and Fv domain was charge-mediated. In addition, molecular dynamics simulations of the FcRn-IgG complexes demonstrated that the flexibility of the Fab arms structurally allows a direct, stabilizing interaction of the Fv domain with the tip of FcRn. To sum up, the charge distribution in the Fv domain, especially in the V_L domain of an antibody influences the FcRn-IgG dissociation. More positively charged regions in the Fv domain resulted in FcRn dissociation at higher pH values.

In **Part 4** the influence of different FcRn-IgG dissociations on FcRn-dependent PK was analyzed. Therefore four antibodies (Briakinumab, Ustekinumab, mAb 8 and mAb 9) conducted a PK study in human FcRn transgenic and in FcRn knockout mice. The best PK parameter to describe differences in FcRn-mediated IgG-recycling is the terminal half-life. Dissociation of antibodies at higher pH values resulted in reduced terminal half-lives in human FcRn transgenic mice. More precisely, FcRn-IgG dissociation pHs *in vitro* correlated linearly with *in vivo* terminal half-lives. In conclusion, these findings support the assumption that antibodies showing slower dissociation at higher pH values are transported back into the cell and are subsequently degraded instead of being released back to blood circulation.

In FcRn knockout mice the terminal half-lives were smaller due to missing FcRn-mediated IgG-recycling. The terminal half-lives of Ustekinumab and mAb 9 were identical indicating that differences in human FcRn transgenic mice were FcRn-mediated. Briakinumab showed a much faster clearance in the first hours after administration in both mice types probably due to different distribution processes. However, the terminal half-life was calculated in the elimination phase and was not affected by different distribution processes.

Taken together, larger positively charge regions in the Fv domain are involved in FcRn-IgG dissociation at increased pH values. This slower-than-normal dissociation prevents efficient FcRn-IgG dissociation at physiological pH, thereby reducing FcRn-dependent terminal half-lives.

It remained unknown if charged regions in the Fv domain influence FcRn-IgG interaction in general. Therefore, in **Part 5**, the transferability of the previous results was tested. Bevacizumab was used as second antibody because the charge distribution showed no striking positively or negatively charged regions in the Fv domain. A Bevacizumab-variant was produced that exhibited an additional positively charged region in the V_L domain. Bevacizumab-variant had a slower dissociation from the FcRn than Bevacizumab. In conclusion, positively charged regions in the V_L domain resulted in FcRn-IgG dissociation at higher pH values for both model systems.

Taken together **conclusions from all chapters** it was demonstrated that the charge distribution in the Fv domain of IgGs is involved in excessive binding to FcRn, thereby reducing FcRn-dependent terminal half-lives *in vivo*. These findings contribute to a better understanding of the FcRn-IgG interaction and it could also provide profound potential in FcRn-dependent antibody-engineering of the variable Fab region. For example, in drug development the interaction of FcRn and antibody needs to be analyzed in two separate steps to predict PK behavior as best as possible: pH affinity at pH 6.0 and the dissociation profile at higher pH values. Antibodies that show a slower-than-normal dissociation could be analyzed and screened for positively charged regions in the Fv domain. To increase FcRn-IgG dissociation and thereby most likely improve antibody PK of these antibodies it should be considered to choose an antibody variant that exhibits smaller positively charged regions in the Fv domain. Furthermore FcRn affinity chromatography can be used to identify candidates at risk for poor PK properties with reduced terminal half-lives. The findings of this work contribute to a better understanding of the FcRn-IgG interaction and might allow to “repair” such candidates.

7. Addendum

7.1. Tables

Table 7-1: Serum concentrations of Briakinumab in huFcRn transgenic mice

Serum concentrations are determined after administration of a 10 mg/kg single dose i.v. injection to 6 animals per group. ADA-positive samples are illustrated as * and ** for formation of moderate and severe drug/ADA immune complexes, respectively.

Time [h/d]	M 1 [µg/mL]	M 2 [µg/mL]	M 3 [µg/mL]	M 4 [µg/mL]	M 5 [µg/mL]	M 6 [µg/mL]	Mean [µg/mL]	SD [µg/mL]
0.08	201	174	188	192	214	194	194	13
2	109	105	106	105	110	110	107	2.4
8	50	53	53	54	56	58	54	2.8
24/ 1	37	32	30	34	35	35	34	2.4
48/ 2	27	23	24	27	24	28	25	2.2
168/ 7	6.2	5.4	6.7	6.7 *	6.4	6.8	6.4	0.5
336/ 14	0.4	1.0 *	0.1 **	0.2 **	0.7 *	0.1 **	0.4	0.4
504/ 21	b.l.q.	b.l.q.*	b.l.q.*	b.l.q.*	b.l.q.*	b.l.q.*	b.l.q.	-
672/ 28	b.l.q.	b.l.q.*	b.l.q.	b.l.q.*	b.l.q.*	b.l.q.*	b.l.q.	-

Table 7-2: Serum concentrations of Ustekinumab in huFcRn transgenic mice

Serum concentrations are determined after administration of a 10 mg/kg single dose i.v. injection to 6 animals per group. ADA-positive samples are illustrated as * and ** for formation of moderate and severe drug/ADA immune complexes, respectively.

Time [h/d]	M 1 [µg/mL]	M 2 [µg/mL]	M 3 [µg/mL]	M 4 [µg/mL]	M 5 [µg/mL]	M 6 [µg/mL]	Mean [µg/mL]	SD [µg/mL]
0.08	205	219	212	225	202	226	215	10
2	156	161	191	175	153	215	175	24
8	120	116	110	114	114	115	115	3.2
24/ 1	73	77	72	73*	69	76	73	2.9
48/ 2	58	57	64	57	56	59	59	2.7
168/ 7	18	19	27	22	20	25	22	3.5
336/ 14	7.2	6.8	8.0	6.2	8.3	4.8	6.9	1.3
504/ 21	2.2	2.2	2.5	2.3	2.5	3.0 *	2.5	0.3
672/ 28	0.9	0.8	2.1	1.1	1.0	1.8	1.3	0.5

Table 7-3: Serum concentrations of mAb 8 in huFcRn transgenic mice

Serum concentrations are determined after administration of a 10 mg/kg single dose i.v. injection to 6 animals per group. ADA-positive samples are illustrated as * and ** for formation of moderate and severe drug/ADA immune complexes, respectively.

Time [h/d]	M 1 [µg/mL]	M 2 [µg/mL]	M 3 [µg/mL]	M 4 [µg/mL]	M 5 [µg/mL]	M 6 [µg/mL]	Mean [µg/mL]	SD [µg/mL]
0.08	241	177	174	203	220	217	206	26
2	146	175	155	120	109	146	142	24
8	90	95	97	106	108	85	97	8.7
24/ 1	76	55	55	59	80	72	66	10.9
48/ 2	65	52	56	71	71	68	64	8.1
168/ 7	24	28	25	28	27	21 **	25	2.6
336/ 14	7.7	2.9 *	4.4	1.3 *	2.4 **	6.7 *	4.2	2.5
504/ 21	3.1	0.1 **	2.3	2.1	0.1 **	0.1	1.3	1.4
672/ 28	b.l.q.	b.l.q.	b.l.q.	b.l.q.	b.l.q. *	b.l.q.	b.l.q.	-

Table 7-4: Serum concentrations of mAb 9 in huFcRn transgenic mice

Serum concentrations are determined after administration of a 10 mg/kg single dose i.v. injection to 6 animals per group. ADA-positive samples are illustrated as * and ** for formation of moderate and severe drug/ADA immune complexes, respectively.

Time [h/d]	M 1 [µg/mL]	M 2 [µg/mL]	M 3 [µg/mL]	M 4 [µg/mL]	M 5 [µg/mL]	M 6 [µg/mL]	Mean [µg/mL]	SD [µg/mL]
0.08	194	254	198	270	295	233	241	40
2	151	183	124	143	165	137	150	21
8	126	104	109	89	111	114	109	12
24/ 1	73	80	64	89	94	77	80	11
48/ 2	65	81	66	69	83	60	71	9.2
168/ 7	34	37	31	30 *	38	36	34	3.1
336/ 14	13	15 **	14 **	15 **	13 **	9.6 **	13	1.9
504/ 21	4.2	0.3 **	4.5 *	4.9 **	0.1 **	4.8 **	3.1	2.3
672/ 28	0.1 **	2.4 *	1.4 *	1.5 *	2.5	0.1 *	1.3	1.1

Table 7-5: Serum concentrations of Briakinumab in FcRn knockout mice

Serum concentrations are determined after administration of a 10 mg/kg single dose i.v. injection to 6 animals per group. ADA-positive samples are illustrated as * and ** for formation of moderate and severe drug/ADA immune complexes, respectively.

Time [h/d]	M 1 [µg/mL]	M 2 [µg/mL]	M 3 [µg/mL]	M 4 [µg/mL]	M 5 [µg/mL]	M 6 [µg/mL]	Mean [µg/mL]	SD [µg/mL]
0.08	192	181	200	187	186	178	187	8.0
2	86	79	74	91	89	91	85	7.1
8	31	32	36	31	29	33	32	2.3
24/ 1	6.7	12	7.9	11	6.9	8.0	8.7	2.1
48/ 2	1.8	2.3	2.7	2.6	2.4	2.2	2.3	0.3
168/ 7	b.l.q.	b.l.q.	b.l.q.	b.l.q.	b.l.q.	b.l.q.	b.l.q.	-
192/ 8	b.l.q. *	b.l.q. *	b.l.q.	b.l.q. *	b.l.q.	b.l.q.	b.l.q.	-
216/ 9	b.l.q. *	b.l.q.	b.l.q.	b.l.q.	b.l.q. *	b.l.q. *	b.l.q.	-
336/ 14	b.l.q.	b.l.q.	b.l.q. *	b.l.q.	b.l.q.	b.l.q. *	b.l.q.	-

Table 7-6: Serum concentrations of Ustekinumab in FcRn knockout mice

Serum concentrations are determined after administration of a 10 mg/kg single dose i.v. injection to 6 animals per group.

Time [h/d]	M 1 [µg/mL]	M 2 [µg/mL]	M 3 [µg/mL]	M 4 [µg/mL]	M 5 [µg/mL]	M 6 [µg/mL]	Mean [µg/mL]	SD [µg/mL]
0.08	209	221	229	228	220	219	221	7.4
2	153	164	158	155	157	149	156	4.8
8	80	95	88	96	104	95	93	8.0
24/ 1	50	47	37	44	38	37	42	5.5
48/ 2	16	16	17	13	11	14	15	2.2
168/ 7	0.4	0.6	0.4	0.3	0.6	0.4	0.5	0.1
192/ 8	0.5	0.2	0.1	0.1	0.2	0.4	0.2	0.2
216/ 9	b.l.q.	b.l.q.	b.l.q.	b.l.q.	b.l.q.	b.l.q.	b.l.q.	-
336/ 14	b.l.q.	b.l.q.	b.l.q.	b.l.q.	b.l.q.	b.l.q.	b.l.q.	-

Table 7-7: Serum concentrations of mAb 9 in FcRn knockout mice

Serum concentrations are determined after administration of a 10 mg/kg single dose i.v. injection to 6 animals per group. ADA-positive samples are illustrated as * and ** for formation of moderate and severe drug/ADA immune complexes, respectively.

Time [h/d]	M 1 [µg/mL]	M 2 [µg/mL]	M 3 [µg/mL]	M 4 [µg/mL]	M 5 [µg/mL]	M 6 [µg/mL]	Mean [µg/mL]	SD [µg/mL]
0.08	249	292	232	214	242	226	242	27
2	119	130	139	136	123	129	129	7.3
8	62	65	74	80	83	87	75	10
24/ 1	31	37	37	32	35	36	35	2.6
48/ 2	16	15	17	12	13	16	15	1.9
168/ 7	0.2 *	0.4 **	0.5	0.5	0.5	0.3	0.4	0.1
192/ 8	0.2	0.1 **	0.2	0.1 **	0.1 **	0.2	0.2	0.2
216/ 9	b.l.q.	b.l.q.	b.l.q.	b.l.q.	b.l.q.	b.l.q.	b.l.q.	-
336/ 14	b.l.q.	b.l.q.	b.l.q.	b.l.q.	b.l.q.	b.l.q.	b.l.q.	-

7.2. List of abbreviations

ABTS	2,2'-azino-bis(3-ethylbenzothiazoline-6-sulphonic acid)
ACS	American chemical society
ADA	Anti-drug antibody
AUC _{0-inf}	Area under the curve (0 h- infinity)
Bi	Biotin
B.l.q.	Below limit of quantification
β ₂ m	Beta-2-microglobulin
c	Concentration
CDR	Complementarity determining region
Cl	Clearance
Da	Dalton
Dig	Digoxigenin
DTT	Dithiothreitol
ELISA	Enzyme-linked immunosorbent assay
Fab	Fragment antigen-binding
Fc	Fragment crystallizable
FcγR	Fc gamma receptor
FcRn	Neonatal Fc receptor
Fig	Figure
Fv	Variable fragment
h	Hour

huFcRn	Human neonatal Fc receptor
hIL	Human interleukin
His	Histidine
HMWs	Higher molecular weight species
HPLC	High liquid performance chromatography
HRP	Horseradish peroxidase
Id	Idiotypic
IdeS	Immunoglobulin-degrading enzyme from <i>Streptococcus pyogenes</i>
IEC	Ion exchange chromatography
Ig	Immunoglobulin
IL	Interleukin
i.v.	Intravenously
k_a	Association rate constant
k_d	Dissociation rate constant
K_D	Equilibrium dissociation constant
LMWs	Lower molecular weight species
M	Molar
mAb	Monoclonal antibody
MACE	Major adverse cardiovascular event
MES	2-(N-morpholine)-ethanesulfonic acid
mg	Milligram
MHC	Major histocompatibility complex

min	Minute
ml	Milliliter
MPS	Mouse Pool Serum
MS	Mass spectrometry
MTP	Microtiter plate
muFcγR	Murine Fc gamma receptor
muFcRn	Murine neonatal Fc receptor
muIL	Murine interleukin
ng	Nanogram
nM	Nanomolar
OD	Optical density
PBS	Phosphate buffered saline
Ph.Eur.	European pharmacopeia
pI	Isoelectric point
PK	Pharmacokinetics
POD	Peroxidase
PUVA	Psoralen ultraviolet A
QC	Quality control
RES	Reticuloendothelial System
RP-HPLC	Reverse phase HPLC
rpm	rounds per minute
R	Correlation coefficient

RT	Room temperature (15-25°C)
RU	Response unit
SA	Streptavidin
s.c.	subcutaneously
SDS	Sodium dodecyl sulfate
SDS-PAGE	Sodium dodecyl sulfate polyacrylamide gel electrophoresis
SEC	Size exclusion chromatography
SPR	Surface plasmon resonance
T _{1/2}	Terminal half-life
TRIS	Tris(hydroxymethyl)aminomethane
U	Unit
UV	Ultraviolet
VEGF	Vascular endothelial growth factor
V _{ss}	Volume of distribution at Steady-State
WT	Wild type

7.3. List of figures

<i>Figure 1-1: Schematic IgG structure</i>	<i>2</i>
<i>Figure 1-2: FcRn-IgG interaction.....</i>	<i>8</i>
<i>Figure 1-3: IgG-recycling mechanism</i>	<i>10</i>
<i>Figure 3-1: Photometric absorbance</i>	<i>33</i>
<i>Figure 3-2: Purity and molecular weight.....</i>	<i>34</i>
<i>Figure 3-3: SEC chromatogram with included integration borders.....</i>	<i>35</i>
<i>Figure 3-4: HIC chromatogram with reference samples</i>	<i>36</i>
<i>Figure 3-5: iCE chromatogram with pI markers</i>	<i>37</i>
<i>Figure 3-6: Antibody cleavage using IdeS</i>	<i>39</i>
<i>Figure 3-7: Principle of the specific ELISA</i>	<i>41</i>
<i>Figure 3-8: FcRn column elution pH plotted against the retention time</i>	<i>46</i>
<i>Figure 3-9: ELISA-Design for mAb detection in human serum samples</i>	<i>50</i>
<i>Figure 3-10: ELISA-Design for detection of drug/ADA immune complexes</i>	<i>54</i>
<i>Figure 3-11: ELISA-Design for Bevacizumab detection.....</i>	<i>58</i>
<i>Figure 4-1: Alignment of Briakinumab and Ustekinumab</i>	<i>61</i>
<i>Figure 4-2: Purity and molecular weight.....</i>	<i>65</i>
<i>Figure 4-3: SEC chromatogram.....</i>	<i>66</i>
<i>Figure 4-4: HIC chromatogram.....</i>	<i>67</i>
<i>Figure 4-5: Charge distribution of Briakinumab and Ustekinumab.....</i>	<i>73</i>
<i>Figure 4-6: Charge distribution of all mAbs.....</i>	<i>74</i>
<i>Figure 4-7: Charge distribution of the FcRn</i>	<i>74</i>
<i>Figure 4-8: Molecular weight of IdeS-cleaved mAbs</i>	<i>75</i>
<i>Figure 4-9: Apparent molecular weight of Briakinumab and Ustekinumab after IdeS cleavage.</i>	<i>76</i>
<i>Figure 4-10: IL-12 interaction of Briakinumab, Ustekinumab and mAb 1-6</i>	<i>78</i>
<i>Figure 4-11: IL-12 interaction of Briakinumab, Ustekinumab and mAb 7-10</i>	<i>79</i>
<i>Figure 4-12: SPR sensorgrams (concentration series) of Briakinumab binding to IL- 12.</i>	<i>80</i>
<i>Figure 4-13: Binding levels to IL-12/-23 of different species</i>	<i>82</i>

Figure 4-14: Binding levels to μ Fc γ RI	82
Figure 4-15: Principle FcRn affinity chromatography	86
Figure 4-16: FcRn column chromatogram of Briakinumab and Ustekinumab	87
Figure 4-17: FcRn column chromatogram of IdeS-cleaved Fc regions.....	87
Figure 4-18: FcRn column chromatogram of Fv-exchanged variants.....	88
Figure 4-19: FcRn column chromatogram of LC-exchanged variants	89
Figure 4-20: FcRn column chromatogram of CDRs-exchanged variants	89
Figure 4-21: FcRn column chromatogram of Ustekinumab-IL-12 complex.....	90
Figure 4-22: FcRn column chromatogram of Briakinumab-IL-12 complex.....	91
Figure 4-23: FcRn column chromatogram under higher ionic strength conditions ...	92
Figure 4-24: Salt-dependent FcRn-mAb interaction of Briakinumab and Ustekinumab.....	92
Figure 4-25: FcRn column chromatogram of Briakinumab-variants with modified charge distribution in the V_H domain.....	93
Figure 4-26: FcRn column chromatogram of Briakinumab-variants with modified charge distribution in the V_H and V_L domain.....	94
Figure 4-27: pH-dependent FcRn-mAb interaction of all mAbs	96
Figure 4-28: Salt-dependent FcRn-mAb interaction of all mAbs.....	97
Figure 4-29: FcRn column chromatogram of antibodies used in mouse PK study.....	98
Figure 4-30: Blood level curves in human FcRn transgenic mice	99
Figure 4-31: Correlation between terminal half-life and isoelectric point or hydrophobicity.....	100
Figure 4-32: Correlation between in vivo terminal half-life and FcRn column elution pH.....	101
Figure 4-33: Blood level curves in FcRn knockout mice	103
Figure 4-34: LC-alignment of Bevacizumab and Bevacizumab-variant.....	105
Figure 4-35: Molecular weight of Bevacizumab and Bevacizumab-variant and DTT- reduced mAbs.....	107
Figure 4-36: Charge distribution of Bevacizumab and Bevacizumab-variant	108
Figure 4-37: VEGF binding of Bevacizumab and Bevacizumab-variant.....	108
Figure 4-38: FcRn column chromatogram of Bevacizumab and Bevacizumab-	

<i>variant</i>	109
<i>Figure 5-1: HeLa^{FcRn} cells incubated with Briakinumab and Ustekinumab</i>	123

7.4. List of tables

Table 1-1:	<i>Properties of human IgG subclasses.....</i>	3
Table 2-1:	<i>Reagents and chemicals</i>	21
Table 2-2:	<i>Kits</i>	23
Table 2-3:	<i>Instruments and chromatography columns.....</i>	23
Table 2-4:	<i>Antibodies and proteins.....</i>	25
Table 2-5:	<i>Mice.....</i>	27
Table 2-6:	<i>Buffer compounds.....</i>	28
Table 2-7:	<i>Software.....</i>	30
Table 2-8:	<i>Consumable supplies.....</i>	30
Table 3-1:	<i>Blood sampling schedule- human FcRn transgenic mice</i>	49
Table 3-2:	<i>Blood sampling schedule- FcRn knockout mice.....</i>	50
Table 3-3:	<i>MTP allocation.....</i>	51
Table 3-4:	<i>MTP allocation for the drug/ADA immune complex assay.....</i>	55
Table 4-1:	<i>Systematically engineered variants of Briakinumab and Ustekinumab.....</i>	63
Table 4-2:	<i>Overview biochemical characterization of all mAbs</i>	68
Table 4-3:	<i>Protein concentration, size and MW after freeze-thaw stress.....</i>	69
Table 4-4:	<i>Protein concentration, size and MW after storage-temperature stress ..</i>	70
Table 4-5:	<i>Isoelectric points of Briakinumab and Ustekinumab</i>	71
Table 4-6:	<i>Net charges of all mAbs</i>	72
Table 4-7:	<i>SPR parameters of mAbs and IL-12.....</i>	81
Table 4-8:	<i>Relative K_{DS} of all mAbs to FcRn.....</i>	84
Table 4-9:	<i>K_D of Briakinumab and Ustekinumab to FcRn</i>	85
Table 4-10:	<i>FcRn affinities, calculated net charges and hydrophobicity.....</i>	95
Table 4-11:	<i>PK parameters in human FcRn transgenic mice</i>	99
Table 4-12:	<i>ADA-positive samples after Briakinumab administration in human FcRn transgenic mice.....</i>	102
Table 4-13:	<i>PK parameters in FcRn knockout mice.....</i>	103
Table 4-14:	<i>ADA-positive samples after Briakinumab administration in FcRn knockout mice.....</i>	104

<i>Table 4-15: Bevacizumab and Bevacizumab-variant with additional positively charged regions in the V_L domain.....</i>	<i>106</i>
<i>Table 4-16: Overview biochemical characterization of Bevacizumab and Bevacizumab-variant</i>	<i>106</i>
<i>Table 7-1: Serum concentrations of Briakinumab in huFcRn transgenic mice</i>	<i>134</i>
<i>Table 7-2: Serum concentrations of Ustekinumab in huFcRn transgenic mice</i>	<i>135</i>
<i>Table 7-3: Serum concentrations of mAb 8 in huFcRn transgenic mice.....</i>	<i>135</i>
<i>Table 7-4: Serum concentrations of mAb 9 in huFcRn transgenic mice.....</i>	<i>136</i>
<i>Table 7-5: Serum concentrations of Briakinumab in FcRn knockout mice.....</i>	<i>136</i>
<i>Table 7-6: Serum concentrations of Ustekinumab in FcRn knockout mice.....</i>	<i>137</i>
<i>Table 7-7: Serum concentrations of mAb 9 in FcRn knockout mice</i>	<i>137</i>

7.5. References

- Akilesh, S., Christianson, G. J., Roopenian, D. C., and Shaw, A. S. (2007). "Neonatal FcR expression in bone marrow-derived cells functions to protect serum IgG from catabolism." *J. Immunol.*, 179(7), 4580-4588.
- Ballabh, P., Braun, A., and Nedergaard, M. (2004). "The blood-brain barrier: an overview: structure, regulation, and clinical implications." *Neurobiol. Dis.*, 16(1), 1-13.
- Behring, E., and Kitasato, S. (1890). "Ueber das Zustandekommen der Diphtherie-Immunität und der Tetanus-Immunität bei Thieren." *Deutsche Medizinische Wochenschrift*, 16 (49), 1113-1116.
- Benet, L. Z. (1984). "Pharmacokinetic parameters: which are necessary to define a drug substance?" *Eur. J. Respir. Dis. Suppl.*, 134, 45-61.
- Benson, J. M., Peritt, D., Scallon, B. J., Heavner, G. A., Shealy, D. J., Giles-Komar, J. M., and Mascelli, M. A. (2011). "Discovery and mechanism of ustekinumab: a human monoclonal antibody targeting interleukin-12 and interleukin-23 for treatment of immune-mediated disorders." *MAbs.*, 3(6), 535-545.
- Bertolotti-Ciarlet, A., Wang, W., Lownes, R., Pristatsky, P., Fang, Y., McKelvey, T., Li, Y., Li, Y., Drummond, J., Prueksaritanont, T., and Vlasak, J. (2009). "Impact of methionine oxidation on the binding of human IgG1 to Fc Rn and Fc gamma receptors." *Mol. Immunol.*, 46(8-9), 1878-1882.
- Bjorkman, P. J., and Parham, P. (1990). "Structure, function, and diversity of class I major histocompatibility complex molecules." *Annu. Rev. Biochem.*, 59, 253-288.
- Bleeker, W. K., Teeling, J. L., and Hack, C. E. (2001). "Accelerated autoantibody clearance by intravenous immunoglobulin therapy: studies in experimental models to determine the magnitude and time course of the effect." *Blood*, 98(10), 3136-3142.
- Blumberg, R. S., Koss, T., Story, C. M., Barisani, D., Polischuk, J., Lipin, A., Pablo, L., Green, R., and Simister, N. E. (1995). "A major histocompatibility complex class I-related Fc receptor for IgG on rat hepatocytes." *J. Clin. Invest.*, 95(5), 2397-2402.

- Borvak, J., Richardson, J., Medesan, C., Antohe, F., Radu, C., Simionescu, M., Ghetie, V., and Ward, E. S. (1998). "Functional expression of the MHC class I-related receptor, FcRn, in endothelial cells of mice." *Int. Immunol.*, 10(9), 1289-1298.
- Boswell, C. A., Tesar, D. B., Mukhyala, K., Theil, F. P., Fielder, P. J., and Khawli, L. A. (2010). "Effects of charge on antibody tissue distribution and pharmacokinetics." *Bioconjug. Chem.*, 21(12), 2153-2163.
- Braghiroli, M. I., Sabbaga, J., and Hoff, P. M. (2012). "Bevacizumab: overview of the literature." *Expert. Rev. Anticancer Ther.*, 12(5), 567-580.
- Brambell, F. W. (1966). "The transmission of immunity from mother to young and the catabolism of immunoglobulins." *Lancet*, 2(7473), 1087-1093.
- Brambell, F. W., Hemmings, W. A., and Morris, I. G. (1964). "A Theoretical Model of Gamma-Globulin Catabolism." *Nature*, 203, 1352-1354.
- Brinks, V., Jiskoot, W., and Schellekens, H. (2011). "Immunogenicity of Therapeutic Proteins: The Use of Animal Models." *Pharm. Res.*.
- Burton, D. R., and Woof, J. M. (1992). "Human antibody effector function." *Adv. Immunol.*, 51, 1-84.
- Campbell, N. A., and Reece, J. B. (2006). "Biologie." Pearson Education Deutschland GmbH.
- Casadevall, N., Nataf, J., Viron, B., Kolta, A., Kiladjian, J. J., Martin-Dupont, P., Michaud, P., Papo, T., Ugo, V., Teyssandier, I., Varet, B., and Mayeux, P. (2002). "Pure red-cell aplasia and antierythropoietin antibodies in patients treated with recombinant erythropoietin." *N. Engl. J. Med.*, 346(7), 469-475.
- Chandler, D. (2005). "Interfaces and the driving force of hydrophobic assembly." *Nature*, 437(7059), 640-647.
- Chaudhury, C., Mehnaz, S., Robinson, J. M., Hayton, W. L., Pearl, D. K., Roopenian, D. C., and Anderson, C. L. (2003). "The major histocompatibility complex-related Fc receptor for IgG (FcRn) binds albumin and prolongs its lifespan." *J. Exp. Med.*, 197(3), 315-322.
- Cianga, C., Cianga, P., Plamadeala, P., and Amalinei, C. (2011). "Nonclassical major histocompatibility complex I-like Fc neonatal receptor (FcRn) expression in neonatal human tissues." *Hum. Immunol.*, 72(12), 1176-1187.

- Dall'Acqua, W. F., Kiener, P. A., and Wu, H. (2006). "Properties of human IgG1s engineered for enhanced binding to the neonatal Fc receptor (FcRn)." *J. Biol. Chem.*, 281(33), 23514-23524.
- Datta-Mannan, A., Witcher, D. R., Tang, Y., Watkins, J., Jiang, W., and Wroblewski, V. J. (2007). "Humanized IgG1 variants with differential binding properties to the neonatal Fc receptor: relationship to pharmacokinetics in mice and primates." *Drug Metab Dispos.*, 35(1), 86-94.
- Diehl, K. H., Hull, R., Morton, D., Pfister, R., Rabemampianina, Y., Smith, D., Vidal, J. M., and van, d., V (2001). "A good practice guide to the administration of substances and removal of blood, including routes and volumes." *J. Appl. Toxicol.*, 21(1), 15-23.
- Ding, C., Xu, J., and Li, J. (2008). "ABT-874, a fully human monoclonal anti-IL-12/IL-23 antibody for the potential treatment of autoimmune diseases." *Curr. Opin. Investig. Drugs*, 9(5), 515-522.
- Duncan, A. R., Woof, J. M., Partridge, L. J., Burton, D. R., and Winter, G. (1988). "Localization of the binding site for the human high-affinity Fc receptor on IgG." *Nature*, 332(6164), 563-564.
- Elliott, M., Benson, J., Blank, M., Brodmerkel, C., Baker, D., Sharples, K. R., and Szapary, P. (2009). "Ustekinumab: lessons learned from targeting interleukin-12/23p40 in immune-mediated diseases." *Ann. N. Y. Acad. Sci.*, 1182, 97-110.
- European Medicines Agency (2009a) Avastin-Bevacizumab. *retrieved from* www.ema.europa.eu/ema/index.jsp?curl=pages/medicines/human/medicines/000582/human_med_000663.jsp&mid=WC0b01ac058001d124
- European Medicines Agency (2009b) Ustekinumab-Stelara. *retrieved from* www.ema.europa.eu/ema/index.jsp?curl=pages/medicines/human/medicines/000958/human_med_001065.jsp&mid=WC0b01ac058001d124
- European Medicines Agency (2011) Abbott Laboratories limited withdraws its marketing authorisation application for Ozespa (briakinumab). *retrieved from* www.ema.europa.eu/ema/index.jsp?curl=pages/news_and_events/news/2011/01/news_detail_001181.jsp&mid=WC0b01ac058004d5c1
- Faber, C., Shan, L., Fan, Z., Guddat, L. W., Furebring, C., Ohlin, M., Borrebaeck, C.

- A., and Edmundson, A. B. (1998). "Three-dimensional structure of a human Fab with high affinity for tetanus toxoid." *Immunotechnology.*, 3(4), 253-270.
- Gandhi, M., Alwawi, E., and Gordon, K. B. (2010). "Anti-p40 antibodies ustekinumab and briakinumab: blockade of interleukin-12 and interleukin-23 in the treatment of psoriasis." *Semin. Cutan. Med. Surg.*, 29(1), 48-52.
- Ghetie, V., Hubbard, J. G., Kim, J. K., Tsen, M. F., Lee, Y., and Ward, E. S. (1996). "Abnormally short serum half-lives of IgG in beta 2-microglobulin-deficient mice." *Eur. J. Immunol.*, 26(3), 690-696.
- Ghetie, V., Popov, S., Borvak, J., Radu, C., Matesoi, D., Medesan, C., Ober, R. J., and Ward, E. S. (1997). "Increasing the serum persistence of an IgG fragment by random mutagenesis." *Nat. Biotechnol.*, 15(7), 637-640.
- Ghetie, V., and Ward, E. S. (2000). "Multiple roles for the major histocompatibility complex class I- related receptor FcRn." *Annu. Rev. Immunol.*, 18, 739-766.
- Ghetie, V., and Ward, E. S. (2002). "Transcytosis and catabolism of antibody." *Immunol. Res.*, 25(2), 97-113.
- Gibiansky, L., and Gibiansky, E. (2009). "Target-mediated drug disposition model: relationships with indirect response models and application to population PK-PD analysis." *J. Pharmacokinet. Pharmacodyn.*, 36(4), 341-351.
- Giragossian, C., Clark, T., Piche-Nicholas, N., and Bowman, C. J. (2013). "Neonatal fc receptor and its role in the absorption, distribution, metabolism and excretion of immunoglobulin g-based biotherapeutics." *Curr. Drug Metab.*, 14(7), 764-790.
- Goebel, N. A., Babbey, C. M., tta-Mannan, A., Witcher, D. R., Wroblewski, V. J., and Dunn, K. W. (2008). "Neonatal Fc receptor mediates internalization of Fc in transfected human endothelial cells." *Mol. Biol. Cell*, 19(12), 5490-5505.
- Gottlieb, A. B., Cooper, K. D., McCormick, T. S., Toichi, E., Everitt, D. E., Frederick, B., Zhu, Y., Pendley, C. E., Graham, M. A., and Mascelli, M. A. (2007). "A phase 1, double-blind, placebo-controlled study evaluating single subcutaneous administrations of a human interleukin-12/23 monoclonal antibody in subjects with plaque psoriasis." *Curr. Med. Res. Opin.*, 23(5), 1081-1092.
- Hack, R., Krüger, C., Scherer, K., Thiel, R., and Weinert, H. (2013) Stellungnahme aus dem Ausschuss für Tierschutzbeauftragte zur Applikation in den

- retrobulbären Venenplexus bei Mäusen. *retrieved from www. gv-solas.de/assets/files/PDFs/pdf_STELLUNGNAHME/stell_appl-retrob2012. pdf*
- Haverick, M., Mengisen, S., Shameem, M., and Ambrogelly, A. (2014). "Separation of mAbs molecular variants by analytical hydrophobic interaction chromatography HPLC: overview and applications." *MAbs.*, 6(4).
- Haymann, J. P., Levraud, J. P., Bouet, S., Kappes, V., Hagege, J., Nguyen, G., Xu, Y., Rondeau, E., and Sraer, J. D. (2000). "Characterization and localization of the neonatal Fc receptor in adult human kidney." *J. Am. Soc. Nephrol.*, 11(4), 632-639.
- Hinton, P. R., Johlfs, M. G., Xiong, J. M., Hanestad, K., Ong, K. C., Bullock, C., Keller, S., Tang, M. T., Tso, J. Y., Vasquez, M., and Tsurushita, N. (2004). "Engineered human IgG antibodies with longer serum half-lives in primates." *J. Biol. Chem.*, 279(8), 6213-6216.
- Hinton, P. R., Xiong, J. M., Johlfs, M. G., Tang, M. T., Keller, S., and Tsurushita, N. (2006). "An engineered human IgG1 antibody with longer serum half-life." *J. Immunol.*, 176(1), 346-356.
- Hötzel, L., Theil, F. P., Bernstein, L. J., Prabhu, S., Deng, R., Quintana, L., Lutman, J., Sibia, R., Chan, P., Bumbaca, D., Fielder, P., Carter, P. J., and Kelley, R. F. (2012). "A strategy for risk mitigation of antibodies with fast clearance." *MAbs.*, 4(6), 753-760.
- Huber, A. H., Kelley, R. F., Gastinel, L. N., and Bjorkman, P. J. (1993). "Crystallization and stoichiometry of binding of a complex between a rat intestinal Fc receptor and Fc." *J. Mol. Biol.*, 230(3), 1077-1083.
- Igawa, T., Tsunoda, H., Tachibana, T., Maeda, A., Mimoto, F., Moriyama, C., Nanami, M., Sekimori, Y., Nabuchi, Y., Aso, Y., and Hattori, K. (2010). "Reduced elimination of IgG antibodies by engineering the variable region." *Protein Eng Des Sel*, 23(5), 385-392.
- Inzinger, M., Weger, W., Salmhofer, W., and Wolf, P. (2012). "Differential response of chronic plaque psoriasis to briakinumab vs. ustekinumab." *Acta Derm. Venereol.*, 92(4), 357-358.
- Israelachvili, J. N. (1985). "*Intermolecular and Surface Forces*." Academic Press Inc..
- Janeway, C. A. Jr., Travers, P., Walport, M., and Shlomchick, M. J. (2001).

- "Immunobiology: The Immune System in Health and Disease." Garland Publishing.
- Jefferis, R. (2009). "Recombinant antibody therapeutics: the impact of glycosylation on mechanisms of action." *Trends Pharmacol. Sci.*, 30(7), 356-362.
- Johansson, B. P., Shannon, O., and Bjorck, L. (2008). "IdeS: a bacterial proteolytic enzyme with therapeutic potential." *PLoS. One.*, 3(2), e1692.
- Jones, E. A., and Waldmann, T. A. (1972). "The mechanism of intestinal uptake and transcellular transport of IgG in the neonatal rat." *J. Clin. Invest*, 51(11), 2916-2927.
- Joubert, M. K., Luo, Q., Nashed-Samuel, Y., Wypych, J., and Narhi, L. O. (2011). "Classification and characterization of therapeutic antibody aggregates." *J. Biol. Chem.*, 286(28), 25118-25133.
- Junghans, R. P. (1997). "Finally! The Brambell receptor (FcRB). Mediator of transmission of immunity and protection from catabolism for IgG." *Immunol. Res.*, 16(1), 29-57.
- Kauffman, C. L., Aria, N., Toichi, E., McCormick, T. S., Cooper, K. D., Gottlieb, A. B., Everitt, D. E., Frederick, B., Zhu, Y., Graham, M. A., Pendley, C. E., and Mascelli, M. A. (2004). "A phase I study evaluating the safety, pharmacokinetics, and clinical response of a human IL-12 p40 antibody in subjects with plaque psoriasis." *J. Invest Dermatol.*, 123(6), 1037-1044.
- Keizer, R. J., Huitema, A. D., Schellens, J. H., and Beijnen, J. H. (2010). "Clinical pharmacokinetics of therapeutic monoclonal antibodies." *Clin. Pharmacokinet.*, 49(8), 493-507.
- Khawli, L. A., Goswami, S., Hutchinson, R., Kwong, Z. W., Yang, J., Wang, X., Yao, Z., Sreedhara, A., Cano, T., Tesar, D., Nijem, I., Allison, D. E., Wong, P. Y., Kao, Y. H., Quan, C., Joshi, A., Harris, R. J., and Motchnik, P. (2010). "Charge variants in IgG1: Isolation, characterization, in vitro binding properties and pharmacokinetics in rats." *MAbs.*, 2(6), 613-624.
- Khawli, L. A., Mizokami, M. M., Sharifi, J., Hu, P., and Epstein, A. L. (2002). "Pharmacokinetic characteristics and biodistribution of radioiodinated chimeric TNT-1, -2, and -3 monoclonal antibodies after chemical modification with biotin." *Cancer Biother. Radiopharm.*, 17(4), 359-370.
- Kim, H., Fariss, R. N., Zhang, C., Robinson, S. B., Thill, M., and Csaky, K. G.

- (2008). "Mapping of the neonatal Fc receptor in the rodent eye." *Invest Ophthalmol. Vis. Sci.*, 49(5), 2025-2029.
- Kim, J., Bronson, C. L., Hayton, W. L., Radmacher, M. D., Roopenian, D. C., Robinson, J. M., and Anderson, C. L. (2006). "Albumin turnover: FcRn-mediated recycling saves as much albumin from degradation as the liver produces." *Am. J. Physiol Gastrointest. Liver Physiol*, 290(2), G352-G360.
- Kobayashi, N., Suzuki, Y., Tsuge, T., Okumura, K., Ra, C., and Tomino, Y. (2002). "FcRn-mediated transcytosis of immunoglobulin G in human renal proximal tubular epithelial cells." *Am. J. Physiol Renal Physiol*, 282(2), F358-F365.
- Köhler, G., and Milstein, C. (1975). "Continuous cultures of fused cells secreting antibody of predefined specificity." *Nature*, 256(5517), 495-497.
- Kuo, T. T., Baker, K., Yoshida, M., Qiao, S. W., Aveson, V. G., Lencer, W. I., and Blumberg, R. S. (2010). "Neonatal Fc receptor: from immunity to therapeutics." *J. Clin. Immunol.*, 30(6), 777-789.
- Kuo, T. T., de Muinck, E. J., Claypool, S. M., Yoshida, M., Nagaishi, T., Aveson, V. G., Lencer, W. I., and Blumberg, R. S. (2009). "N-Glycan Moieties in Neonatal Fc Receptor Determine Steady-state Membrane Distribution and Directional Transport of IgG." *J. Biol. Chem.*, 284(13), 8292-8300.
- Kurzeja, M., Rudnicka, L., and Olszewska, M. (2011). "New interleukin-23 pathway inhibitors in dermatology: ustekinumab, briakinumab, and secukinumab." *Am. J. Clin. Dermatol.*, 12(2), 113-125.
- Leach, J. L., Sedmak, D. D., Osborne, J. M., Rahill, B., Lairmore, M. D., and Anderson, C. L. (1996). "Isolation from human placenta of the IgG transporter, FcRn, and localization to the syncytiotrophoblast: implications for maternal-fetal antibody transport." *J. Immunol.*, 157(8), 3317-3322.
- Lima, X. T., Abuabara, K., Kimball, A. B., and Lima, H. C. (2009). "Briakinumab." *Expert. Opin. Biol. Ther.*, 9(8), 1107-1113.
- Lin, Y. S., Nguyen, C., Mendoza, J. L., Escandon, E., Fei, D., Meng, Y. G., and Modi, N. B. (1999). "Preclinical pharmacokinetics, interspecies scaling, and tissue distribution of a humanized monoclonal antibody against vascular endothelial growth factor." *J. Pharmacol. Exp. Ther.*, 288(1), 371-378.
- Ling, J., Zhou, H., Jiao, Q., and Davis, H. M. (2009). "Interspecies scaling of therapeutic monoclonal antibodies: initial look." *J. Clin. Pharmacol.*, 49(12),

1382-1402.

Lobo, E. D., Hansen, R. J., and Balthasar, J. P. (2004). "Antibody pharmacokinetics and pharmacodynamics." *J. Pharm. Sci.*, 93(11), 2645-2668.

Loomes, L. M., Kerr, M. A., and Senior, B. W. (1993). "The cleavage of immunoglobulin G in vitro and in vivo by a proteinase secreted by the urinary tract pathogen *Proteus mirabilis*." *J. Med. Microbiol.*, 39(3), 225-232.

Low, S. C., and Mezo, A. R. (2009). "Inhibitors of the FcRn:IgG protein-protein interaction." *AAPS. J.*, 11(3), 432-434.

Luo, J., Wu, S. J., Lacy, E. R., Orlovsky, Y., Baker, A., Teplyakov, A., Obmolova, G., Heavner, G. A., Richter, H. T., and Benson, J. (2010). "Structural basis for the dual recognition of IL-12 and IL-23 by ustekinumab." *J. Mol. Biol.*, 402(5), 797-812.

Mager, D. E. (2006). "Target-mediated drug disposition and dynamics." *Biochem. Pharmacol.*, 72(1), 1-10.

Mahmood, I., and Green, M. D. (2005). "Pharmacokinetic and pharmacodynamic considerations in the development of therapeutic proteins." *Clin. Pharmacokinet.*, 44(4), 331-347.

Montano, R. F., and Morrison, S. L. (2002). "Influence of the isotype of the light chain on the properties of IgG." *J. Immunol.*, 168(1), 224-231.

Montoyo, H. P., Vaccaro, C., Hafner, M., Ober, R. J., Mueller, W., and Ward, E. S. (2009). "Conditional deletion of the MHC class I-related receptor FcRn reveals the sites of IgG homeostasis in mice." *Proc. Natl. Acad. Sci. U. S. A.*, 106(8), 2788-2793.

Mould, D. R., and Green, B. (2010). "Pharmacokinetics and pharmacodynamics of monoclonal antibodies: concepts and lessons for drug development." *BioDrugs.*, 24(1), 23-39.

Nimmerjahn, F., and Ravetch, J. V. (2008). "Fcγ receptors as regulators of immune responses." *Nat. Rev. Immunol.*, 8(1), 34-47.

Ober, R. J., Martinez, C., Lai, X., Zhou, J., and Ward, E. S. (2004a). "Exocytosis of IgG as mediated by the receptor, FcRn: an analysis at the single-molecule level." *Proc. Natl. Acad. Sci. U. S. A.*, 101(30), 11076-11081.

- Ober, R. J., Martinez, C., Vaccaro, C., Zhou, J., and Ward, E. S. (2004b). "Visualizing the site and dynamics of IgG salvage by the MHC class I-related receptor, FcRn." *J. Immunol.*, 172(4), 2021-2029.
- Ober, R. J., Radu, C. G., Ghetie, V., and Ward, E. S. (2001). "Differences in promiscuity for antibody-FcRn interactions across species: implications for therapeutic antibodies." *Int. Immunol.*, 13(12), 1551-1559.
- Oganesyan, V., Damschroder, M. M., Cook, K. E., Li, Q., Gao, C., Wu, H., and Dall'Acqua, W. F. (2014). "Structural insights into neonatal Fc receptor-based recycling mechanisms." *J. Biol. Chem.*, 289(11), 7812-7824.
- Pendley, C., Schantz, A., and Wagner, C. (2003). "Immunogenicity of therapeutic monoclonal antibodies." *Curr. Opin. Mol. Ther.*, 5(2), 172-179.
- Perens, G., Levi, D. S., Alejos, J. C., and Wetzel, G. T. (2007). "Muronomab-CD3 for pediatric acute myocarditis." *Pediatr. Cardiol.*, 28(1), 21-26.
- Perini, P., Facchinetti, A., Bulian, P., Massaro, A. R., Pascalis, D. D., Bertolotto, A., Biasi, G., and Gallo, P. (2001). "Interferon-beta (INF-beta) antibodies in interferon-beta1a- and interferon-beta1b-treated multiple sclerosis patients. Prevalence, kinetics, cross-reactivity, and factors enhancing interferon-beta immunogenicity in vivo." *Eur. Cytokine Netw.*, 12(1), 56-61.
- Petkova, S. B., Akilesh, S., Sproule, T. J., Christianson, G. J., Al, K. H., Brown, A. C., Presta, L. G., Meng, Y. G., and Roopenian, D. C. (2006). "Enhanced half-life of genetically engineered human IgG1 antibodies in a humanized FcRn mouse model: potential application in humorally mediated autoimmune disease." *Int. Immunol.*, 18(12), 1759-1769.
- Prabhat, P., Gan, Z., Chao, J., Ram, S., Vaccaro, C., Gibbons, S., Ober, R. J., and Ward, E. S. (2007). "Elucidation of intracellular recycling pathways leading to exocytosis of the Fc receptor, FcRn, by using multifocal plane microscopy." *Proc. Natl. Acad. Sci. U. S. A.*, 104(14), 5889-5894.
- Putnam, W. S., Prabhu, S., Zheng, Y., Subramanyam, M., and Wang, Y. M. (2010). "Pharmacokinetic, pharmacodynamic and immunogenicity comparability assessment strategies for monoclonal antibodies." *Trends Biotechnol.*, 28(10), 509-516.
- Qiao, S. W., Kobayashi, K., Johansen, F. E., Sollid, L. M., Andersen, J. T., Milford, E., Roopenian, D. C., Lencer, W. I., and Blumberg, R. S. (2008). "Dependence of antibody-mediated presentation of antigen on FcRn." *Proc.*

Natl. Acad. Sci. U. S. A., 105(27), 9337-9342.

Raghavan, M., and Bjorkman, P. J. (1996). "Fc receptors and their interactions with immunoglobulins." *Annu. Rev. Cell Dev. Biol.*, 12, 181-220.

Raghavan, M., Bonagura, V. R., Morrison, S. L., and Bjorkman, P. J. (1995). "Analysis of the pH dependence of the neonatal Fc receptor/immunoglobulin G interaction using antibody and receptor variants." *Biochemistry*, 34(45), 14649-14657.

Raghavan, M., Chen, M. Y., Gastinel, L. N., and Bjorkman, P. J. (1994). "Investigation of the interaction between the class I MHC-related Fc receptor and its immunoglobulin G ligand." *Immunity.*, 1(4), 303-315.

Reff, M. E., and Heard, C. (2001). "A review of modifications to recombinant antibodies: attempt to increase efficacy in oncology applications." *Crit Rev. Oncol. Hematol.*, 40(1), 25-35.

Rodewald, R. (1976). "pH-dependent binding of immunoglobulins to intestinal cells of the neonatal rat." *J. Cell Biol.*, 71(2), 666-669.

Roopenian, D. C., and Akilesh, S. (2007). "FcRn: the neonatal Fc receptor comes of age." *Nat. Rev. Immunol.*, 7(9), 715-725.

Roopenian, D. C., Christianson, G. J., and Sproule, T. J. (2010). "Human FcRn transgenic mice for pharmacokinetic evaluation of therapeutic antibodies." *Methods Mol. Biol.*, 602, 93-104.

Roopenian, D. C., Christianson, G. J., Sproule, T. J., Brown, A. C., Akilesh, S., Jung, N., Petkova, S., Avanesian, L., Choi, E. Y., Shaffer, D. J., Eden, P. A., and Anderson, C. L. (2003). "The MHC class I-like IgG receptor controls perinatal IgG transport, IgG homeostasis, and fate of IgG-Fc-coupled drugs." *J. Immunol.*, 170(7), 3528-3533.

Rosen, L. S. (2005). "VEGF-targeted therapy: therapeutic potential and recent advances." *Oncologist.*, 10(6), 382-391.

Russell, W. M. S., and Burch, R. L. (1959). "The Principles of Humane Experimental Technique."

Sanchez, L. M., Penny, D. M., and Bjorkman, P. J. (1999). "Stoichiometry of the interaction between the major histocompatibility complex-related Fc receptor and its Fc ligand." *Biochemistry*, 38(29), 9471-9476.

- Schlachetzki, F., Zhu, C., and Pardridge, W. M. (2002). "Expression of the neonatal Fc receptor (FcRn) at the blood-brain barrier." *J. Neurochem.*, 81(1), 203-206.
- Schlothauer, T., Rueger, P., Stracke, J. O., Hertenberger, H., Fingas, F., Kling, L., Emrich, T., Drabner, G., Seeber, S., Auer, J., Koch, S., and Papadimitriou, A. (2013). "Analytical FcRn affinity chromatography for functional characterization of monoclonal antibodies." *MAbs.*, 5(4), 576-586.
- Shields, R. L., Namenuk, A. K., Hong, K., Meng, Y. G., Rae, J., Briggs, J., Xie, D., Lai, J., Stadlen, A., Li, B., Fox, J. A., and Presta, L. G. (2001). "High resolution mapping of the binding site on human IgG1 for Fc gamma RI, Fc gamma RII, Fc gamma RIII, and FcRn and design of IgG1 variants with improved binding to the Fc gamma R." *J. Biol. Chem.*, 276(9), 6591-6604.
- Simister, N. E., and Mostov, K. E. (1989). "An Fc receptor structurally related to MHC class I antigens." *Nature*, 337(6203), 184-187.
- Simister, N. E., and Rees, A. R. (1985). "Isolation and characterization of an Fc receptor from neonatal rat small intestine." *Eur. J. Immunol.*, 15(7), 733-738.
- Simister, N. E., Story, C. M., Chen, H. L., and Hunt, J. S. (1996). "An IgG-transporting Fc receptor expressed in the syncytiotrophoblast of human placenta." *Eur. J. Immunol.*, 26(7), 1527-1531.
- Skoog, B., and Wichman, A. (1986). "Calculation of the isoelectric points of polypeptides from the amino acid composition." *Trends Anal. Chem.*, 5, 82-83.
- Stapleton, N. M., Andersen, J. T., Stermerding, A. M., Bjarnarson, S. P., Verheul, R. C., Gerritsen, J., Zhao, Y., Kleijer, M., Sandlie, I., de, H. M., Jonsdottir, I., van der Schoot, C. E., and Vidarsson, G. (2011). "Competition for FcRn-mediated transport gives rise to short half-life of human IgG3 and offers therapeutic potential." *Nat. Commun.*, 2, 599.
- Stubenrauch, K., Mackeben, K., Vogel, R., and Heinrich, J. (2012). "Generic anti-drug antibody assay with drug tolerance in serum samples from mice exposed to human antibodies." *Anal. Biochem.*, 430(2), 193-199.
- Stubenrauch, K., Wessels, U., Essig, U., Vogel, R., and Schleypen, J. (2010). "Evaluation of a generic immunoassay with drug tolerance to detect immune complexes in serum samples from cynomolgus monkeys after administration of human antibodies." *J. Pharm. Biomed. Anal.*, 52(2), 249-254.

- Suzuki, T., Ishii-Watabe, A., Tada, M., Kobayashi, T., Kanayasu-Toyoda, T., Kawanishi, T., and Yamaguchi, T. (2010). "Importance of neonatal FcR in regulating the serum half-life of therapeutic proteins containing the Fc domain of human IgG1: a comparative study of the affinity of monoclonal antibodies and Fc-fusion proteins to human neonatal FcR." *J. Immunol.*, 184(4), 1968-1976.
- Tabrizi, M. A., Tseng, C. M., and Roskos, L. K. (2006). "Elimination mechanisms of therapeutic monoclonal antibodies." *Drug Discov. Today*, 11(1-2), 81-88.
- Ternant, D., and Pintaud, G. (2005). "Pharmacokinetics and concentration-effect relationships of therapeutic monoclonal antibodies and fusion proteins." *Expert. Opin. Biol. Ther.*, 5 Suppl 1, S37-S47.
- Toutain, P. L., and Bousquet-Melou, A. (2004). "Volumes of distribution." *J. Vet. Pharmacol. Ther.*, 27(6), 441-453.
- Traczewski, P., and Rudnicka, L. (2012). "Briakinumab for the treatment of plaque psoriasis." *BioDrugs.*, 26(1), 9-20.
- Vaccaro, C., Bawdon, R., Wanjie, S., Ober, R. J., and Ward, E. S. (2006). "Divergent activities of an engineered antibody in murine and human systems have implications for therapeutic antibodies." *Proc. Natl. Acad. Sci. U. S. A.*, 103(49), 18709-18714.
- Vaccaro, C., Zhou, J., Ober, R. J., and Ward, E. S. (2005). "Engineering the Fc region of immunoglobulin G to modulate in vivo antibody levels." *Nat. Biotechnol.*, 23(10), 1283-1288.
- van Beers, M. M., Jiskoot, W., and Schellekens, H. (2010). "On the role of aggregates in the immunogenicity of recombinant human interferon beta in patients with multiple sclerosis." *J. Interferon Cytokine Res.*, 30(10), 767-775.
- Vieira, P., and Rajewsky, K. (1988). "The half-lives of serum immunoglobulins in adult mice." *Eur. J. Immunol.*, 18(2), 313-316.
- von Pawel-Rammingen, U., Johansson, B. P., and Bjorck, L. (2002). "IdeS, a novel streptococcal cysteine proteinase with unique specificity for immunoglobulin G." *EMBO J.*, 21(7), 1607-1615.
- Waldmann, T. A., and Strober, W. (1969). "Metabolism of immunoglobulins." *Prog. Allergy*, 13, 1-110.

- Wang, W., Lu, P., Fang, Y., Hamuro, L., Pittman, T., Carr, B., Hochman, J., and Prueksaritanont, T. (2011). "Monoclonal Antibodies with Identical Fc Sequences Can Bind to FcRn Differentially with Pharmacokinetic Consequences." *Drug Metab Dispos.*
- Wang, W., Wang, E. Q., and Balthasar, J. P. (2008). "Monoclonal antibody pharmacokinetics and pharmacodynamics." *Clin. Pharmacol. Ther.*, 84(5), 548-558.
- Ward, E. S., and Ober, R. J. (2009). "Chapter 4: Multitasking by exploitation of intracellular transport functions the many faces of FcRn." *Adv. Immunol.*, 103, 77-115.
- Weber, J., and Keam, S. J. (2009). "Ustekinumab." *BioDrugs.*, 23(1), 53-61.
- Weger, W., and Weger, W. (2010). "Current status and new developments in the treatment of psoriasis and psoriatic arthritis with biological agents." *Br. J. Pharmacol.*, 160(4), 810-820.
- Yamada, T. (2011). "Therapeutic monoclonal antibodies." *Keio J. Med.*, 60(2), 37-46.
- Yeung, Y. A., Leabman, M. K., Marvin, J. S., Qiu, J., Adams, C. W., Lien, S., Starovasnik, M. A., and Lowman, H. B. (2009). "Engineering human IgG1 affinity to human neonatal Fc receptor: impact of affinity improvement on pharmacokinetics in primates." *J. Immunol.*, 182(12), 7663-7671.
- Zalevsky, J., Chamberlain, A. K., Horton, H. M., Karki, S., Leung, I. W., Sproule, T. J., Lazar, G. A., Roopenian, D. C., and Desjarlais, J. R. (2010). "Enhanced antibody half-life improves in vivo activity." *Nat. Biotechnol.*, 28(2), 157-159.
- Zheng, Y., Tesar, D. B., Benincosa, L., Birnbock, H., Boswell, C. A., Bumbaca, D., Cowan, K. J., Danilenko, D. M., Daugherty, A. L., Fielder, P. J., Grimm, H. P., Joshi, A., Justies, N., Kolaitis, G., Lewin-Koh, N., Li, J., McVay, S., O'Mahony, J., Otteneder, M., Pantze, M., Putnam, W. S., Qiu, Z. J., Ruppel, J., Singer, T., Stauch, O., Theil, F. P., Visich, J., Yang, J., Ying, Y., Khawli, L. A., and Richter, W. F. (2012). "Minipig as a potential translatable model for monoclonal antibody pharmacokinetics after intravenous and subcutaneous administration." *MAbs.*, 4(2).
- Zhou, J., Mateos, F., Ober, R. J., and Ward, E. S. (2005). "Conferring the binding properties of the mouse MHC class I-related receptor, FcRn, onto the human

ortholog by sequential rounds of site-directed mutagenesis." *J. Mol. Biol.*, 345(5), 1071-1081.

Zhu, X., Meng, G., Dickinson, B. L., Li, X., Mizoguchi, E., Miao, L., Wang, Y., Robert, C., Wu, B., Smith, P. D., Lencer, W. I., and Blumberg, R. S. (2001). "MHC class I-related neonatal Fc receptor for IgG is functionally expressed in monocytes, intestinal macrophages, and dendritic cells." *J. Immunol.*, 166(5), 3266-3276.

Zhu, Y., Hu, C., Lu, M., Liao, S., Marini, J. C., Yohrling, J., Yeilding, N., Davis, H. M., and Zhou, H. (2009). "Population pharmacokinetic modeling of ustekinumab, a human monoclonal antibody targeting IL-12/23p40, in patients with moderate to severe plaque psoriasis." *J. Clin. Pharmacol.*, 49(2), 162-175.

7.6. Presentations and publications

Articles

Schoch A, Thorey IS, Engert J, Winter G, and Emrich T (2014).

"Comparison of the lateral tail vein and the retro-orbital venous sinus routes of antibody administration in pharmacokinetic studies." *Lab Anim (NY)*, 43(3), 95-99.

Schoch A, Kettenberger H, Winter G, Engert J, Heinrich J, and Emrich T.
Charge-mediated Influence of the Antibody Variable Domain on FcRn-Dependent Pharmacokinetics.

Submitted, currently under revision

Oral Presentations

Schoch A: Influence of the Fab-FcRn interaction on pharmacokinetics

10th Essential protein engineering summit (PEGS), 2014, Boston, Massachusetts, USA

Poster Presentations

Schoch A, Kettenberger H, Winter G, Engert J, Heinrich J, and Emrich T

"Influence of the Fab-FcRn interaction on pharmacokinetics." 10th Essential protein engineering summit (PEGS), 2014, Boston, Massachusetts, USA

Patents

Emrich T, Kettenberger H, Schlothauer T, **Schoch A**

"In vitro prediction of in vivo half-life"

European Patent Application EP 14161103.8 filed on March 21st, 2014

7.7. Curriculum Vitae

Personal Data

Name	Angela Susanne Schoch
Date of birth	20.07.1985
Place of birth	Heidelberg, Germany
Nationality	German

Education

07 / 2011 – 09 / 2014	Ph.D. thesis Department of Pharmacy, Pharmaceutical Technology and Biopharmaceutics, Ludwig-Maximilians- University in Munich
01 / 2011	License to practice as a Pharmacist (“Approbation”)
10 / 2005 – 10 / 2009	Study of Pharmacy at the Ruprecht-Karls University in Heidelberg

Work Experience

07 / 2011 – 09 / 2014	Ph.D. thesis Department of Large Molecule Bioanalytical Research and Development, Roche Diagnostics GmbH in Penzberg
01 / 2011 – 06 / 2011	Pharmacist at SaniPlus Pharmacy im PEP in Munich
05 / 2010 – 10 / 2010	Internship at Marien Pharmacy in Munich
11 / 2009 – 04 / 2010	Internship at Roche Diagnostics GmbH in Penzberg